# ADVANCED STEEL CONSTRUCTION

*An International Journal*

**Volume 4 Number 1**

**March 2008**

**CONTENTS**

**Technical Papers**



ISSN 1816-112X

Website: *http://www.hkisc.org/*

ADVANCED STEEL CONSTRUCTION

VOL.4, NO.1 (2008)

ADVANCED STEEL CONSTRUCTION

*an International Journal*

*ISSN 1816-112X*

*Volume 4 Number 1* *March 2008*

ISSN 1816-112X

# Advanced Steel Construction
*an international journal*



*Cover: International Commercial Centre in West Kowloon, Hong Kong, China. Courtesy of Sun Hung Kai Properties Limited.*

# General Information
## *Advanced Steel Construction, an international journal*

**Aims and scope**

The International Journal of Advanced Steel Construction provides a platform for the publication and rapid dissemination of original and up-to-date research and technological developments in steel construction, design and analysis. Scope of research papers published in this journal includes but is not limited to theoretical and experimental research on elements, assemblages, systems, material, design philosophy and codification, standards, fabrication, projects of innovative nature and computer techniques. The journal is specifically tailored to channel the exchange of technological know-how between researchers and practitioners. Contributions from all aspects related to the recent developments of advanced steel construction are welcome.

**Instructions to authors**

**Submission of the manuscript.** Authors may submit three double-spaced hard copies of manuscripts together with an electronic copy on a diskette or cd-rom in an editable format (MS Word is preferred). Manuscripts should be submitted to the regional editors as follows for arrangement of review.

| | |
|---|---|
| Asian Pacific , African and organizing editor : | Professor S.L. Chan |
| American editor : | Professor W.F. Chen |
| European editor : | Professor R. Zandonini |

All manuscripts submitted to the journal are highly recommended to accompany with a list of four potential reviewers suggested by the author(s). This list should include the complete name, address, telephone and fax numbers, email address, and at least five keywords that identify the expertise of each reviewer. This scheme will improve the process of review.

**Style of manuscript**

**General.** Author(s) should provide full postal and email addresses and fax number for correspondence. The manuscript including abstract, keywords, references, figures and tables should be in English with pages numbered and typed with double line spacing on single side of A4 or letter-sized paper. The front page of the article should contain:

a) a short title (reflecting the content of the paper);
b) all the name(s) and postal and email addresses of author(s) specifying the author to whom correspondence and proofs should be sent;
c) an abstract of 100-200 words; and
d) 5 to 8 keywords.

The paper must contain an introduction and a conclusion. The length of paper should not exceed 25 journal pages (approximately 15,000 words equivalents).

**Tables and figures.** Tables and figures including photographs should be typed, numbered consecutively in Arabic numerals and with short titles. They should be referred in the text as Figure 1, Table 2, etc. Originally drawn figures and photographs should be provided in a form suitable for photographic reproduction and reduction in the journal.

**Mathematical expressions and units.** The Systeme Internationale (SI) should be followed whenever possible. The numbers identifying the displayed mathematical expression should be referred to in the text as Eq. (1), Eq. (2).

**References.** References to published literature should be referred in the text, in the order of citation with Arabic numerals, by the last name(s) of the author(s) (e.g. Zandonini and Zanon [3]) or if more than three authors (e.g. Zandonini et al. [4]). References should be in English with occasional allowance of 1-2 exceptional references in local languages and reflect the current state-of-technology. Journal titles should be abbreviated in the style of the Word List of Scientific Periodicals. References should be cited in the following style [1, 2, 3].

Journal: [1] Chen, W.F. and Kishi, N., "Semi-rigid Steel Beam-to-column Connections, Data Base and Modelling", Journal of Structural Engineering, ASCE, 1989, Vol. 115, No. 1, pp. 105-119.

Book: [2] Chan, S.L. and Chui, P.P.T., "Non-linear Static and Cyclic Analysis of Semi-rigid Steel Frames", Elsevier Science, 2000.

Proceedings: [3] Zandonini, R. and Zanon, P., "Experimental Analysis of Steel Beams with Semi-rigid Joints", Proceedings of International Conference on Advances in Steel Structures, Hong Kong, 1996, Vol. 1, pp. 356-364.

**Proofs.** Proof will be sent to the corresponding author to correct any typesetting errors. Alternations to the original manuscript at this stage will not be accepted. Proofs should be returned within 48 hours of receipt by Express Mail, Fax or Email.

**Copyright.** Submission of an article to "Advanced Steel Construction" implies that it presents the original and unpublished work, and not under consideration for publication nor published elsewhere. On acceptance of a manuscript submitted, the copyright thereof is transferred to the publisher by the Transfer of Copyright Agreement and upon the acceptance of publication for the papers, the corresponding author must sign the form for Transfer of Copyright.

**Permission.** Quoting from this journal is granted provided that the customary acknowledgement is given to the source.

**Page charge and Reprints.** There will be no page charges if the length of paper is within the limit of 25 journal pages. A total of 30 free offprints will be supplied free of charge to the corresponding author. Purchasing orders for additional offprints can be made on order forms which will be sent to the authors. These instructions can be obtained at the Hong Kong Institute of Steel Construction, Journal website: http://www.hkisc.org

The International Journal of Advanced Steel Construction is published quarterly by non-profit making learnt society, The Hong Kong Institute of Steel Construction, c/o Department of Civil & Structural Engineering, The Hong Kong Polytechnic University, Hung Hom, Kowloon, Hong Kong.



**Subscription inquiries and change of address.** Address all subscription inquiries and correspondence to Member Records, IJASC. Notify an address change as soon as possible. All communications should include both old and new addresses with zip codes and be accompanied by a mailing label from a recent issue. Allow six weeks for all changes to become effective.

**The Hong Kong Institute of Steel Construction**
HKISC
c/o Department of Civil and Structural Engineering,
The Hong Kong Polytechnic University,
Hunghom, Kowloon, Hong Kong, China.
Tel: 852- 2766 6047 Fax: 852- 2334 6389
Email: *ceslchan@polyu.edu.hk* Website: *http://www.hkisc.org/*
**ISSN 1816-112X**

ISSN 1816-112X



# Advanced Steel Construction
## an international journal

**VOLUME 4 NUMBER 1 MARCH 2008**

**Technical Papers**

# EXPERIMENTAL AND NUMERICAL INVESTIGATIONS FOR I-GIRDERS IN BENDING AND SHEAR STIFFENED BY TRAPEZOIDAL STIFFENERS

N. Boissonnade[1,*], H. Degée[1], J. Naumes[2] and M. Oppe[2]

*1ArGEnCo Department, University of Liège, Liège, Belgium*
*[2]Lehrstuhl für Stahlbau, RWTH Aachen, Aachen, Germany*
*[*](Corresponding author: E-mail: N.Boissonnade@ulg.ac.be)*

*Received: 15 January 2007; Revised: 6 April 2007; Accepted: 20 April 2007*

**ABSTRACT:** The paper investigates the shear resistance of I-girders longitudinally stiffened by trapezoidal stiffeners. It first reports on 4 full-scale tests performed at RWTH Aachen, on stiffened panels with strong closed stiffeners. As expected, failure in the subpanels has been governing. A devoted FEA shell model is then described and validated towards these results and other experimental sources. Parametric studies led with the numerical tool help pointing out several aspects where the Eurocode 3 Part 1.5 recommendations on stiffened panels in bending and shear may be improved.

**Keywords:** Stiffened plate, trapezoidal stiffener, experimental test, numerical model, shear buckling

## 1. INTRODUCTION

This paper presents part of the research work developed in the frame of a European RFCS project designated as "ComBri" [1] (Competitive Steel and Composite Bridges by improved Steel Plated Structures). Within this project, several aspects of steel and composite bridge design such as resistance to bending, to shear, to patch loading or bridge launching have been studied.

Present paper focuses on the problem of stiffened web panels in shear or in combined bending and shear, the use of strong closed longitudinal stiffeners becoming more and more widespread since it is shown to allow for a more economic design. The main purpose is here to improve the design of longitudinally stiffened I-girders so that to benefit from the increased resistance of panels stiffened by a few strong closed stiffeners. Indeed, web subpanels adjacent to a closed (trapezoidal) stiffener may be significantly strengthened by the high torsional stiffness of the longitudinal stiffener that improves the subpanels' resistance to shear buckling. In addition, buckling of the whole stiffened panel may be significantly restrained by the use of a trapezoidal stiffener. The problem is here to determine in what extent this may positively affect the resistance of the whole girder.

In this field, Eurocode 3 Part 1.5 [2] appears to be one of the most advanced set of design rules. It proposes general recommendations, but the particular case of closed stiffeners is not especially addressed. Part 1.5 rules are indeed based on the so-called "rotated stress field method", that have first been developed for unstiffened webs with large aspect ratios. Then, the method has been further extended to longitudinally stiffened girders, and validated through tests and FEA numerical calculations. Nevertheless, it seems that very few developments and data towards the derivation of specific rules for strong closed stiffeners have been collected.

In this respect, this paper first briefly reports on a series of four shear buckling tests performed at RWTH Aachen, where the test specimens were designed with strong longitudinal trapezoidal stiffeners ensuring a local failure in the subpanels. Then, the paper describes the development and assessment of FEA shell models towards several sources of experimental data. On the basis of the developed numerical tools, parametric studies have been conducted, and the results of a comparison between these numerical results and the application of Eurocode 3 Part 1.5 rules are presented.

Conclusions on the ability of the code to provide safe and accurate results when the girder comprises longitudinal closed stiffeners are finally given.

## 2. SHEAR BUCKLING TESTS (RWTH AACHEN)

Four full-scale tests on I-girders with slender webs have been performed at RWTH Aachen [3]. They consist of 3-point bending tests (see Figure 1) prepared and performed to serve as a reference for the validation of FEA models. They have been designed so that to exhibit the increase of resistance brought by a strong closed longitudinal stiffener. Accordingly, two specimens were designed with non-stiffened webs while the other two have been prepared with the same material and dimensions but also with a longitudinal stiffener.

The longitudinal stiffeners have been chosen so that to lead to a low global panel slenderness (i.e. including the restraining effect of the stiffener) that ensures failure in the subpanels. Therefore, the beneficial effect of the stiffener is maximised [1].

The material properties of the tested specimen are given in Table 1.

Table 1. Material Properties

| | *Web* | *Flanges* | *Longitudinal stiffener* | *Transverse stiffener* |
|---|---|---|---|---|
| *E [GPa]* | 210 | 210 | 210 | 210 |
| $f_y$ *[MPa]* | 399 | 433 | 399 | 433 |

Different measurement devices have been used during the tests. They have been chosen so that to get exploitable information for further comparison with numerical simulations. In addition to the load cell, 6 strain gauges and 10 3D-rosettes have been placed on the specimens (see Figure 2). Furthermore, photogrammetric measurements by means of three digital cameras have been used to determine the spatial evolution of displacements during loading. For that purpose, a regular grid of targets has been placed on the web surface (Figure 2). The three-dimensional displacements have been obtained through an appropriate numerical treatment of two or three images. This photogrammetric system has also been used to provide information on the initial geometrical imperfections.

Figure 3 reports on the obtained load-displacement curves. As can be seen, the results obtained with the stiffened girders (Test 2a and Test 2b) are significantly higher than with the unstiffened girders (Test 1a and Test 1b). This clearly points out how much additional resistance can be provided through the use of a longitudinal stiffener being able to prevent global panel buckling. These results are further compared with FEA results in the next section.

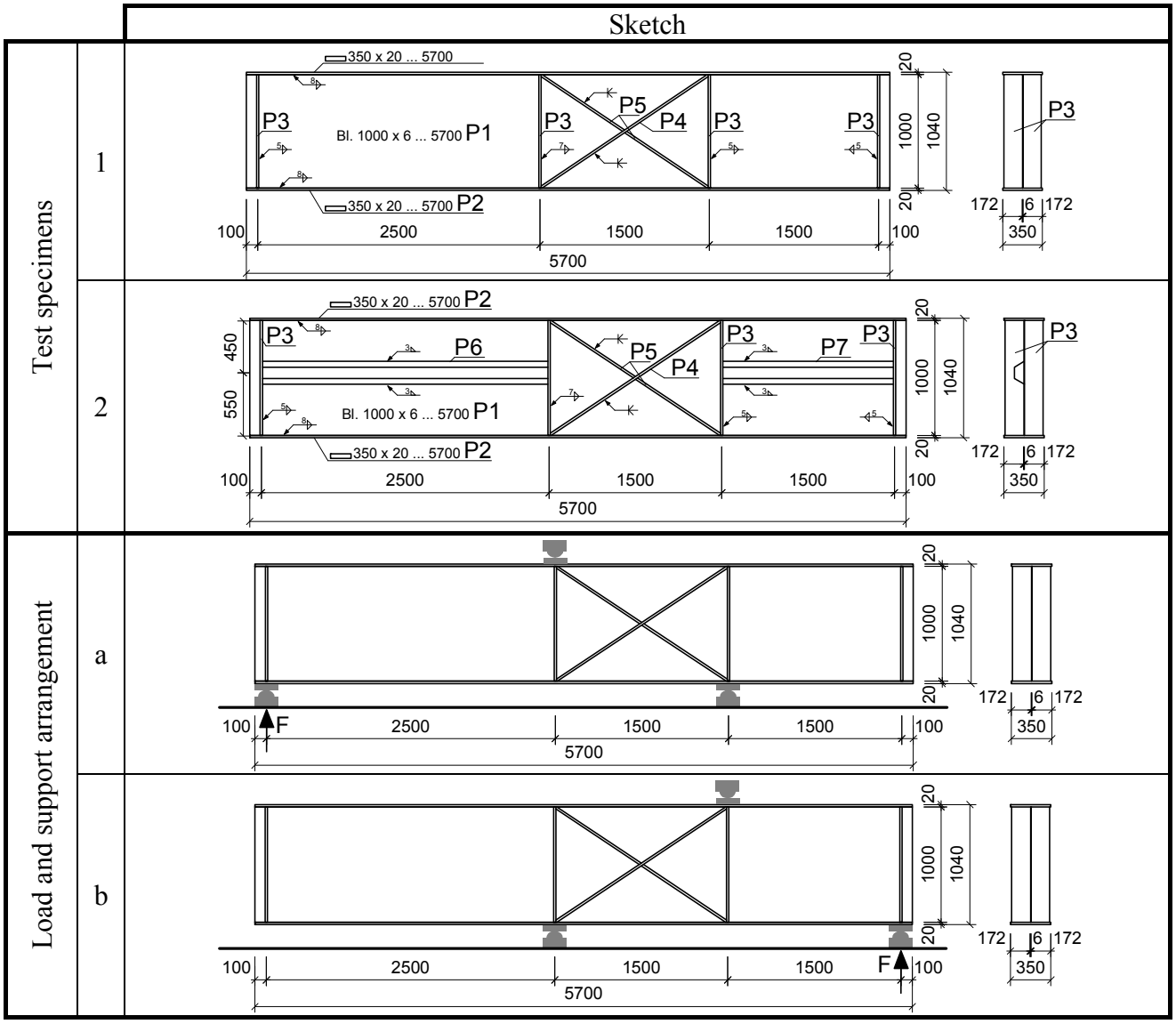


Figure 1. Test Program for Shear Buckling Tests

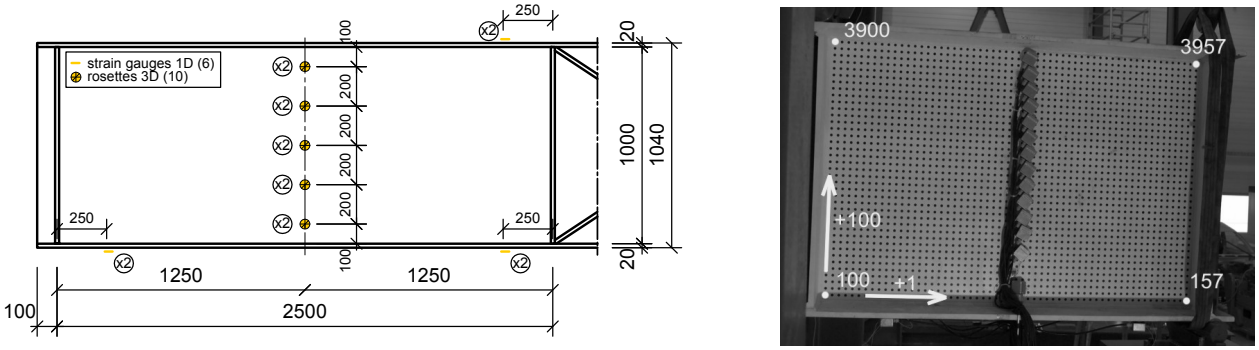


Figure 2. Rosettes and Strain Gauges Locations – Test Grid of Targets

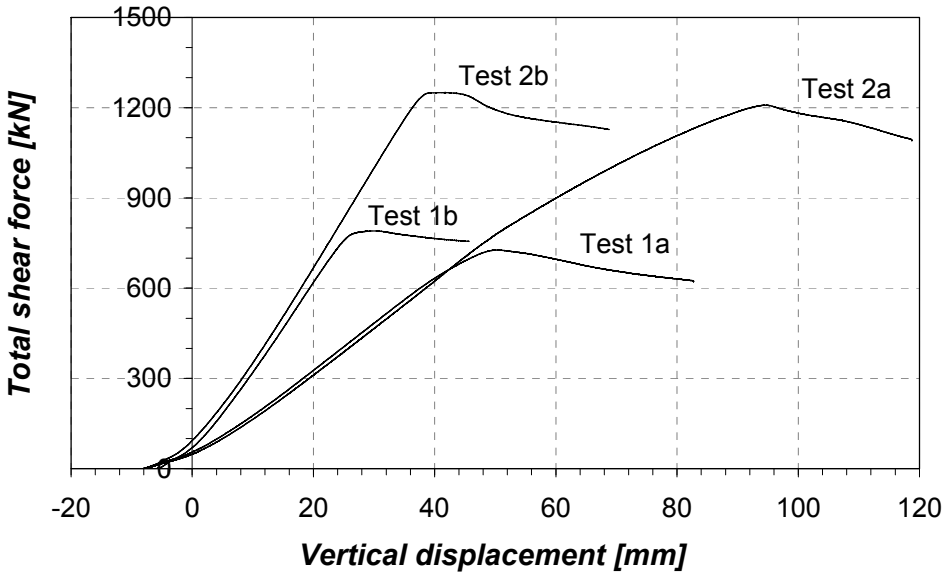


Figure 3. Experimental Load-displacement Curves

## 3. DEVELOPMENT AND ASSESSMENT OF FEA MODELS

### 3.1 Description of the FEA Models

Several FEA non-linear models have been derived both at RWTH Aachen with MARC-Software and at M&S Liège with FINELg. Because the uses of both software lead to very close results, no distinction is made here from the different numerical sources.

The geometry of the I-girder is accounted for by means of shell elements, with mesh densities that have been shown to be sufficient for a reasonably accurate calculation of a shear buckling situation (see Figure 4). The support conditions are derived in order to fulfil the three-point bending load case, and the applied force consists in a linearly distributed load along the flange width, as was done in the experimental tests. The material is assumed as elastic-plastic with no strain hardening, and residual stresses are not accounted for. Deeper details on the shell elements and modelling assumptions may be found in [4].

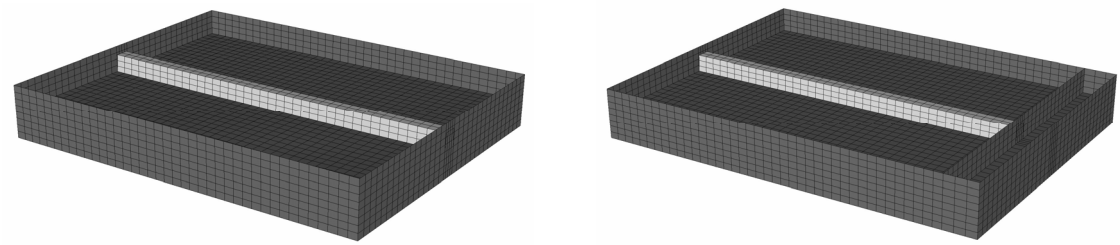

Figure 4. FEA Shell Models: Simple Model (RWTH Tests) and Refined Model (Stuttgart Tests)

As can be seen on Figure 4, two different FEA models have been derived: a first simple model that is dedicated to the simulation of the RWTH Aachen tests, and a more refined model allowing dealing with rigid or non-rigid end-posts.

As a particular point, the introduction of geometrical imperfections in the FEA calculations is worthy of further discussion. Indeed, several possibilities to combine global panel default with local subpanels imperfections were seen to lead to non-negligible discrepancies on the carrying capacity of the girder.

In accordance with Eurocode 3 Part 1.5 recommendations for FEA modelling, both global and local imperfections have been taken into account. The *global* imperfection was assumed to be a bow imperfection with maximum amplitude equal to $a$ / 400, $a$ being the length of the web panel. The *local* subpanel imperfection has to be set affine to the considered subpanel buckling shape, with an amplitude of min ($a$ / 200; $b$ / 200), where $a$ and $b$ are the dimensions of the subpanel.

Then, several combinations of these isolated defaults may be defined. According to Eurocode 3, a leading imperfection has to be accompanied by a secondary imperfection with 70% of its recommended amplitude. The determination of the imperfection that should be considered as the major one then implies to perform two calculations where the global and local defaults play the major role alternatively. In addition, the direction of each imperfection has to be defined since each one can be either on the same side as the stiffener or on the opposite side. As a consequence, several calculations need to be achieved, and the minimum obtained capacity shall be kept as the reference value.

It has been shown [1] that, concerning the present problem, the combination where the global subpanel imperfection is chosen as the major imperfection on the stiffener's side together with a local default on the opposite side lead to the most conservative results.

Besides this "code" combination procedure, a second method to account for the geometrical imperfection has been used. It consists of using the displacements pattern from the last step of the "code" non-linear calculation (i.e. in the post-buckling range) with adequate amplitude as the initial imperfection. This allows studying directly the "worst" imperfection shape where global and local imperfections are merged. An amplitude equal to $a$ / 800 has been shown to be appropriate and safe, the influence of the shape being more important than the value of the initial amplitude.

The influence of initial residual stresses has not been taken into account, since it is known to have a very small influence on this type of results, especially regarding shear behaviour where the welding affects a quite limited zone [1].

### 3.2 Assessment of FEA Models

The results obtained from the numerical model have been compared with the experimental results. Figure 5 presents the obtained load-displacement curves, where the FEA calculations have been achieved through the "code" procedure described in Section 3.1.

As can be seen, the different FEA curves are in quite good agreement with their respective experimental counterparts. It is to be noted that a good correspondence for the whole load-displacements curves has only be made possible through an appropriate modelling of the supports with non fully-rigid but elastic supports, the spring stiffness of the latter being the measured ones.

Finally, additional numerical calculations have been performed with the "real" initial geometrical imperfection pattern, see Figure 6. Indeed, as explained in Section 2, the photogrammetric system has been prepared so that to be able to provide such data. A linear interpolation between the measurements got from the physical test grid of targets and the FEA model mesh has been used to convert the necessary data in the numerical model. Figure 7 compares the results of these calculations with those obtained in the "code" procedure.

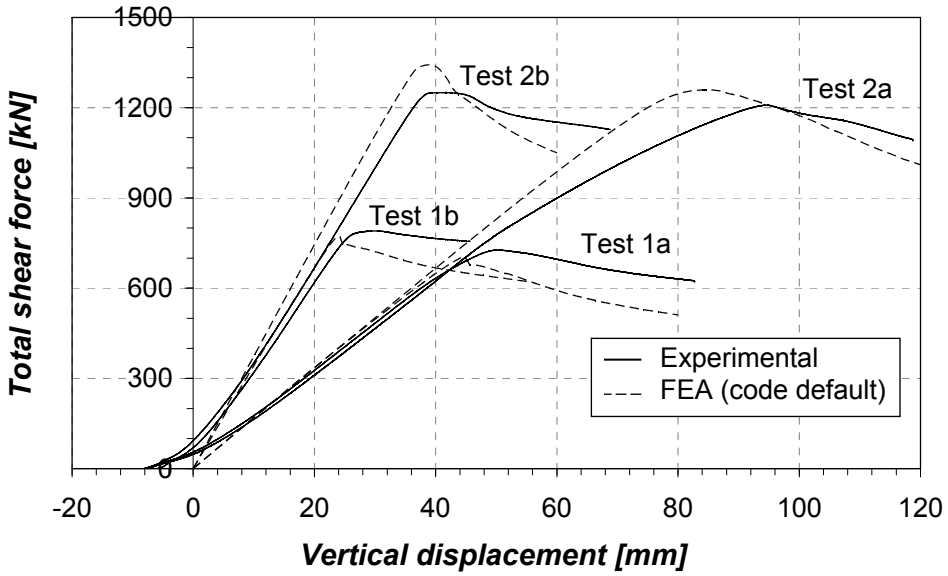


Figure 5. FEA vs. Test Load-displacement Curves

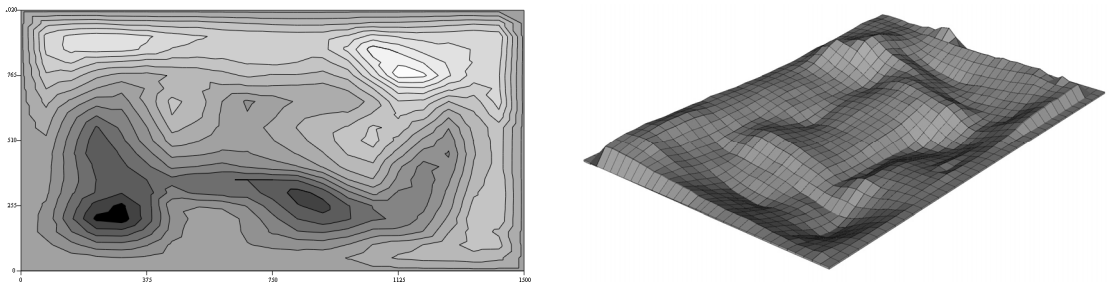

Figure 6. Measured Distribution of Initial Imperfections and Associated FEA Mesh (Amplified)

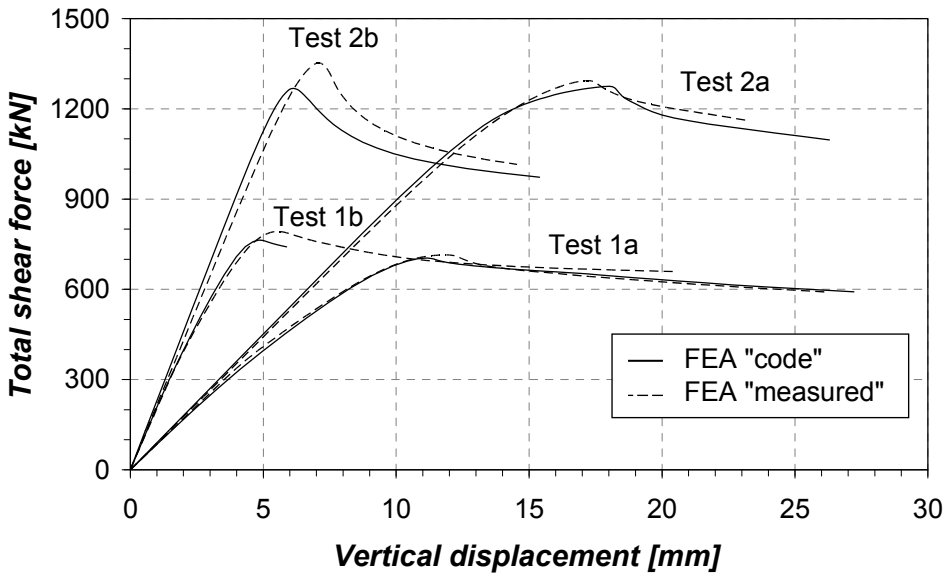


Figure 7. FEA Results for "Code" and Measured Imperfections (No Springs at Supports)

As a very good accordance between all calculations is observed, the different procedures described above to deal with the geometrical imperfections are found appropriate.

In order to further assess the ability of the models to simulate accurately the shear buckling behaviour of I-girders, additional comparisons have been carried out with other similar tests performed in Stuttgart ([5], [6], [7]).

In these four "Stuttgart tests", the longitudinal (closed) stiffeners dimensions have been chosen so that to cover different situations, from weak to strong stiffeners. So-called "weak" stiffeners are such that they buckle together with the subpanels when shear buckling occurs (i.e. global panel buckling), while stronger stiffeners restricts shear buckling to the weakest subpanel.

Table 2. Results for Stuttgart Shear Tests (Loads in kN)

| *Girder* | $G_1$ | $G_2$ | $G_3$ | $G_4$ |
|---|---|---|---|---|
| *Experimental* | 1453 | 1569 | 1412 | 1591 |
| *FEA code* | 1494 | 1524 | 1428 | 1468 |
| *FEA post* | 1408 | 1446 | 1355 | 1408 |
| $\%_{FEA\ code}$ | -2.7 | 3.0 | -1.1 | 8.4 |
| $\%_{FEA\ post}$ | 3.2 | 8.5 | 4.2 | 13.0 |

As can be seen in Table 2, the correspondence between experimental and numerical results is quite good. The design of these tests being completely different from the tests performed in Aachen, the quality of the obtained results further ensures the reliability of the developed FEA models. On the basis of these results, the models are found safe and accurate. They have been extensively used in the parametric studies described in the following.

## 4. PARAMETRIC STUDIES

The validity of the FEA models being confirmed, parametric studies have been led with respect to a 3-point bending arrangement represented in Figure 8. They are mainly dedicated to the shear behaviour of the stiffened girder.

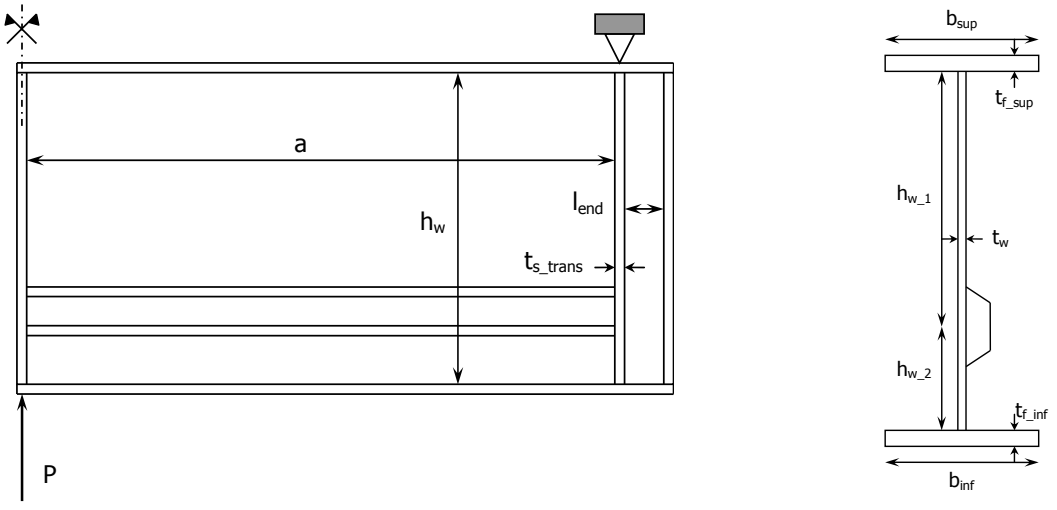


Figure 8. Loading, Support Conditions and Geometrical Definitions for the Investigated System

The following parameters have been taken into account in a first parametric study:
- 2 different trapezoidal stiffeners ("weak" and "strong");
- Web thickness equal to 6 or 12 mm;
- 3 aspect ratios for the web: 1.0, 3.0 and 5.0;
- 2 web depths $h_w$: 1000 and 2000 mm;

– 2 positions for the longitudinal stiffener: at 0.5 $h_w$ or 0.3 $h_w$;
– Rigid or non-rigid end-posts;
– "Code" or "post" initial geometrical imperfection.
– Closed or open trapezoidal stiffeners, or no stiffener;

In addition, a second parametric study on stiffened girders with higher web depths has been led, according to the following parameters:
– 2 different trapezoidal stiffeners ("weak" and "strong");
– Web thickness equal to 20 mm;
– 3 aspect ratios for the web: 1.0, 1.5 and 2.0
– 3 web depths $h_w$: 2000, 3000 and 4000 mm;
– 2 positions for the longitudinal stiffener: at 0.5 $h_w$ or 0.3 $h_w$;
– Rigid or non-rigid end-posts;
– "Code" or "post" initial geometrical imperfection.
– Closed or open trapezoidal stiffeners, or no stiffener;

As both "code"- or "post"-type initial imperfections calculations have been performed, the lowest ultimate loads have been kept as the FEA reference. In total, 1260 FEA-shell non-linear calculations have been performed (refined model).

Cases where the trapezoidal stiffener is said to be "open" aims at testing the influence of the torsional stiffness brought by the longitudinal stiffener. For such particular cases, the flange of the trapezoidal stiffener is assumed to be cut in its middle; as a consequence, the stiffener, still of trapezoidal shape, only brings a torsional stiffness corresponding to that of an open section, i.e. that is much lower than for a closed section shape.

All the results provided by the parametric studies have been compared to the corresponding Eurocode 3 Part 1.5 results. According to the code, the following resistance checks have to be performed within the present loading and support conditions:
– Bending resistance check at mid-span with a gross (Class 3) cross-section ("Gross");
– Bending resistance check at a distance equal to min (0.4 $a$; 0.5 $b$) from mid-span ("Bending");
– Shear buckling resistance check ("Shear");
– Possible interaction between bending and shear at a distance equal to 0.5 $h_w$ from mid-span ("Interaction").

All Eurocode 3 Part 1.5 results presented in the following correspond to the minimum load obtained in accordance with the four above-listed criteria.

Besides a strict application of Eurocode 3 rules, additional code-type calculations have been performed, where the buckling stresses are determined numerically. Eurocode 3 Part 1.5 indeed offers the opportunity to calculate separately the elastic plate buckling stresses, and use of EBPlate software has been made [8]. It allows getting quite accurate numerical values in many situations, and, in particular, dealing with the influence of the longitudinal stiffeners on global panel behaviour [9] or the beneficial effect of flanges and transverse stiffeners.

Accordingly, three different code-type calculations are presented in the following Figures:
– The first one corresponds to a strict application of Eurocode 3 recommendations, i.e. in line with the procedures proposed in Part 1.5 Annex A for the evaluation of bending and shear critical stresses ("Pure EC3");

– A second calculation includes the beneficial effect of the girder's flanges on the stability of the adjacent panels (including possible shear lag in the flanges), that may no more be considered as simply supported ("EC3 2 edges");
– A third calculation takes in addition advantage of the transverse stiffeners on the global panel stability ("EC3 4 edges").

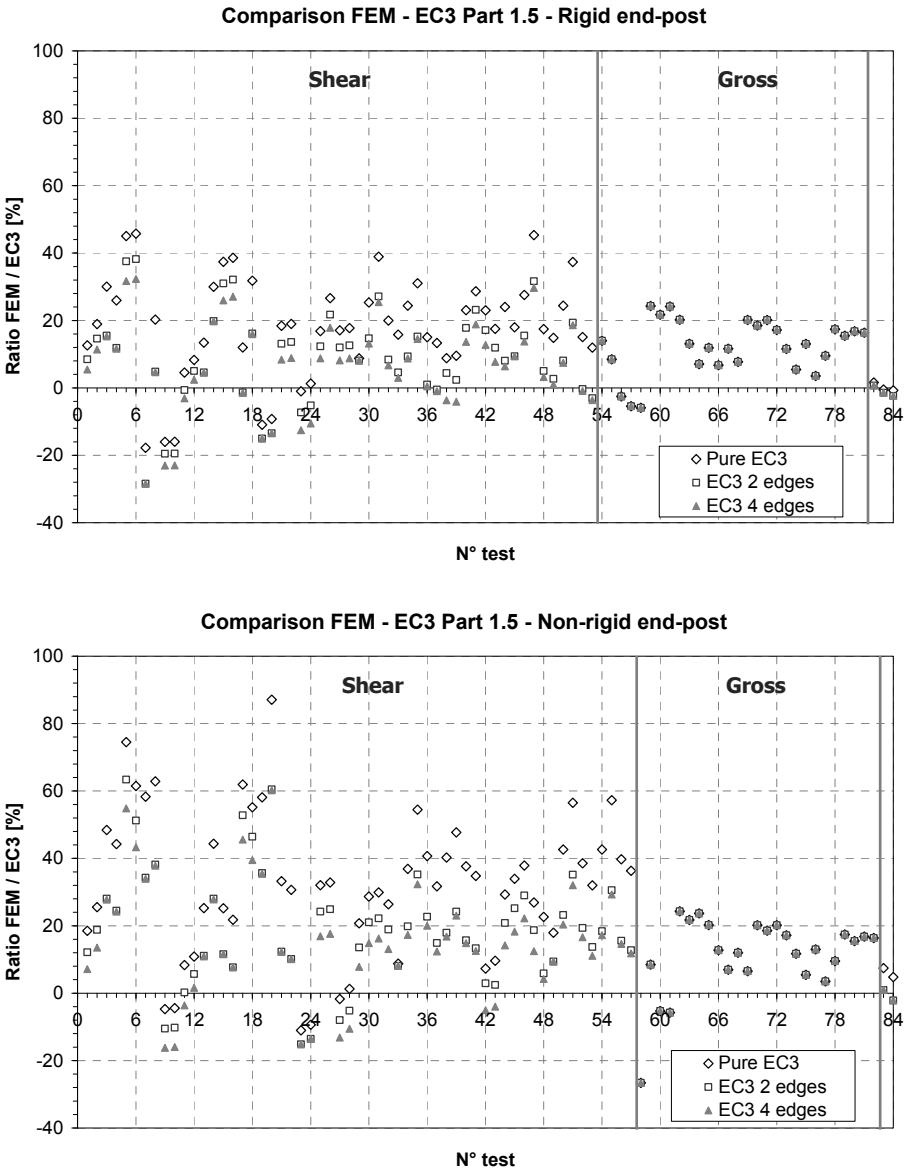


Figure 9. Comparison of Results for Closed Stiffeners

Figure 9 reports on the accuracy of these three approaches for respectively rigid and non-rigid end-post cases, when the results are sorted by failure type (according to Eurocode 3 criteria). On this Figure, the different geometric situations tested are plotted versus the percentage of difference in ultimate loads between the code result and the reference FEA result.

It is first seen that the "Shear" and "Gross" failure modes mainly govern in the different situations chosen. Then, it clearly appears that the results provided in the rigid end-post situation are much more accurate than in the non-rigid end-post case, in comparison with the FEA references. Whereas the levels of accuracy and safety appear to be quite acceptable when the "Gross" criterion governs (i.e. girders with high aspect ratios $\alpha$), situations where shear is the leading phenomenon exhibit a highly varying level of accuracy, even more for the non-rigid end-post cases. That may be explained

by the fact that the trapezoidal shape of the stiffener significantly improves the lateral resistance of the transversal stiffener of the non-rigid end-post. Therefore, no penalty on the shear buckling resistance of the stiffened web should be applied, as is nevertheless recommended by Eurocode 3 Part 1.5 rules.

It is also shown, as expected, that when the calculations of critical stresses get more and more refined, the obtained results get more and more accurate. Figure 10 also leads to the same conclusion in case of an open stiffener. In cases where the web panel is unstiffened, the distinction between rigid and no-rigid end-post appears to be justified [1].

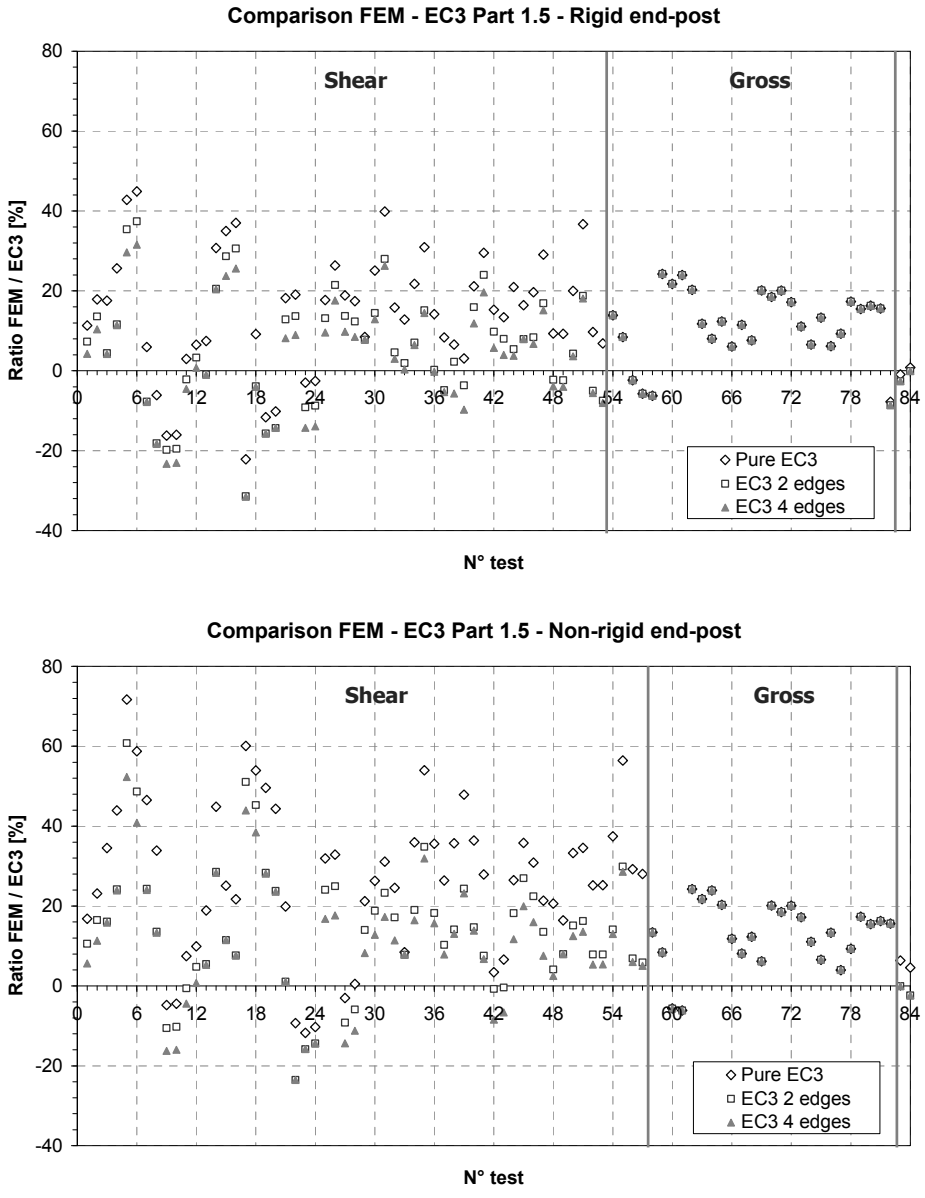


Figure 10. Comparison of Results for Open Stiffeners

Figure 11 proposes another plotting of the results, as a function of the global web relative slenderness to shear $\lambda_w$. This permits to exhibit in which extent an accurate determination of the critical stress positively affects the value of $\lambda_w$, thus the carrying capacity. It appears however that Eurocode 3 Part 1.5 rules may lead to slightly unsafe results for low value of $\lambda_w$. This was shown to be due to the fact that Part 1.5 accounts for a beneficial effect of strain hardening on the shear resistance that was disregarded in the FEA calculations.

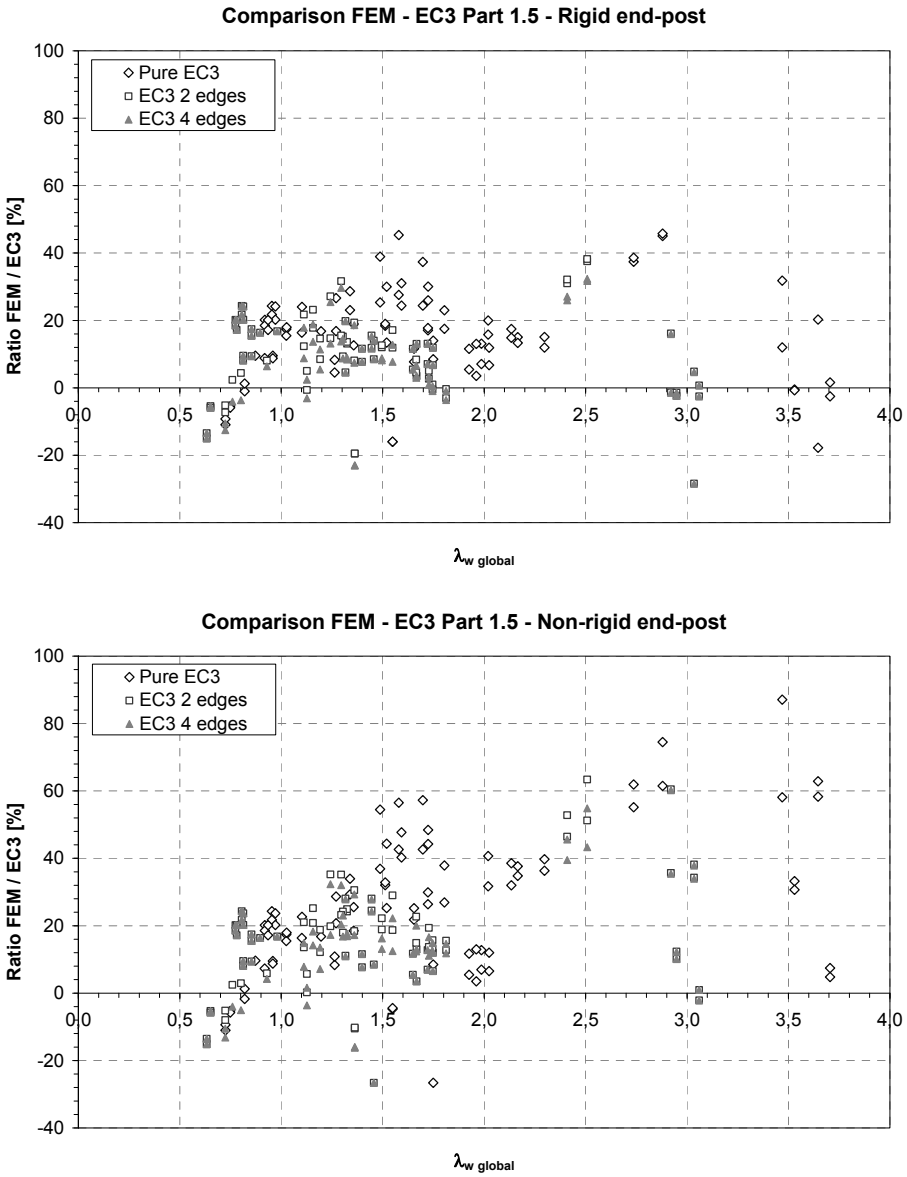


Figure 11. Influence of the Determination Procedure for Critical Stresses (Closed Stiffener)

## 5. CONCLUSION

Through extensive results from a validated numerical FEA tool, the paper has shown that the Eurocode 3 Part 1.5 recommendations could be improved for the specific cases of I-girders in shear stiffened by closed trapezoidal stiffeners. Indeed, especially for non-rigid end-post situations, the results provided by the application of Eurocode 3 Part 1.5 rules exhibit over-conservative design that could be improved. This may be due to the quite stiff shape of the trapezoidal stiffener since results for open stiffener also lead to the same conclusion.

In addition, it is shown that the possibility offered by the code to calculate separately (i.e. from numerical sources) the critical plate buckling stresses lead to more satisfactory results, for all cases involving longitudinal stiffeners.

Several possibilities for improvement in this way are actually under development, and are planned to be achieved within the end of the “ComBri” project.

## ACKNOWLEDGEMENTS

The authors deeply acknowledge the Research Fund for Coal and Steel (RFCS) of the European Union for their financial support.

## REFERENCES

[1] ComBri 2004 – 2006, RFCS Contract n RFS-CR-03018 "ComBri", Technical Reports n 4-5-6, 2004-2006.

[2] Eurocode 3 Part 1.5 2004, prEN1993-1-5: Design of Steel Structures – Plated Structural Elements, 2004.

[3] Naumes, J., Oppe, M., "ComBri" Competitive Steel and Composite Bridges by Improved Steel Plated Structures. Test Report – Shear Buckling Tests. RWTH Aachen, 2006.

[4] Boissonnade, N., Degée, H., "ComBri" Competitive Steel and Composite Bridges by Improved Steel Plated Structures. Background Document to Work Package 1.2 – Numerical and Code Aspects, University of Liège, 2006.

[5] Pavlovcic L., Seitz M., Detzel A., Kuhlmann U., Beg D., "Report on Tests and FE Study on Longitudinally Stiffened Web of Plate Girders in Shear", Institut für Konstruktion und Entwurf, Stahl- Holz- und Verbundbau, Universität Stuttgart, 2003.

[6] Pavlovcic L., Detzel A., Kuhlmann U., Beg D., "Shear Resistance of Longitudinally Stiffened Panels – Part 1: Tests and Numerical Analysis of Imperfections, Journal of Constructional Steel Research, March 2007, Vol. 63, Issue 3, pp. 337-350.

[7] Pavlovcic L., Detzel A., Kuhlmann U., Beg D., "Shear Resistance of Longitudinally Stiffened Panels – Part 2: Numerical Parametric Study", Journal of Constructional Steel Research, March 2007, Vol. 63, Issue 3, pp. 351-364.

[8] EBPlate, "Elastic Buckling of Plates", Software Developed by CTICM in the Frame of the ComBri Project, RFCS Contract n RFS-CR-03018, 2006.

[9] Galéa Y., Martin P.O., "Plate Type Behaviour – Use of EBPlate to Calculate $\sigma_{cr,p}$. Working Document", Stuttgart Meeting, December 2005.

# CONCEPTIONS OF EQUIVALENT IMPERFECTIONS IN ANALYSIS OF STEEL FRAMES

A. Machowski[1] and I. Tylek [2,*]
[1]*Assoc. Prof. D. Sc. Ph. D., Faculty of Civil Engineering, Cracow University of Technology, ul. Warszawska 24, 31-155 Cracow, Poland*
[2] *M. Sc , Faculty of Civil Engineering, Cracow University of Technology, ul. Warszawska 24, 31-155 Cracow, Poland*
[*]*(Corresponding author: E-mail: ik2@poczta.fm)*

*Received: 17 October 2006; Revised: 2 May 2007; Accepted: 22 June 2007*

**ABSTRACT:** Bases of four different conceptions of the equivalent initial tilt utilized in elastic and post-elastic analyses of steel frames are under consideration. It turns out that conception and value of equivalent initial tilt depend on method of analysis and limit state conception. Reduction of initial tilt depending on number of columns per story is motivated if statistically based stationary gaussian random noise model of initial column tilt and bar-disk mechanical model of skeletal structure are applied.

**Keywords:** Steel frames, equivalent imperfection

## 1. INTRODUCTION

Formulas for initial frame tilt recommended by different normalization commissions and individual authors have similar multiplicative form

$$\phi_0 = \phi_0^{(1)} \cdot k_c(m) \cdot k_s(n). \tag{1}$$

However these formulas have very different coefficients: $k_c(m) \le 1$ and $k_s(n) \le 1$, depending on number of columns on story $m$ and number of stories $n$ applied for reduction of basic value of equivalent single story column tilt $\phi_0^{(1)}$ (usually $\phi_0^{(1)} = 1/200$).

Application of the equivalent initial tilt in steel frames analysis for the first time has been recommended in ECCS [1] Specifications – without reduction (Figure 1) of basic value $\phi_0^{(1)}$ ($k_c = k_s = 1$).

| No. | Source | $k_c(m)$ | $k_s(n)$ |
|---|---|---|---|
| 1 | ECCS [1] | 1,0 | 1,00 |
| 2 | ECCS [2] | $\frac{1}{2}\cdot\left(1+\frac{1}{m}\right)$ | 1,00 |
| 3 | PKNMiJ [3] | $\frac{1}{2}\cdot\left(1+\frac{1}{\sqrt{m}}\right)$ | $\sqrt{\frac{5}{h}} \le 1$ |
| 4 | CEN [4] | $\sqrt{0{,}5+\frac{1}{m}} \le 1$ | $\sqrt{0{,}2+\frac{1}{n}} \le 1$ |
| 5 | Beaulieu & Adams [5] | $m^{-0.455}$ | 1,00 |

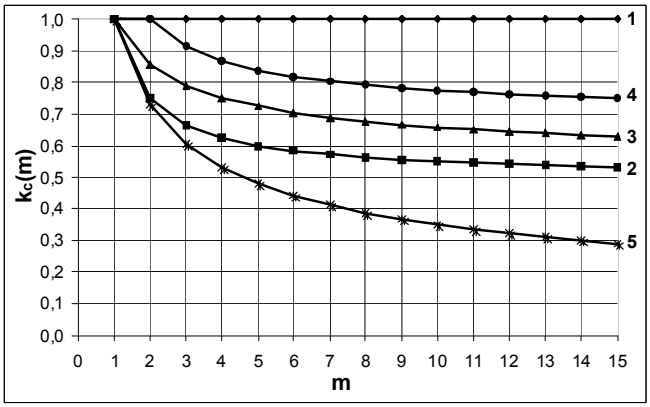


Figure 1. Comparison of Different Reduction Coefficients $k_c(m)$ and $k_s(n)$ or $k_s(h)$; $h$ – Frame Height

The smallest values of the reduction factor $k_c(m)$ have been proposed by Beaulieu and Adams (Beaulieu and Adams [5]), however they assume $k_s(n) \equiv 1$. In the paper mentioned above a letter $m$ denotes the number of columns on building story as a whole (not in single planar frame) – in contrast with other recommendations. Three factors in formula (1) are not yet satisfactorily justified. They are associated with steel frame erection tolerances and results of statistical analysis of post-erection column out-of-plumb measurements.

Applications of conclusions obtained from statistical analysis of column out-of-plumbs have been proposed among others by: Beaulieu and Adams (Beaulieu and Adams [5]) and Machowski (Machowski [6]). From theoretical analysis of the equivalent initial tilt problem utilizing statistically based initial column out-of-plumb model (Machowski [6], Machowski and Tylek [7]) follows that application of reduction coefficient $k_s(n) < 1$ is not justified in general case of multistory frame analysis. However, applying other conceptions of equivalent initial tilt, some reduction coefficient $k_s(n)$ is justified, what is shown below.

## 2. STATISTICALLY BASED INITIAL COLUMN TILT

Column out-of-plumbs are related to orthogonal Cartesian coordinates system with axes parallel to structural system axes ($i$, $j$, $k$) with $z$ axis oriented vertically and $x$ axis oriented along the building. With regards to statistical analysis it was more convenient to introduce initial tilt (interstory drift to story height ratio) as non-dimensional out-of-plumbness measure instead of horizontal deviations of column nodes. Definition of column $i$-th story initial tilts: $\phi_i^x$ and $\phi_i^y$ is illustrated in Figure 2.

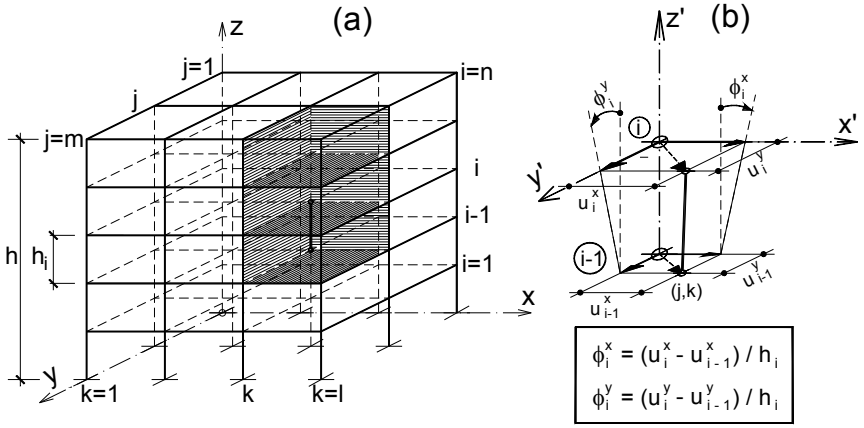


Figure 2. Elements of Columns Initial Tilt Matrix Definition

Horizontal deviations of column nodes from vertical lines, driven from central points of column bottom cross-sections: $u_i^x$, $u_i^y$, $u_{i-1}^x$, $u_{i-1}^y$ – respectively, are measured after all frame erection and after construction of all floors (post-fabrication measurements).

Statistical analysis of initial tilt measurements (Machowski [6], [8]) showed that mathematical model of stationary gaussian random noise $\phi_{ijk}^x$ and $\phi_{ijk}^y$ (stationary random series with mean value $E\{\phi\} = 0$ and constant variance $D_\phi = \sigma_\phi^2 = \text{const.}$) is justified if empirical variance fulfils a constraint

$$D_\phi = \sigma_\phi^2 \le 3(‰)^2 . \tag{2}$$

The second conclusion of this analysis was that exist only weak autocorrelation dependence between tilts of columns in the same vertical planar frames and lack of correlation between any other tilts. Proposed estimations of correlation coefficients extreme values are shown in Figure 3.

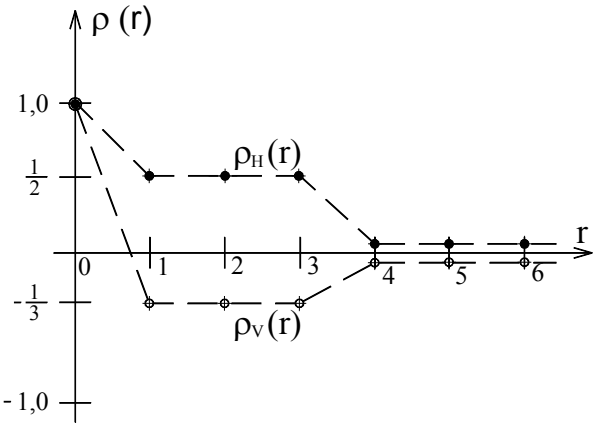


Figure 3. Assessment of Autocorrelation Dependences in Random Series of Initial Tilts ($\rho_H(r)$ – Autocorrelation in Horizontal Series, $\rho_V(r)$ – Autocorrelation in Vertical Series)

For upper value of initial tilts according to Eq. 2 we obtain, in case of normal distribution, for allowable defectiveness $w$ = 5% limit of tolerance applied in reception of structure

$$\phi^t = 1{,}96 \cdot \sigma_\phi = 1{,}96 \cdot \sqrt{3}‰ \cong 1/295 \cong 1/300 . \tag{3}$$

The equivalent value of initial tilt from standard recommendation $\phi_z$ = 1/200 = 5 ‰ has been justified in (Machowski [6]) as characteristic value of random variable which replace: initial column out-of-plumb, eccentricity in column splice and residual stresses. Respective value of variance $\sigma^2_{\phi z} = (1/200 / 1{,}96)^2 \cong (2{,}5\ ‰)^2 \cong 6\ (‰)^2$.

## 3. EQUIVALENT INITIAL TILT IN ELASTIC analysis

Determination of substitute random initial tilt for *i*-th story of building as a whole is the first step to determination of the equivalent initial tilt for all building.

Post erectional column out-of-plumbs cause additional bending moments $\underline{M}^{\phi x}$ and $\underline{M}^{\phi y}$ from vertical load for frame as vertical cantilever. A sequence of these cumulative moments $\underline{M}_i^{\phi}$ for *i*-th story and selective direction of initial tilt (*x* or *y*) may be written in following form

$$\underline{M}_i^{\phi} = \underline{M}_{i+1}^{\phi} + \Delta\underline{M}_i^{\phi}, \tag{4}$$

(random values are underlined)

For bar-disk analytical scheme (Machowski and Tylek [9]) of multistory skeletal structure (Figure 4) with rigid floor-disks effective initial random tilt for *i*-th story of building $\underline{\phi}_i^{eff}$ may follow from conservation of global moment increment condition (if torsional effect for building as vertical cantilever is neglected)

$$\Delta \underline{M}_i^{\phi} = \sum_{p=1}^{s} P_{ip} \cdot h_i \cdot \underline{\phi}_{ip} = P_i \cdot h_i \cdot \underline{\phi}_i^{eff} , \tag{5}$$

where: $P_i = \Sigma P_{ip}$, ($p = 1 \ldots s.$) - sum of all vertical loads acting on building above $i$-th story,
$P_{ip}$ (for $s$ columns $p = 1, 2, \ldots, s.$ on $i$-th story of building) – sum of vertical loads above $i$-th story in $p$-th column.

From Eq. 5

$$\underline{\phi}_i^{eff} = \sum_{p=1}^{s} w_{ip} \cdot \underline{\phi}_{ip} = \mathbf{w}_i \, \boldsymbol{\phi}_i^{\mathrm{T}} . \tag{6}$$

Random tilt $\underline{\phi}_i^{eff}$ is therefore a linear transformation of finite discrete gaussian noise $\boldsymbol{\phi}_i = [\underline{\phi}_{i1} \ldots \underline{\phi}_{ip} \ldots \underline{\phi}_{is}]$ with deterministic weight-vector $\mathbf{w}_i = [w_{i1} \ldots w_{ip} \ldots w_{is}]$, where weights $w_{ip} = P_{ip}/P_i$ fulfil normalization condition $\Sigma w_{ip} = 1$, ($p = 1 \ldots s.$), is normal random variable with parameters:

$$\mathrm{E}\left\{\underline{\phi}_i^{eff}\right\} = 0, \quad \sigma_{\phi \mathrm{i}}^2 = k_{c,i}^2 \cdot \sigma_{\phi}^2 , \tag{7}$$

where:

$$k_{c,i}^2 = \mathbf{w}_i \boldsymbol{\rho}_s \mathbf{w}_i^{\mathrm{T}} = \sum_{p=1}^{s} w_{ip} \cdot \sum_{q=1}^{s} w_{iq} \cdot \rho_{pq} . \tag{8}$$

A right side of expression Eq. 8 is positively defined quadratic form of $s$-variable: $w_{i1}, \ldots, w_{ip}, \ldots w_{is}$. with symmetric matrix of coefficients $\boldsymbol{\rho}_s$ equal to normalized correlation matrix $\boldsymbol{\rho}_s$ of random vector $\boldsymbol{\phi}_i$. Values of reduction coefficient $k_{c,i}$ according to Eq. 8 have been analysed in detail in (Machowski [6]) considering statistically based correlation matrix $\boldsymbol{\rho}_s$ and realistic range of weight-vector $\mathbf{w}_i$ configurations.

Safe approximation of effective random initial tilt for frame as a whole may be defined as follows

$$\underline{\phi}^{EFF} = \max_{i=1}^{n} \left| \underline{\phi}_i^{EFF} \right| , \tag{9}$$

where:

$$\underline{\phi}_i^{EFF} = \sum_{t=i}^{n} V_t \cdot \sum_{q=i}^{t} h_q \cdot \underline{\phi}_q^{eff} \cdot \left( \sum_{t=i}^{n} V_t \cdot \sum_{q=i}^{t} h_q \right)^{-1} \tag{10}$$

– effective random initial tilt for frame as a whole, which guarantee safe estimation of additional bending moment $\underline{M}_i^{\phi}$ for $i$-th story of frame as vertical cantilever,
$\underline{\phi}_i^{eff}$ – according to Eq. 6,

$V_t$ – sum of vertical loads imposed immediately to $t$-th story.

The particular analysis of Eq. 9 and mentioned below numerical analysis has been made in (Machowski [6]).

The numerically determined: probability density function f($\xi$) and distribution function F($\xi$), for effective frame initial tilt $\underline{\xi} = \left| \underline{\phi}^{\mathrm{EFF}} \right|$, are showed in Figure 5.

The half-normal probability distribution of $\underline{\xi}$ for $n = 1$ is assumed (Machowski [6]). Top quantiles of $\underline{\xi}$ (for example associated with value $F(\underline{\xi}) = 0{,}95$) are almost independent on the number of stories (Figure 5). Therefore reduction of initial tilt standard deviation and characteristic value depending on story number $n$ is unfounded – in contrast to reduction depending on number of columns per story $m$.

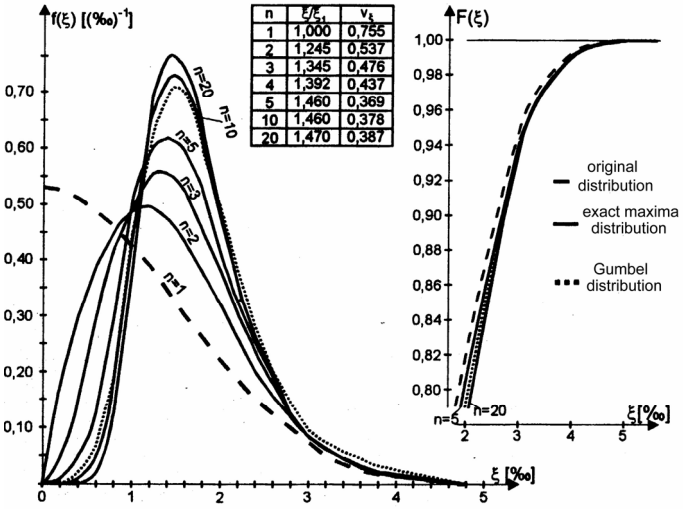


| n | $\xi_n/\xi_1$ | $v_\xi$ |
|---|---|---|
| 1 | 1,000 | 0,755 |
| 2 | 1,245 | 0,537 |
| 3 | 1,345 | 0,476 |
| 4 | 1,392 | 0,437 |
| 5 | 1,460 | 0,369 |
| 10 | 1,460 | 0,378 |
| 20 | 1,470 | 0,387 |

Figure 5. Comparison of Numerical Results for Equivalent Random initial Tilt of Frame as a Whole $\underline{\xi} = \left| \underline{\phi}^{\mathrm{EFF}} \right|$ ($n$ – Number of Stories)

Mentioned above conception of global effects of imperfection load conservation, independent on frame behaviour (elastic or post-elastic), may be replaced by conception of local effects of imperfection load conservation (i.e. in beam-column element of the skeleton). Using simplyfied linear beam-column resistance formula (Machowski [6])

$$\Delta S = \left|\Delta N\right| + 0{,}9 \cdot \varphi_y \cdot \left|\Delta M_y\right| / r_y = \left|\Delta N\right| + b \cdot \left|\Delta M_y\right|, \tag{11}$$

where: $r_y = W_y/A$.

The absolute value of equivalent initial tilt of frame as a whole is obtained from condition of local effect $\Delta S$ Eq. 11 conservation

$$\underline{\phi}^{EFF} \cong \left( \left| \sum_{i=1}^{n} a_{N,i} \cdot \underline{\phi}_i^{eff} \right| + b \cdot \left| \sum_{i=1}^{n} a_{M,i} \cdot \underline{\phi}_i^{eff} \right| \right) \Big/ \left( \left| \sum_{i=1}^{n} a_{N,i} \right| + b \cdot \left| \sum_{i=1}^{n} a_{M,i} \right| \right), \tag{12}$$

where: $a_{N,i}$ ; $a_{M,i}$ - coefficients of equivalent initial tilt of $i$-th story $\underline{\phi}_i^{eff}$ influence on axial force and bending moment, adequately, in selected element of the frame.

This conception was analysed on the example of the 5-story building B1 (Figure 6).

Building B1 has been designed according to the Polish Standard (PKNMiJ [3]) considering Polish load conditions. In this building five transversal steel rigid frames are braced by three longitudinal

two-bay rigid frames, building has rigid in own plane reinforced concrete floors and light-weight curtain walls.

Tilt in *x* axis direction of longitudinal frame in axis C-C was under consideration.

Substituting to Eq. 12 $a_{N,i}$, $a_{M,i}$ and $b$ for the exterior column of the first floor of analysed frame and neglecting values of $a_{N,i}$ much smaller than $b \cdot a_{M,i}$, coefficient for conversion of variance of equivalent initial tilt of *i*-th floor $\sigma^2\{\phi_i^{eff}\}$ on variance of equivalent initial tilt of whole building $\sigma^2\{\phi^{EFF}\}$ is obtained

$$k_s^2 \cong \left|\sum_{i=1}^{5} a_{M,i}^2\right| \Big/ \left|\sum_{i=1}^{5} a_{M,i}\right|^2 . \tag{13}$$

Taking into consideration negative autocorrelation of $\phi_i^{eff}$ (in the plumb-line), reduction coefficient $k_s$ in analysed case is, according to Eq. 13, equal to 0,894. If this autocorrelation is passed over reduction coefficient $k_s$ obtained a little larger value ($k_s$ = 0,907).

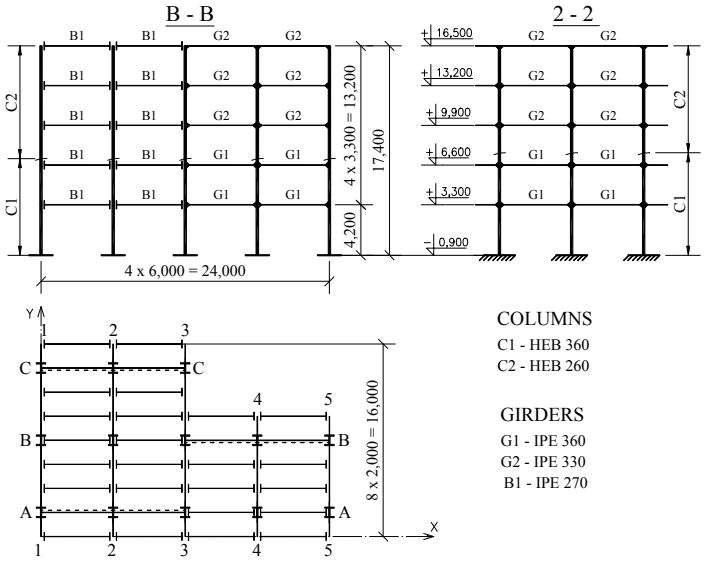


Figure 6. Analysed Skeletal Framed Steel Structure – Building B1 (5-Story)

## 4. SUBSTITUTE INITIAL TILT IN POST-ELASTIC ANALYSIS

Safe conception Eq. 9 of effective random initial tilt of frame, may be replaced by conditions of strength of frame (rigid-plastic or elastic-plastic) conservation.

To analyse conception of frame strength conservation four skeletal steel framed structures of multistory buildings were chosen (Figure 6 – 9). Structures were analysed in post-elastic range with application of bar-disk analytical scheme (Machowski and Tylek [9]) neglecting torsional effects for building as vertical cantilever.

Tilt of transversal rigid frame in axis 4-4 is analysed in building B2 (Figure 7). This is the 9-story framed structure with 8 transversal carrying frames braced by 9 one-bay longitudinal rigid frames.

16-story structure of building B3 (Figure 8) consist of 9 transversal carrying frames braced by 4 vertical trusses in longitudinal direction. Tilt of transversal frame in axis 5-5 is under consideration. Carrying system of 24-story building B-4 (Figure 9) has 4 transversal and 4 longitudinal steel rigid frames. Tilt of frame in axis 3-3 is analysed.

All skeletal structures under consideration have been designed according to the Polish Standard (PKNMiJ [3]) considering Polish load conditions. Buildings have rigid in own plane reinforced concrete floors and light-weight curtain walls.

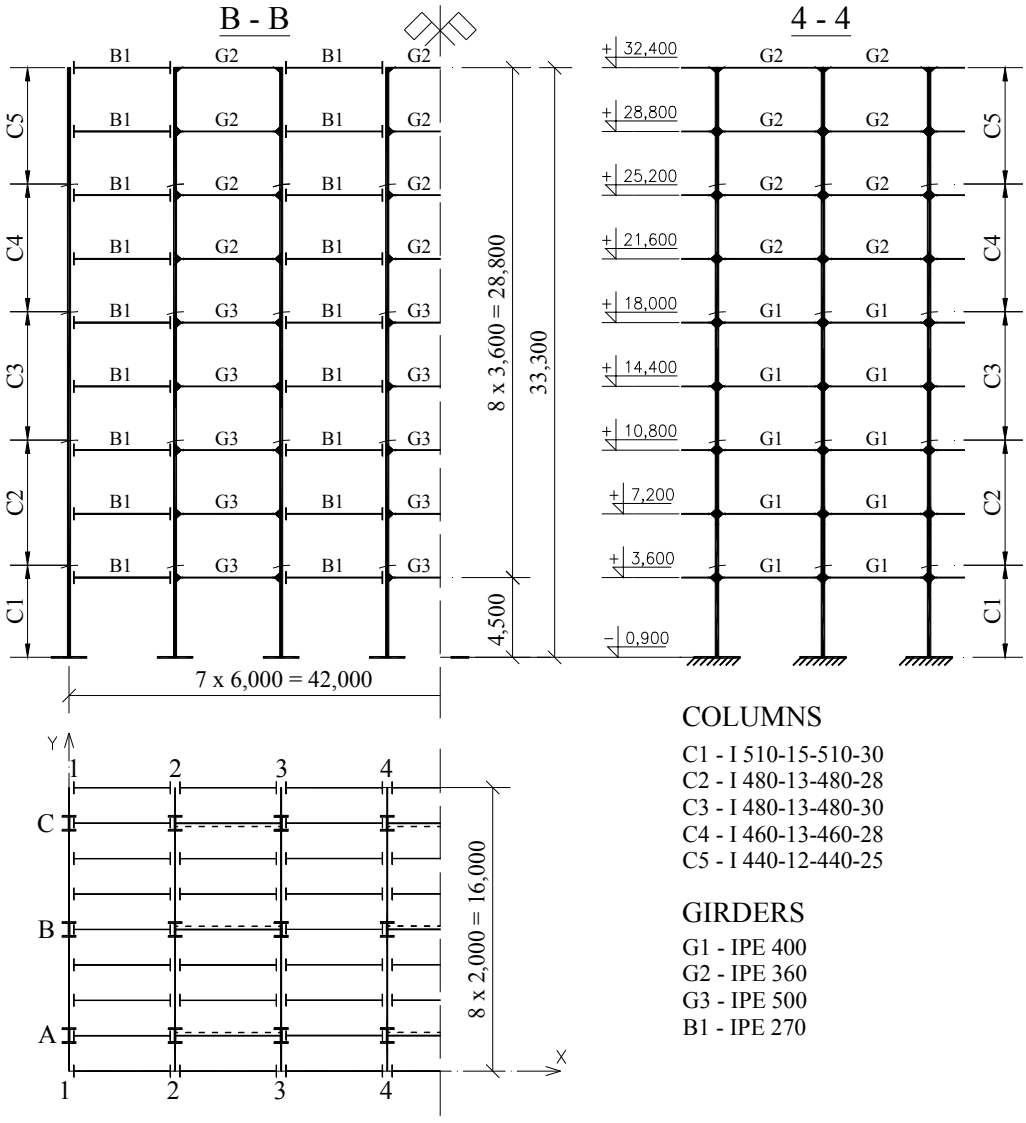


Figure 7. Analysed Skeletal Framed Steel Structure – Building B2 (9-Story)

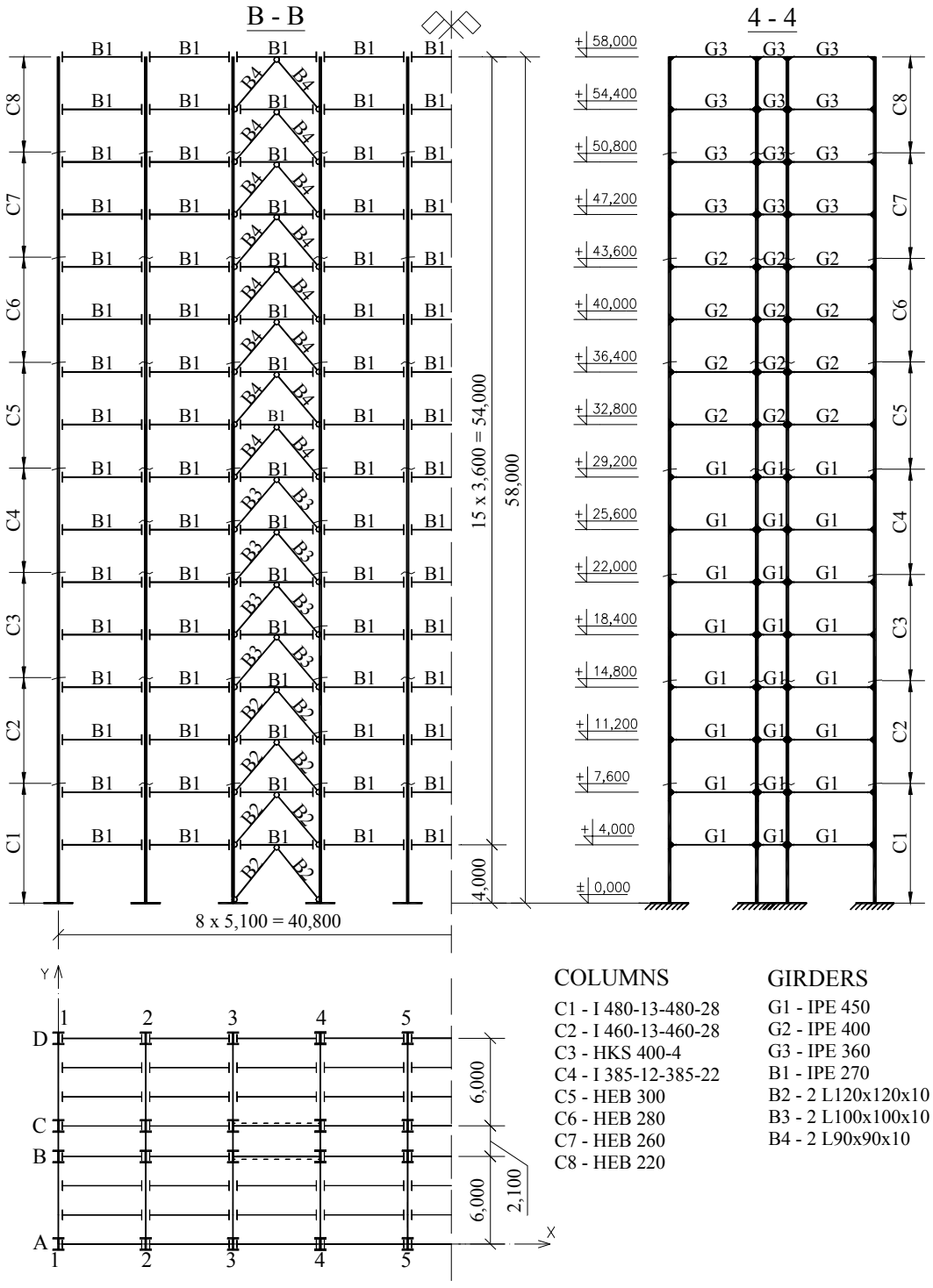


Figure 8. Analysed Skeletal Framed Steel Structure – Building B3 (16-Story)

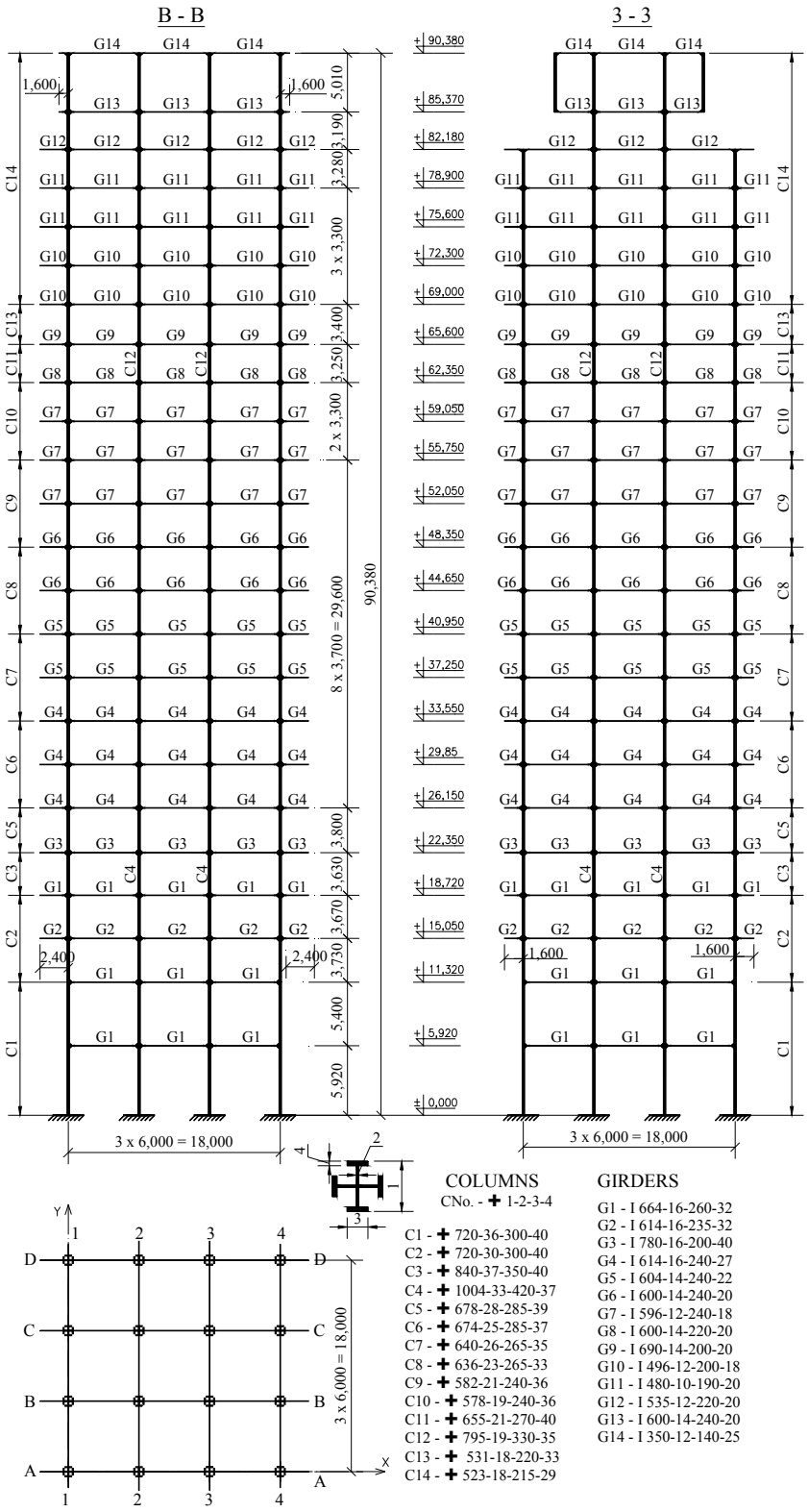


Figure 9. Analysed Skeletal Framed Steel Structure – Building B4 (24-Story)

In order to establish effective initial tilt two conceptions of frame strength conservation may be applied:

(A) conservation of power dissipated in plastic flow mechanism of complete solution and
(B) conservation of limit strength value associated with limit point *G* on frame equilibrium path.

According to ECCS recommendation (ECCS 1985) simple conception (A) is only valid if condition of "strong columns" (columns which remain elastic up to plastic mechanism formation) is fulfilled. Beams are designed in the first step (according to plastic mechanism) and next elastic columns are selected with application of equilibrium conditions.

Finally checking according to Merchant-Wood interaction formula is accomplished.

This design procedure is applied especially if seismic or other extraordinary loads are under consideration.

If random vector of initial effective story tilts ($\underline{\phi}_I \equiv \underline{\phi}_i^{eff}$ – according to Eq. 6) is replaced by a set of couples of forces $P_i \cdot \underline{\phi}_i$, according to Figure 10, then plastic mechanism with straight rigid columns and plastic hinges in beams may be under consideration. Conservation of dissipated power condition may be recorded in form (Figure 10)

$$\dot{\omega} \cdot \sum_{i=1}^{n} P_i \cdot h_i \cdot \underline{\phi}_i = \dot{\omega} \cdot \underline{\phi}^{EFF} \cdot \sum_{i=1}^{n} P_i \cdot h_i , \tag{14}$$

where $P_i$ – as in Eq. 5,
from here effective initial tilt for frame as a whole may be expressed as linear transformation of vector of effective story tilts

$$\underline{\phi}^{EFF} = \sum_{i=1}^{n} d_i \cdot \underline{\phi}_i , \tag{15}$$

where: $d_i = P_i \cdot h_i \Big/ \sum_{i=1}^{n} P_i \cdot h_i$, $\sum_{i=1}^{n} d_i = 1$.

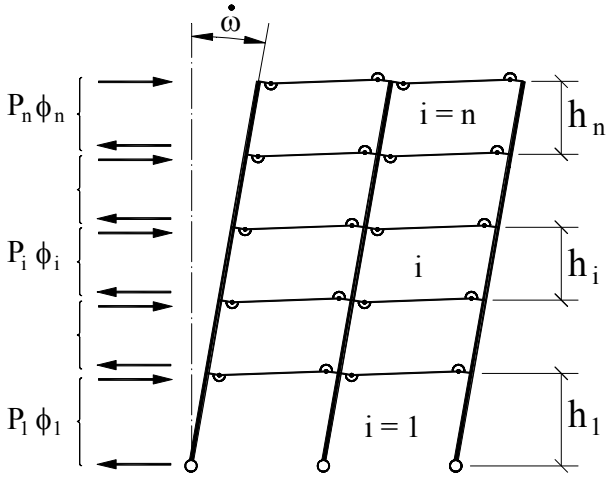


Figure 10. Collapse Mechanism of Frame with Strong (Rigid) Columns and Couples of Forces Replacing Random Initial Tilts of Stories

Reduction coefficients $k_s(n) = \sigma_{\phi EFF} / \sigma_{\phi i}$ – obtained according to Eq. 15 for buildings B1 – B4 are compared in Figure 13 with other results.

Application of conception (B) (conservation of limit strength of frame value) to frames B1 – B4 requires appropriate computer application program. Program ANSYS has been utilized in order to obtain frame limit strength corresponding to limit point on equilibrium path (limit value of vertical load on frame $V_R$ corresponding to limit point on equilibrium path $G$ in Figure 11).

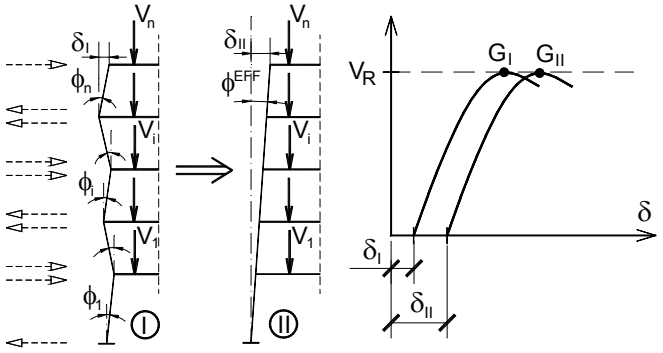


Figure 11. Sequence of Story Initial tilts, Effective Frame Initial Tilt $\phi^{EFF}$, Respective Couples of Forces and Equilibrium Paths

Elastic-plastic model of material with strain hardening coefficient (1/10000) $E$ ($E$ = 205 GPa) has been assumed. Post-limit (descending) part of equilibrium path has been obtained thanks to consideration of extended system of equations with nonlinear constraints equation (Crisfield's equation).

According to applied simulation procedure; for every realization of random effective story initial tilts sequence: $\underline{\phi}_1,\ldots,\underline{\phi}_i,\ldots,\underline{\phi}_n$. respective frame equilibrium path (Figure. 11) has been determined. A concept of couples of forces replacing initial tilt of story is utilized. Next the effective initial tilt of frame as a whole $\underline{\phi}^{EFF}$ has been chosen in agreement with condition $V_R(G_I) = V_R(G_{II})$ (Figure 11).

The results of calculations for building B2, as an example, are shown in Figure 12. According to results of statistical tests probability distribution of effective frame initial tilt $\underline{\phi}^{EFF}$ may be approximated by normal distribution.

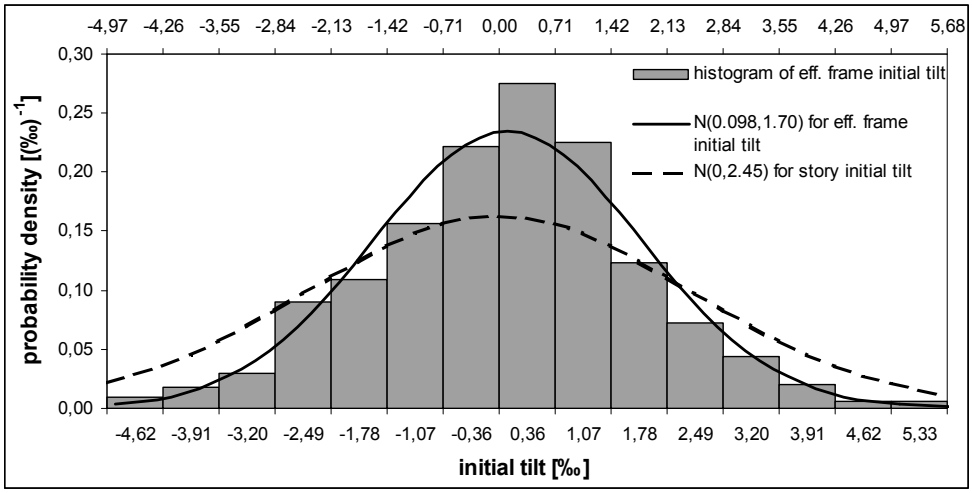


Figure 12. The example (building B2) of comparison story initial tilt and effective frame initial tilt $\underline{\phi}^{EFF}$ probability distribution

Numerical results obtained for elastic and post-elastic analysis are compared with different codified recommendations for coefficient of reduction $k_s(n)$ in Figure 13.

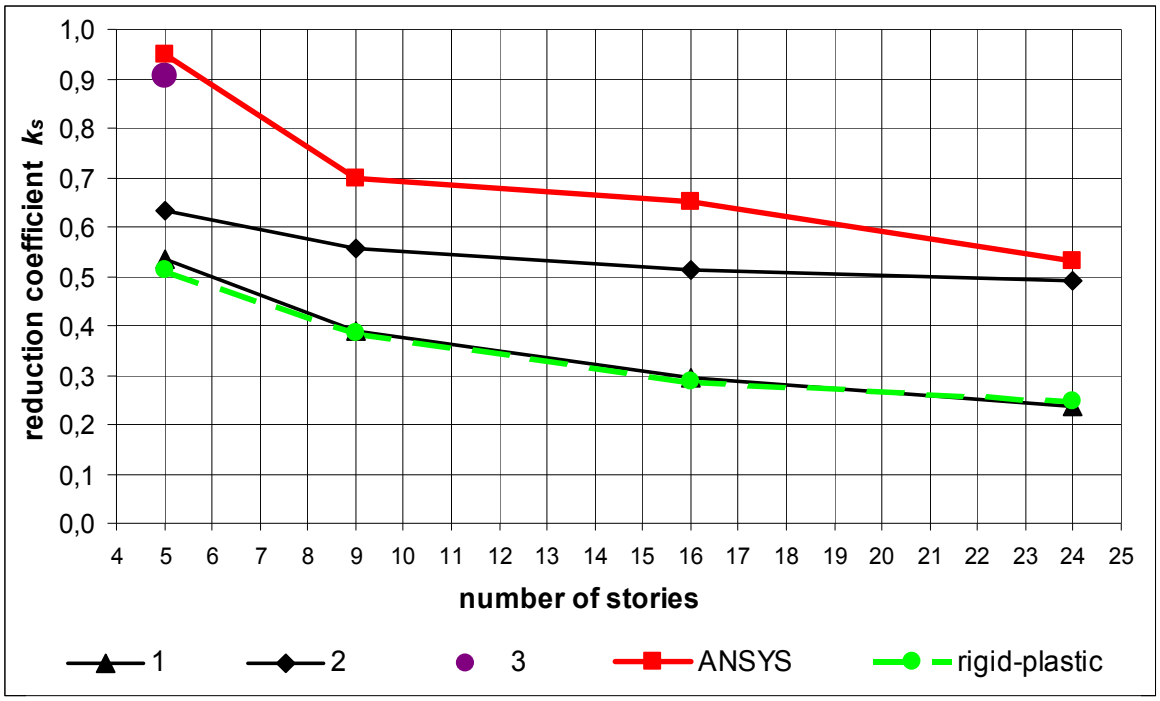


Figure 13. Comparison of Numerical Results and Reduction Coefficient $k_s(n)$ According to Different Suggestions (1: $k_s = \sqrt{5/h}$, $h$ – height of the building , 2: $k_s = \sqrt{0{,}2 + 1/n}$, $n$ – number of stories ,3: $k_s$ according to (I) conception)

## 5. CONCLUDING REMARKS

Main conclusion of conducted analysis may be formulated as follows: equivalent geometrical imperfection strongly depends on assumed ultimate limit state definition and method of analysis (elastic or post-elastic) so uniform formulae given in standards are questionable and are criticized in this article.

Reduction of the substitute initial tilt of steel frame depending on number of columns per story is sufficiently motivated if conception of bar-disk scheme and conservation of story moment conditions are accepted. This reduction may be applied in the same manner in elastic and post-elastic analysis.

A safe reduction of global imperfection depending on number of story is unjustified in general case. Some reduction of the equivalent initial tilt depending on number of stories is motivated if one of the following conceptions is applied: (I) imperfection load local effect conservation (in elastic analysis), conservation of limit strength (II) or dissipated power (III) (in post-elastic frame analysis). Values of reduction coefficient $k_s(n)$ determined for the same building according to these three conceptions differ from each other (i.e. for building B1 $k_s(n)$ = 0,907 according to (I), $k_s(n)$ = 0,944 according to (II) and $k_s(n)$ = 0,494 according to (III)), what shows that standard recommendations for reduction factor $k_s(n)$ are unconservative in general case. It also indicate need of diversity of equivalent initial tilt value depending on type of analysis (elastic or elastic-plastic) and on conception of limit state (i.e. limit strength value associated with limit point on frame equilibrium path).

## REFERENCES

[1] ECCS 1974, European Specifications for Steel Structures, 1st Ed., 1974.
[2] ECCS 1984, Eurocode 3, Design of Steel Structures, 1984.
[3] PKNMiJ 1990, PN-90/B-03200, Steel Structures, Design Rules (in Polish), 1990.
[4] CEN 1990, CEN/TC 250, Eurocode 3: Design of Steel Structures, Part 1.1. General Rules and Rules for Buildings, 1990.
[5] Beaulieu, D. and Adams, P.F.,. "Significance of Structural Out-of-plumb Forces and Recommendations for Design", Canadian Journal of Civil Engineering, 1980, Vol. 7, pp.105-113.
[6] Machowski, A., "Problems of Limit States and Reliability of Steel Multistory Building Frames" (in Polish), Politechnika Krakowska, Monografia 262, Seria Inżynieria Lądowa, 1999.
[7] Machowski, A. and Tylek, I., "The Equivalent Imperfection Concepts of Steel Frame" (in Polish), L Konferencja KILiW PAN i KN PZiTB Krynica 2004a, Tom II, pp. 269-276.
[8] Machowski, A., "Initial Random Out-of-plumbs of Steel Frame Columns", Archives of Civil Engineering, 2002, XLVIII, Vol. 2, pp. 205-226.
[9] Machowski, A. and Tylek, I., "Application of bar-disk Systems in Analysis of Steel Frames" (in Polish), Czasopismo Techniczne, Politechnika Krakowska, 2004b, Budownictwo, Zeszyt Vol. 11, pp. 59-80.

# SEISMIC UPGRADING OF EXISTING RC BUILDINGS BY SLENDER STEEL SHEAR PANELS: A FULL-SCALE EXPERIMENTAL INVESTIGATION

A. Formisano[1], G. De Matteis[2,*] S. Panico[3] and F. M. Mazzolani[4]

[1] *PhD, Department of Structural Engineering, University of Naples "Federico II", Naples, Italy*
[2] *Associate Professor, Department of Design, Rehabilitation and Control of Architectural Structures, University of Chieti/Pescara "G. d'Annunzio", Pescara, Italy*
[3] *PhD, Department of Structural Engineering, University of Naples "Federico II", Naples, Italy*
[4] *Full Professor, Department of Structural Engineering, University of Naples "Federico II", Naples, Italy*
** (Corresponding author: E-mail: dematteі@unina.it)*

*Received: 27 November 2006; Revised: 2 May 2007; Accepted: 22 June 2007*

**ABSTRACT:** In the present paper the seismic upgrading of an existing RC structure by using slender steel shear panels is examined. Based on a preliminarily experimental evaluation of the performance of the bare RC structure, an *ad hoc* design procedure has been developed in the framework of the performance based design methodology. The applied device, whose configuration has been defined also according to both simplified and refined numerical analyses, is able to significantly enhance both the strength and the stiffness of the primary structure. It has been installed within a reaction steel frame, positioned into the bare RC structure, which is composed by members designed in order to remain in elastic regimen under the tension field action developed by plates. Since the original RC module was not able to withstand significant values of horizontal forces, the reinforcing of both the first level beam and the foundation beam by means of coupled channel steel profiles and threaded bars has been done. Finally, in order to assess the reliability of the proposed intervention, a full scale cyclic experimental test has been performed on the upgraded structure, confirming the effectiveness of the adopted technique as well as the validity of the proposed design procedure.

**Keywords:** Slender steel shear panels, seismic upgrading, GLD building, experimental test, tension field mechanism, plate buckling

## 1. INTRODUCTION

In the framework of new seismic design approaches for upgrading existing reinforced concrete buildings, the development of innovative intervention techniques, based on either the reinforcement of existing structural elements or the introduction of new resisting systems, the metal-based technology approach can be considered very profitable [1]. Such a technique is founded on the energy dissipation capacity of special metallic devices able to achieve or improve the structural safety of the original structure under seismic actions.

Within this category, the solution based on using metal shear panels can result particularly effective, due to the limited weight, the reduced volume obstruction, the easy insertion and the meaningful structural contribution offered by the applied devices in terms of strength, stiffness and ductility. In addition, it is important to observe that the self-weight of steel panels is rather low, if compared with the one of a reinforced concrete shear wall, determining in this way a reduction of gravitational loads and therefore of seismic actions transmitted to the foundation.

Nowadays, metal shear panels adopted in seismic applications can be subdivided in two main behavioural classes: 1) the so-called "compact" panels, mainly made of low strength metallic materials (LYS steel or pure aluminium) and properly stiffened in order to avoid elastic shear buckling phenomena, which have been recently proposed for high steel buildings and also for reinforcement of RC buildings [2]; 2) the "slender" shear panels, made of thin steel plates, which have been widely studied and applied both in North America and in Japan mainly for applications

into new buildings [3]. In particular, the latter typology can be effectively used in case of primary structures characterized by limited lateral stiffness and reduced over-strength. In fact, slender shear panels may behave as stiffening devices also, rather than as hysteretic dampers only. As a consequence, the contribution provided by shear panels could significantly reduce the damageability of the primary structure, which is usually a key point in case of old existing structures.

## 2. STEEL PLATE SHEAR WALLS

### 2.1 General

Shear walls realized with either slender or compact shear panels are able to offer significant resistance against seismic actions, conferring high ductility, stable hysteretic characteristics and good initial stiffness to the structure in which they are installed. Besides, they could provide a significant over-strength and also ability to absorb seismic energy input in a wide deformation range. In shear panels the energy dissipation takes place mainly for shear mechanism, by means of either pure shear stress action (Figure 1a) or tension field action (Figure 1b) [4]. In the latter, owing to the high slenderness of the plate, premature shear buckling in the elastic field occurs and the lateral shear forces are carried by means of diagonal tensile stresses developing in the web plates parallel to the directions of the principal stresses. Such a behaviour, which is typical of slender shear panels, produces both a poor dissipative behaviour, with a pronounced slip-type hysteretic response, and a strong flexural interaction with beams and columns of the primary frame. On the other hand, a pure shear dissipative mechanism is of concern for compact shear panels, it allowing both a stable inelastic cyclic behaviour and a uniform yielding spread over the entire plate. In order to have a pure shear dissipative mechanism, shear panels should be designed and ribbed in such a way to avoid any buckling phenomenon up to the required plastic deformation level.

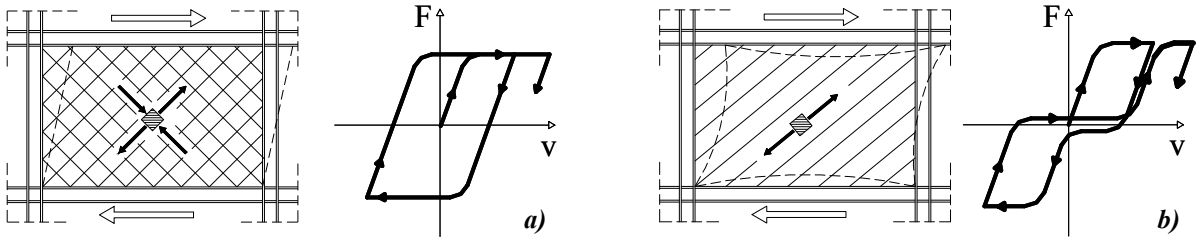


Figure 1. Shear Energy Dissipation Mechanisms: Pure Shear (a) and Tension Field (b)

In addition, shear panels with pure shear mechanism are also able to enhance the energy dissipation capacity of the whole structure, acting as sacrificial devices, absorbing a large amount of seismic input energy and protecting the primary framed structure from relevant structural damages. Therefore, they can act as hysteretic dampers, whose dissipative function is activated by the inter-storey drifts occurring during the deformation of the structure subjected to horizontal actions.

Although characterised by a poor dissipative behaviour, in the present study, the use of shear walls made of slender steel plates for improving the characteristics of strength and stiffness of existing structures is investigated.

## 2.2 Application of Slender Shear Panels

When acting as bracing system, slender steel plate shear walls can be conformed according to two different configurations [5]. The first solution, defined as standard system, is the one in which the connections among members are schematised as pinned joints (Figure 2a): in such a case, which refers typically to steel structures, the only seismic-resistant system is represented by the shear wall, while the remaining part of the structure must be checked in order to carry vertical loads only. Considering that also hinged beam-to-column connections are usually able to absorb some amount of the flexural moment, from 20% to 70% of the plastic moment of the connected beam, the primary structure participates to the absorption of the acting horizontal actions. In this case the members must be opportunely rigid and resistant so that the dissipation mechanism can develop correctly through the whole surface of shear panels: therefore it is necessary that the beams are designed for remaining in the elastic field while the columns do not suffer buckling phenomena.

The second solution, defined as dual system, foresees that the beam-to-column connections are of moment-resisting type (Figure 2b): the reaction frame participates significantly to the absorption of horizontal actions, providing an additional contribution to the lateral resistance given by steel shear walls.

In such a case, which refers to framed (either steel or reinforced concrete) structures, the members have to be checked to support the tension field mechanism produced by the panel, with particular attention to the formation of plastic hinges in the surrounding members. Considering that also the base framed structure participates to the absorption of lateral forces, it should be checked that it is actually able to absorb a part of these actions, which must be determined according to the ratio between the lateral stiffness of the two systems (primary structure and shear wall).

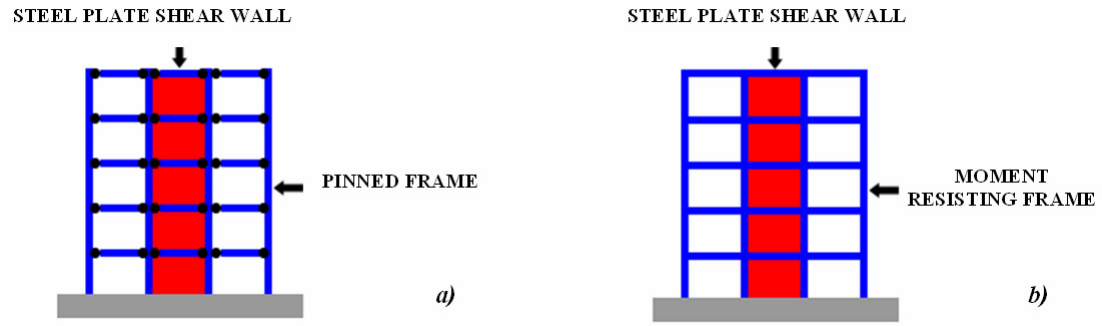


Figure 2. Shear Walls Configurations: a) Standard System; b) Dual System

In such a framework, when framed RC buildings are of concern, metal shear panels should be inserted into a reaction steel frame in order to allow their installation in the primary structure.

The connection between shear panels and the members of the surrounding frame, which can be of simple or moment-resistant type, can be realized by using bolts or by welding the panel to appropriate plates fixed to the beams and columns.

Comparing the current system with the traditional steel stiffening and strengthening techniques (concentric or eccentric bracings), it has to be observed that the former allows to realize easily openings by the insertion of opportune stiffening elements surrounding the opening surface (Figure 3a). Another solution that can be effectively employed for allowing the presence of large openings in steel walls is to use two separate steel shear walls connected among them through the floors beams (Figure 3b).

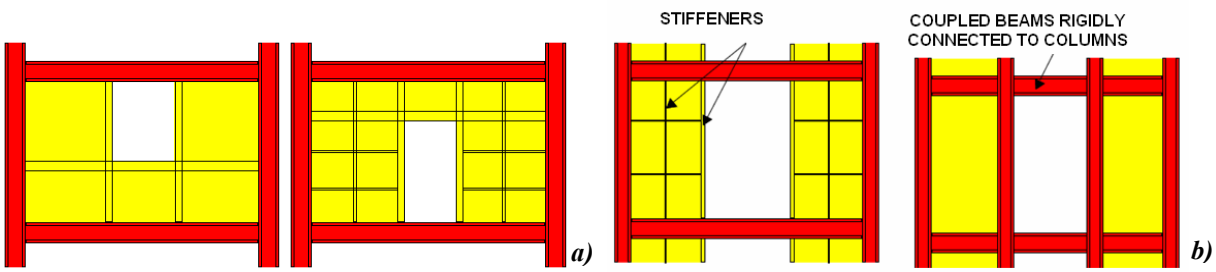


Figure 3. Openings in Simple Steel Plate Shear Walls (a) and Adoption of Coupled Steel Plate Shear Walls (b)

## 3. THE BUILDING UNDER INVESTIGATION

In the field of the seismic retrofitting of existing buildings, the ILVA-IDEM research project (acronym of Intelligent DEMolition) represents an innovative approach aiming at evaluating the effectiveness of different anti-seismic devices based on the use of metallic materials. In particular, the activity foresees the execution of different experimental tests on a reinforced concrete building located in the ex-industrial area ILVA of Bagnoli (Figure 4), located in the suburb of Naples, which is currently interested by a re-qualification process [6]. The building under examination, which has been designed in order to withstand only vertical loads, has rectangular dimensions and is developed on two levels, with not practicable coverage floor.

Figure 4. The Original Building

In order to analyse different retrofitting techniques, the building has been divided into six substructures (modules) by means of cuts performed at the floor levels, removing preliminarily cladding and partition walls (Figure 5).


Figure 5. The Division in Sub-structures (Modules)

In this context, only the employment of shear panels is analysed. In particular, steel shear panels, which are connected with bolted connections to an external reaction steel frame, are longitudinally placed within the RC module identified with number 5 in Figure 5. A general view of both the two levels carpentry and the two orthogonal structural sections of the sub-structure is depicted in Figures 6 and 7, respectively.

The emergent beams, which are placed along the perimeter in longitudinal direction and support a mixed-concrete slab (Figures 8a and b), includes 2ϕ8 on the upper side and 2ϕ10 + 1ϕ12 on the lower one. The strength in transversal direction is supplied by 30x30 cm columns (Figure 8c), having 4ϕ12 longitudinal bars and stirrups ϕ8/30”, connected by the floor slab only.

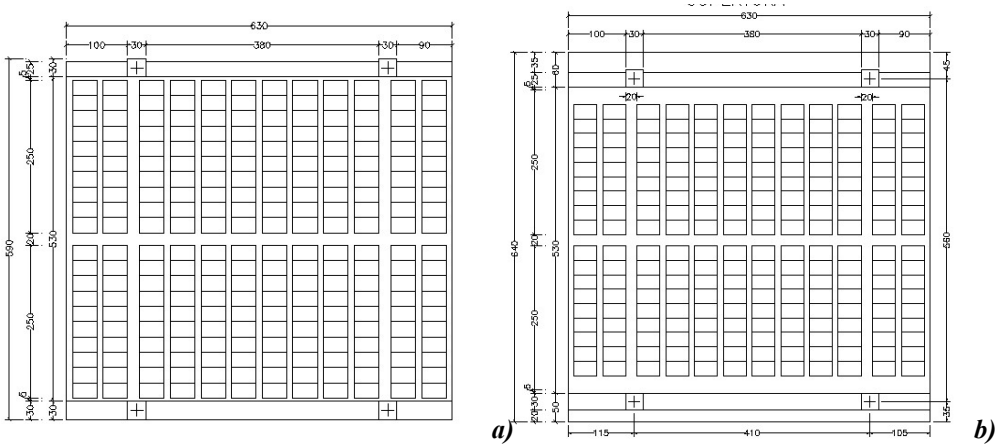


Figure 6. Carpentries of the First (a) and Second Floor (b)

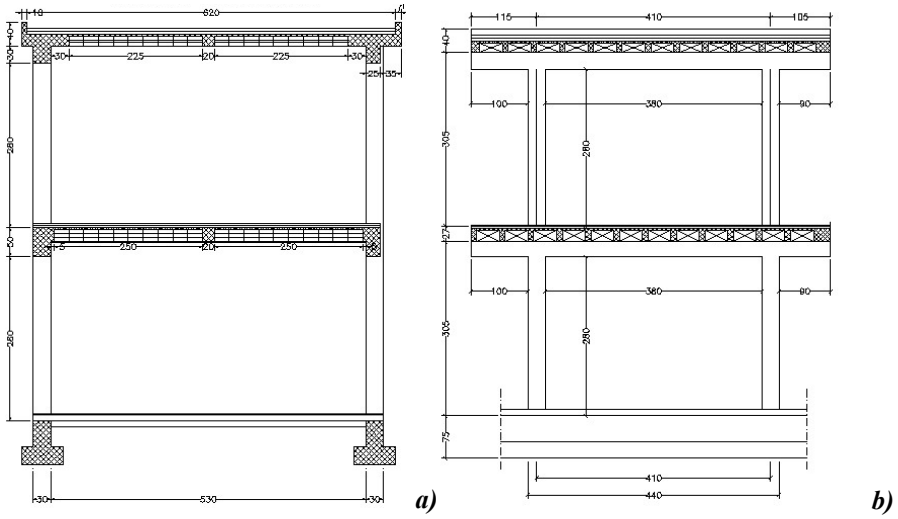


Figure 7. Transversal (a) and Longitudinal (b) Section of the Module Under Study

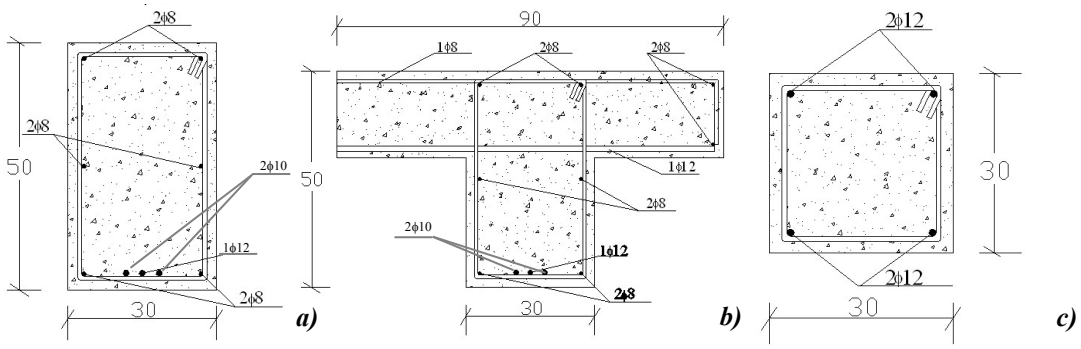


Figure 8. Representative Sections of the Fifth Module:
First (a) and Second (b) Level RC Beam and Column (c)

Aiming at defining the mechanical characteristics of the base materials composing the RC structure, laboratory tests have been carried out at the Department of Structural Engineering of the University of Naples "Federico II" on specimens directly extracted from the structure. Three compression tests (Figure 9) have provided for the concrete an average ultimate strength and Young modulus equal to 20.9 MPa and 17155 MPa, respectively (Table 1). The mechanical properties of the steel bars have been obtained by performing tensile tests, whose results are reported in Table 2.

Figure 9. Compression Test on Concrete Cylindrical Specimen

Table 1. Results of Compression Tests on Concrete Specimens

| Specimen | Unit weight | Elastic modulus | Strength |
|---|---|---|---|
| | [Kg/m$^3$] | [MPa] | [MPa] |
| 1 | 2244 | 18035 | 20.9 |
| 2 | - | 16990 | 21.4 |
| 3 | 2235 | 16442 | 20.3 |
| Average | 2239 | 17155 | 20.9 |

Table 2. Results of Tensile Tests on Steel Bars

| Specimen N. | Diameter [mm] | L [mm] | $N_v$ [kN] | $N_{ult}$ [kN] | $\sigma_{ult}$ [MPa] | $\sigma_v$ [MPa] |
|---|---|---|---|---|---|---|
| 1 | 8 | 1040 | 29.0 | 33.0 | 656.5 | 576.9 |
| 2 | 8 | 975 | - | 41.0 | 815.7 | - |
| 3 | 8 | 500 | 23.1 | 33.4 | 664.5 | 459.6 |
| 4 | 10 | 558 | 39.5 | 59.2 | 753.8 | 502.9 |
| 5 | 10 | 520 | 38.9 | 58.8 | 748.7 | 495.3 |
| 6 | 10 | 485 | - | 62.7 | 798.3 | - |
| 7 | 12 | 850 | 44.1 | 73.8 | 652.5 | 389.9 |
| 8 | 12 | 570 | 53.1 | 82.2 | 726.8 | 469.5 |
| 9 | 12 | 860 | 53.0 | 79.0 | 698.5 | 468.6 |

The selected structural module has been preliminarily tested, without reaching the complete collapse of the system, by means of a pushover test, employing two hydraulic jacks having a capacity of 30 tons (Figure 10).

The test results, reported in terms of Force-Displacement curve of the first storey in Figure 11, provide useful information on the ultimate strength and the exact lateral stiffness levels offered by the primary structure.

Figure 10. Pushover Test on the Module under Study

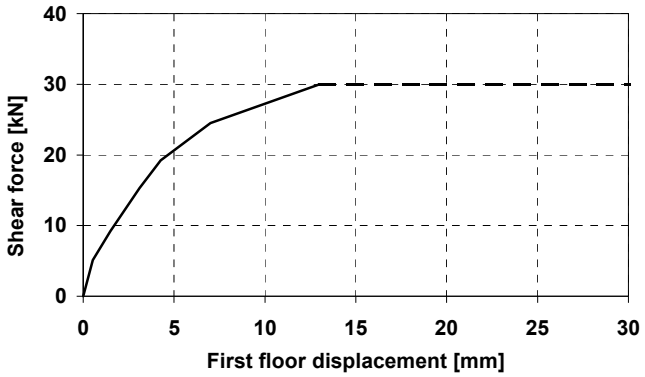


Figure 11. Result of the Experimental Pushover Test

## 4. THE RETROFITTING DESIGN

The choice of an appropriate seismic consolidation strategy depends on the determination of specific performance objectives to be assured as well as on the determination of the reasons why the original structure is not able to provide the required performance. Once the structural deficiencies have been determined, a preliminary retrofitting design can be developed [7]. In particular, after the determination of the displacement level required to the original structure under the design earthquake and the spectral displacement target for the reinforced structure, the shear panel characteristics able to absolve this task can be defined [8, 9]. In order to define the actual geometry of shear panels to be adopted, a sophisticated finite element model has been implemented by means of the ABAQUS v. 6.4 non linear numerical code [10], it being described in detail in [11]. The material used for panel is DX56D steel, whose stress-strain curve is reported in Figure 12, which is employed as a base material for producing cold-formed thin walled sheeting and profiles.

On the basis of existing analytic simplified formulations [12, 13], the panel dimensions have been determined as $b$ = 600 mm, $d$ = 2400 mm and $s$ = 1.15 mm. In order to guarantee a $b/d$ ratio lower than 0.8, that is indicated as the lower bound of the aspect ratio beyond which the development of a correct plastic mechanism is not developed, the insertion of appropriate transversal rectangular stiffeners (height of 100 mm and thickness of 4 mm) along the whole panel length has been foreseen. Therefore, the panel has been subdivided into six parts having $b$ = 600 mm and $d$ = 400 mm. The sub - panels are connected to each other and to the surrounding frame by means of M14 bolts, having a pitch of 50 mm and a edges distance of 25 mm (Figure 13). In order to assess the effectiveness of the adopted connecting systems, preliminary tensile tests on two 150 x 250 mm panel portions, connected by means of 100 x 150 mm fishplates and six M14 bolts, have been carried out (Figure 14a). The corresponding results in terms of force (F) – relative displacement ($\Delta$) are given in Figure 15.

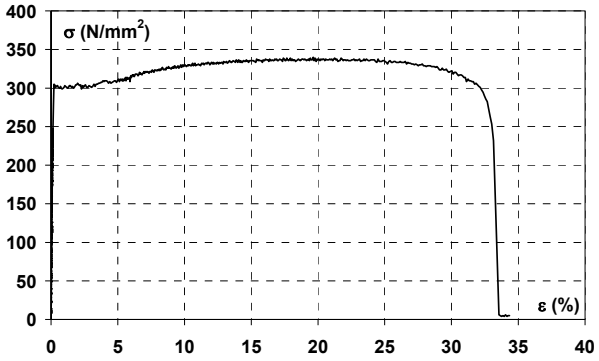


Figure 12. σ–ε Curve of the Adopted Steel

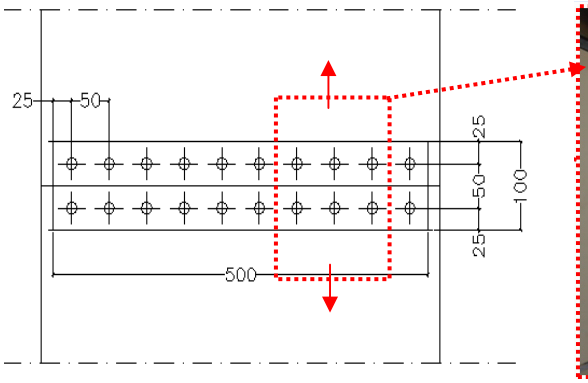


Figure 13. Details of the Panel Connection

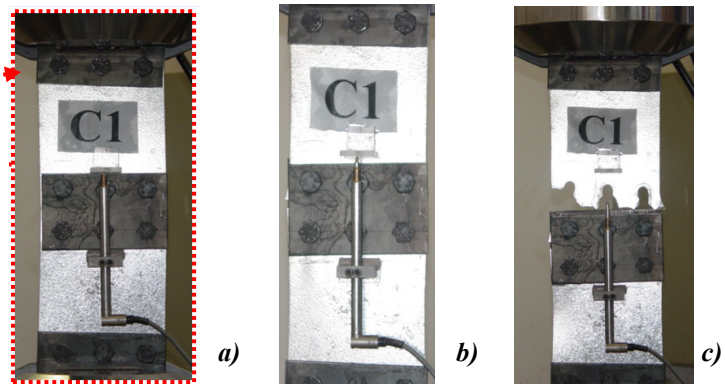


Figure 14. Connection Specimen Before (a), During (b) and After (b) the Test

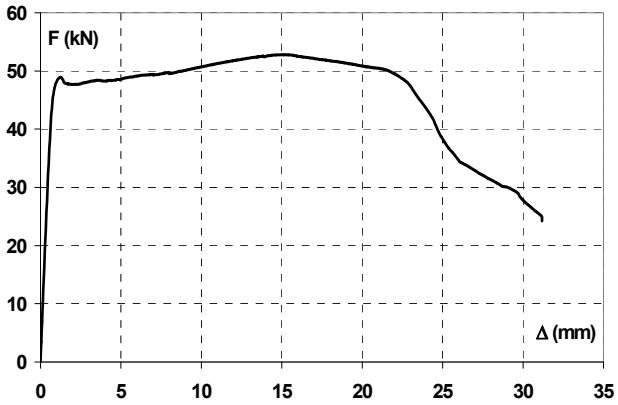


Figure 15. The Experimental Response of the Connection

It is apparent that the shear strength of connections is higher than the yielding resistance of the plate because of the occurrence of the block tearing mechanism, which determines a significant increment of the effective sheeting net section (Figure 14c). Also a significant ductility of the adopted connection, which make it able to restore the panel continuity, is noticeable. In order to confirm the validity of the proposed design solution and for evaluating possible interaction problems between the RC structure and the steel parts, a global analyses of the retrofitted structure, where the shear plates have been modelled according to the “strip model" theory [13], has been performed [14].

## 5. THE EXPERIMENTAL TEST

### 5.1 System Set-up

The proposed technique has been validated by a full scale experimental test. In order to install the steel shear panel into the RC frame, a surrounding hinged steel frame, constituted by members realised with UPN180 coupled profiles, has been introduced (Figure 16).

In order to have an appropriate panel response, represented by the development of a tension field mechanism with an inclination of 45°, the shear plate has been subdivided into two parts, having an aspect ratio equal to 0.50, due to the insertion of intermediate UPN 240 coupled beams, whose configuration is depicted in Figure 17.

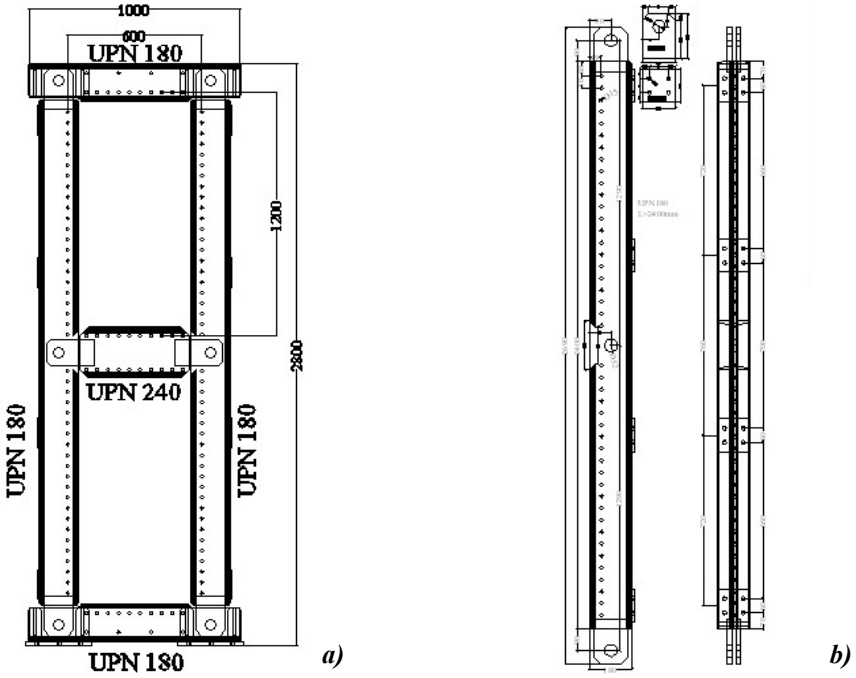


Figure 16. Lateral Reaction Steel Frame
(a) and Particular of Adopted Columns (b)

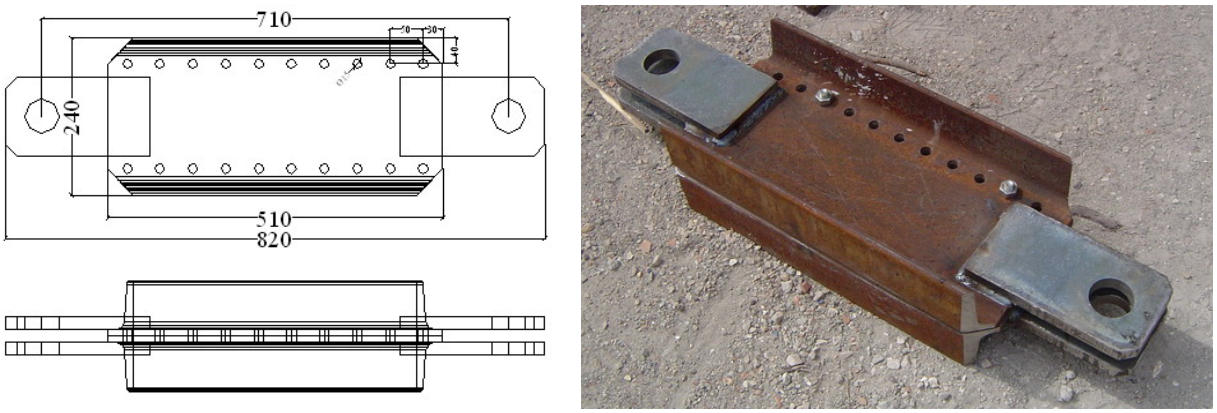


Figure 17. The Intermediate Beam

In particular, aiming at ensuring that the columns could sustain the normal boundary stresses associated with the tension field, considering hinged connections between frame members, the following equation must be satisfied:

$$M_{pf} = \frac{\sigma_{ty} \cdot t \cdot \left(\frac{d}{2}\right)^2 \cdot \cos^2 \Theta}{8} \tag{1}$$

where $t$ and $d$ are the panel thickness and height, respectively, while $\Theta$ is the inclination angle of tensile bands. The Eq. (1), which would allow using a column depth equal to 1/2 of the actual one, has been determined considering the columns as supported on three points. In such a way the bending moment applied to the vertical elements is equal to 1/4 of the one characterising the scheme without the intermediate member [12], thus determining smaller dimensions of the columns. On the other hand, the beams have to be characterised by an adequate flexural stiffness and strength to allow an uniform tension field in the shear panel surface. The minimum plastic resistance of the beam may be determined by the following relationship:

$$M_{pf} = \frac{\sigma_{ty} \cdot t \cdot b^2 \cdot \cos^2 \Theta}{8} \tag{2}$$

where $b$ is the panel width.

The steel frame columns have been connected to RC foundation beams by means of four UPN 220 profiles, adequately stiffened by reinforcing steel plates, and six threaded passing M16 bolts (Figure 18).

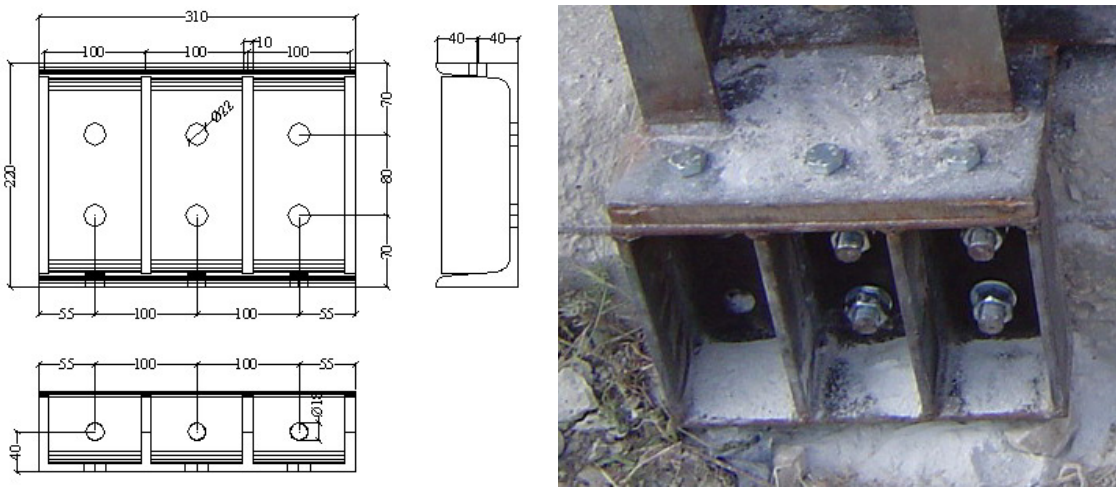


Figure 18. Reaction Steel Frame – Foundation Beam Connection

Moreover, in order to allow the transfer of the forces carried out by the steel panel (approximately 10 times greater than the one of the bare structure) the jacketing of the RC beam, by using two UPN220 profiles, has been executed (Figure 19).

In particular, the connection between the upper member of the reaction steel frame and the RC beam reinforcing one is realised with the system reported in Figure 20, while the details of the hinged beam-to-column connection are illustrated in Figure 21.

The final configuration of the applied system is represented in Figure 22, where the connection details and the intermediate stiffeners of the panel are also visible. In the same figure the installation of St. Andrew cross bracings in the transversal direction of the module is visible, they being able to avoid structural torsional effects during the loading test.

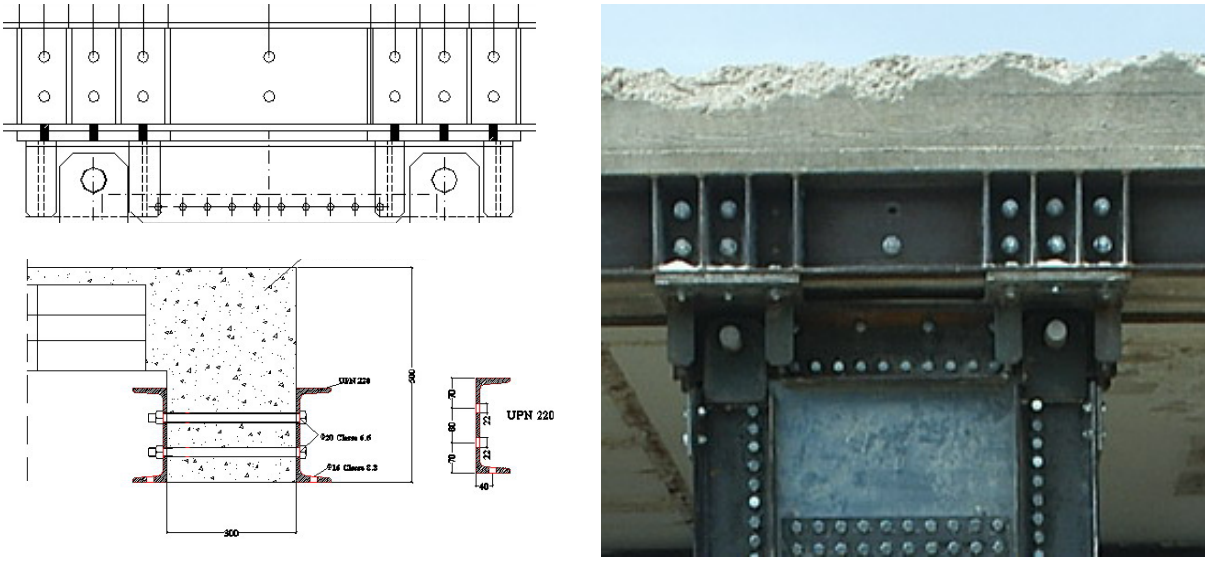


Figure 19. Reaction Steel Frame – RC Beam Connection

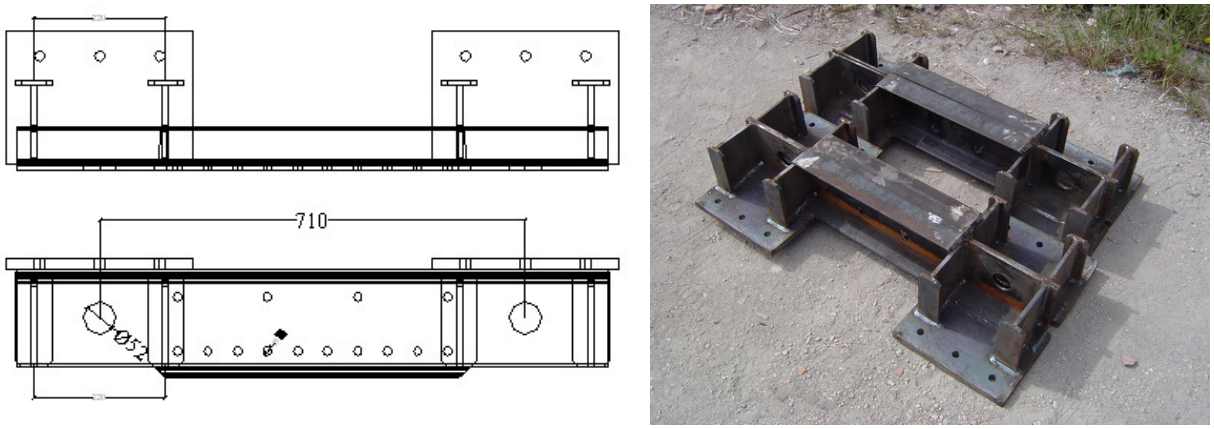


Figure 20. The Connection System between the Jacketing Steel Beam and the Upper one of the Reaction Frame

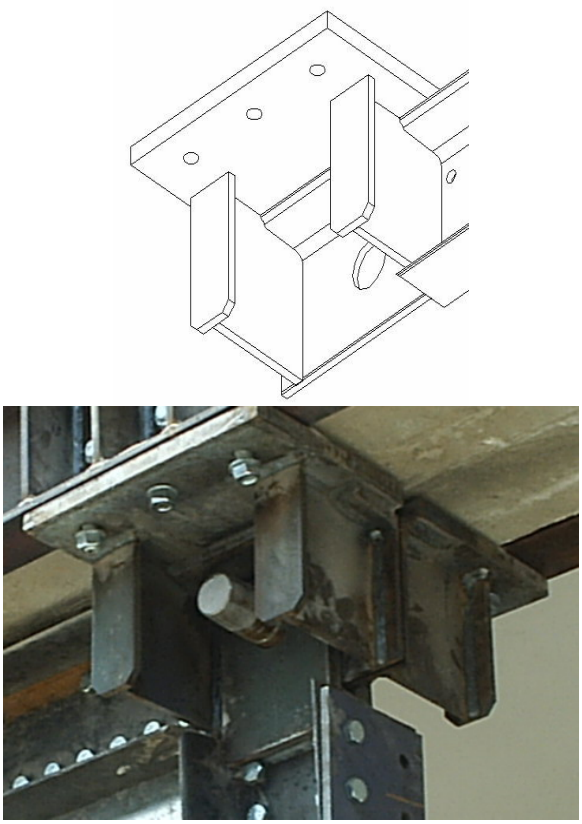

Figure 21. Details of the Hinged Beam-to-column Connection

Figure 22. Global View of the Retrofitted Structure

The retaining structure, which has been applied to the sixth module of the original RC building, is obtained by connecting steel profiles to the foundation beam and to the first level RC beam end (Figure 23).

Figure 23. The Retaining Steel Structure

The lateral load has been applied to the reinforced structure by using hydraulic jacks, which were able to apply tensile and compression actions equal to 200 and 300 kN, respectively.

In the experimental test several measurement devices (continuous transducers) have been employed in order to acquire the following absolute displacements (Figure 24):
- first level floor on both sides of the structure (P3);
- reinforcing steel beam (P4);
- shear wall stiffeners (P5- P7-P8) and intermediate
- UPN 240 beam (P6);
- foundation of shear panel (P9).

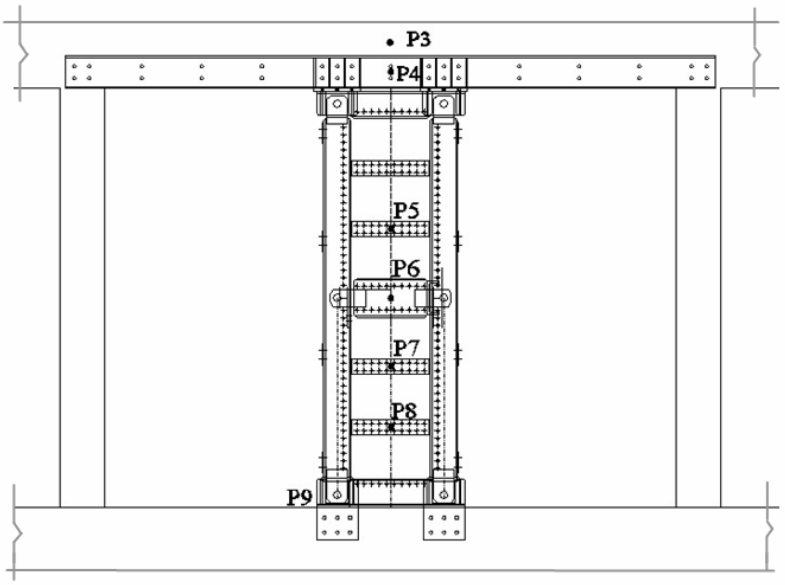


Figure 24. Location of Measurement Instruments

A global view of the used measurement instruments is reported in Figure 25.

Figure 25. Global View of the Measurement Devices Applied on the Upgraded Structure

## 5.2 The Experimental Behaviour

In the experimental test a cyclic loading history under quasi-static conditions has been applied (Figure 26). The load has been increased of 20 kN for each cycle up to the last one, where the increment has been of 60 kN. All loading cycles have been symmetric up to the attainment of 200 kN; hence only the compression load has been increased up to 300 kN.

During the test, any important difference between the displacements measured by two transducers located at the two opposite sides of the building occurred. In addition, the displacements of the transducers fixed on the RC beam and on the reinforcing steel profile have provided the same values, confirming the effectiveness of the connection created between the primary structure and the reinforcing steel beams. The displacements relieved at the base of the steel plate shear wall were very small, providing a maximum amplitude of 1 mm when the peak load of 300 kN was attained.

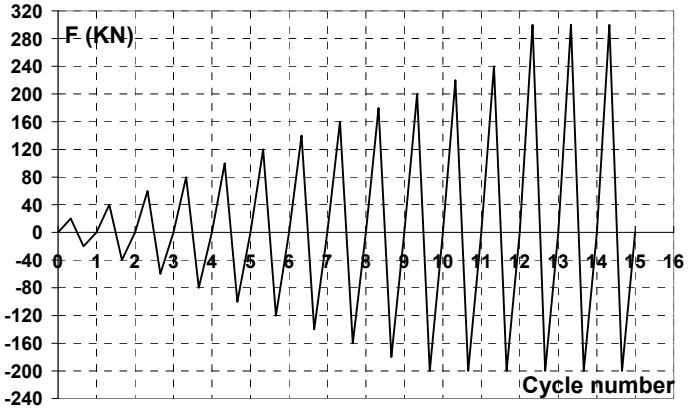


Figure 26. The Applied Loading History

The result of the experimental test in terms of applied force versus the first storey displacement (P3 transducer) is depicted in Figure 27. The behaviour of the retrofitted structure is significantly improved, showing an increase of the initial stiffness and ultimate strength equal to 400% and 1000%, respectively. Also, the deformation capacity of the structure results to be very large,

without the involvement of any brittle collapse mode up to a deformation amplitude equal to 85 mm, corresponding an inter-storey drift equal to 3.5%. Finally, it should be observed that the dissipation capacity of the structure is quite satisfactory, showing a combined mechanism between plastic hinges in the beam-to-column joint of the RC frame and plastic deformation of tensioned diagonals of the applied steel shear panel.

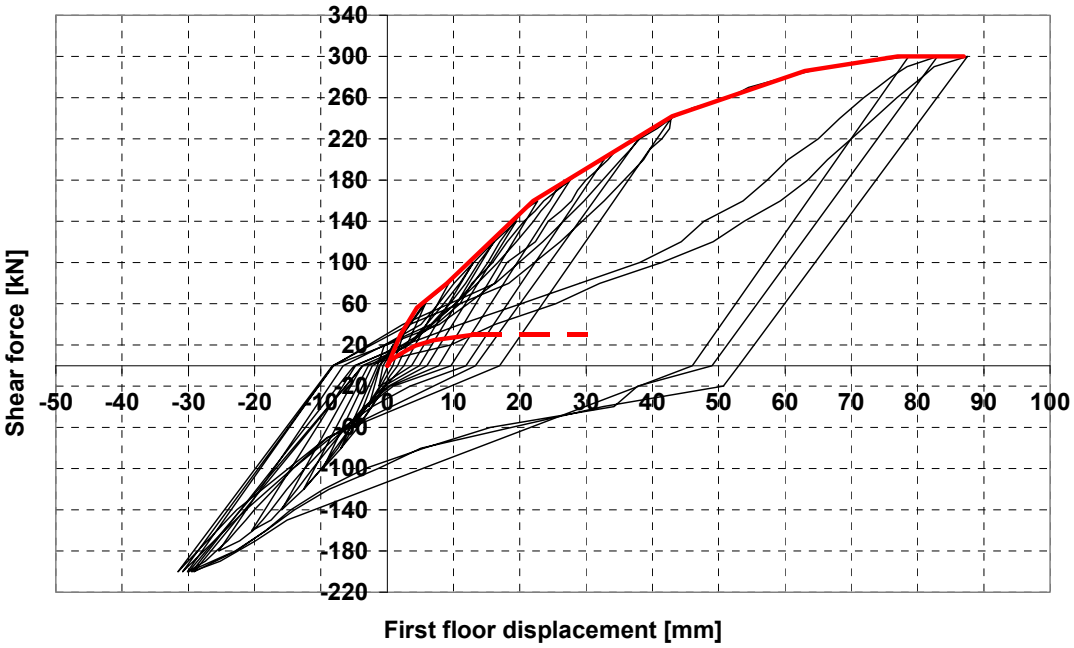


Figure 27. The Experimental Response of the Retrofitted Structure

In the Figures 28-to-33, a detailed representation of significant phenomena occurred in the shear panels during the test is presented. In particular, in the second cycle, for a displacement of 2.94 mm, the occurrence of buckling in the upper sub-panel was evident (see Figure 28). Such a phenomenon was due to the global flexural action on the shear wall which, due to the compression load generating in the steel column and the development of slips in the beam-to-column connection of the retaining steel frame, caused the buckling of the panel portions subjected to the maximum compression loading.

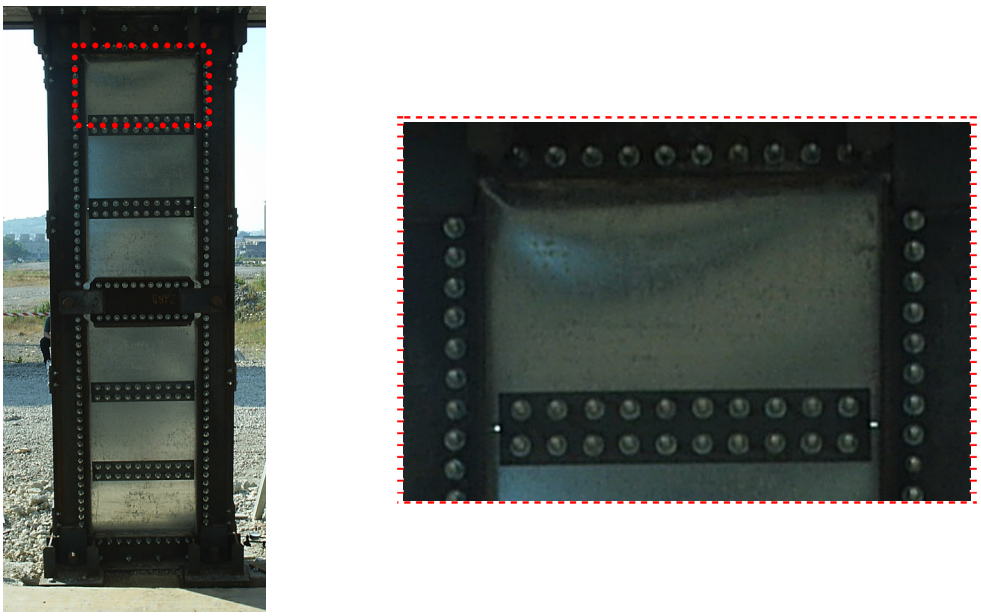

Figure 28. The Shear Panel Response during the Second Cycle of the Loading Test

In the third cycle, for an applied total force of 60 kN and a displacement of about 6 mm, the instability of each panel portions, with a more remarkable development of the buckled shape in the upper one, occurred (Figure 29).

In the fifth cycle, when a global lateral action equal to 100 kN, producing a structural displacement of 13 mm, has been applied, the buckling behaviour involved more panel portions (Figure 30), while starting from the ninth cycle permanent waves developed on the surface of each sub-panel. In particular, at this stage, which is characterized by a total force of 220 kN and a displacement of 37.90 mm, the tension field mechanism was activated also in the upper panel portion (Figure 31).

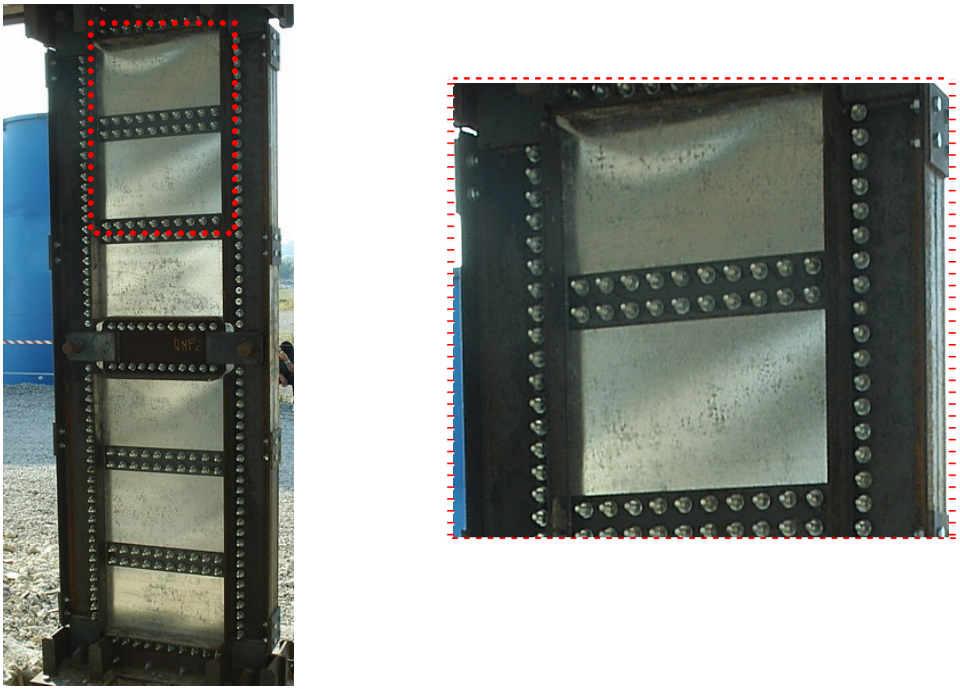

Figure 29. The Shear Panel Response during the Third Cycle of the Loading Test

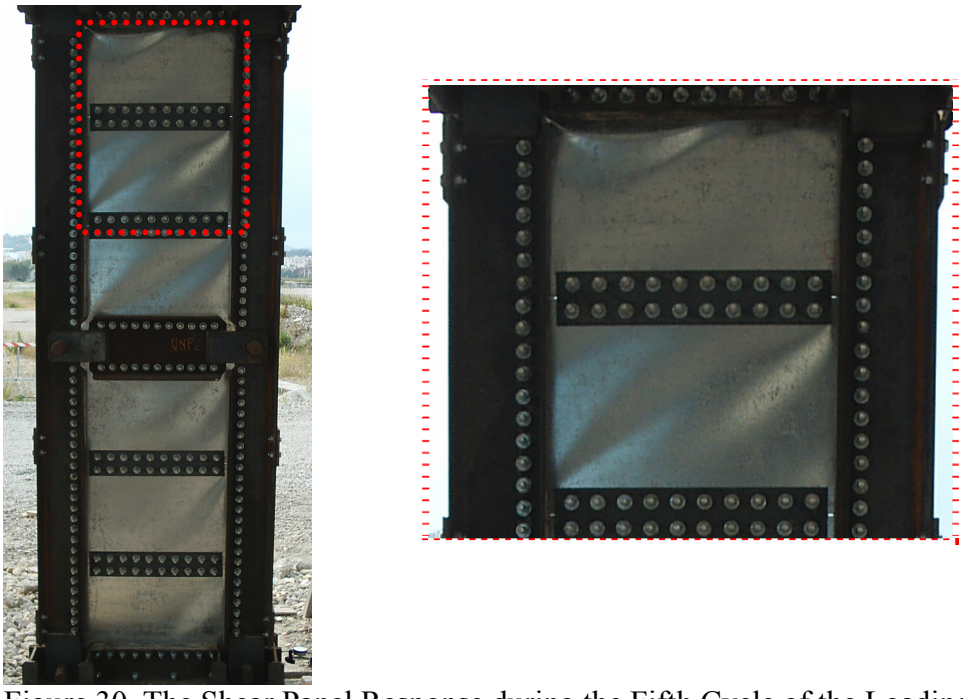

Figure 30. The Shear Panel Response during the Fifth Cycle of the Loading Test

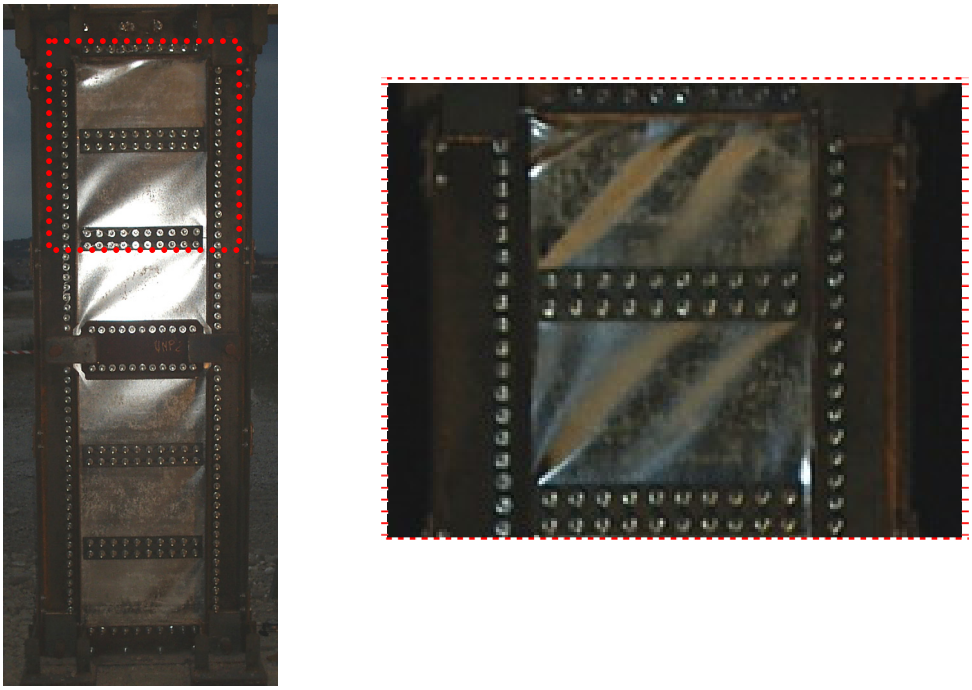

Figure 31. The Shear Panel Response during the Ninth Cycle of the Loading Test

In the twelfth cycle a partial plastic behaviour of the panel, with the significant development of permanent waves on each plate portion, appeared (Figure 32). In this phase, corresponding to an applied global load and displacement of 240 kN and 42.80 mm, respectively, the buckled shape occurred in the upper panel portion during the initial loading stage disappeared.

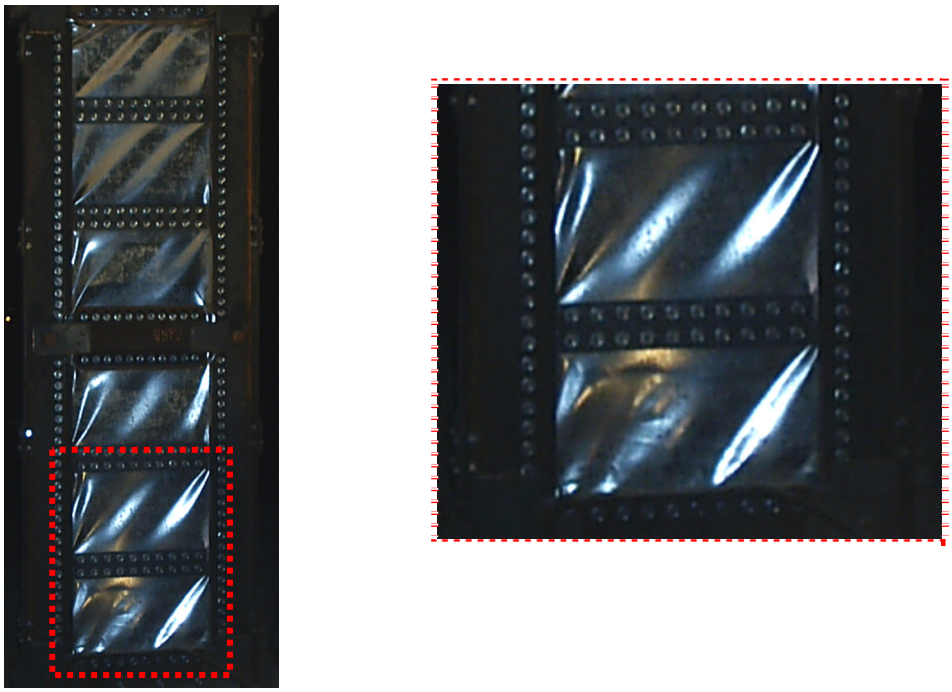

Figure 32. The Shear Panel Response during the Twelfth Cycle of the Loading Test

The final deformed shape of shear panels at the end of the test (15$^{th}$ cycle), where a force of 300 kN and a displacement of 87.55 mm were applied, is depicted in Figure 33, where it is apparent as the entire panel surface is strongly involved in plastic deformation.

Finally, experimental results have confirmed the effectiveness of the proposed design procedure since the consequently implemented non linear finite element model of the steel shear panel exhibited a very good agreement in terms of deformed shape with the real final deformation of the used system, as shown in Figure 33. The same results have been also achieved by modeling the steel shear panel through equivalent truss elements, according to the strip model theory, as it is exhaustively reported in [15]

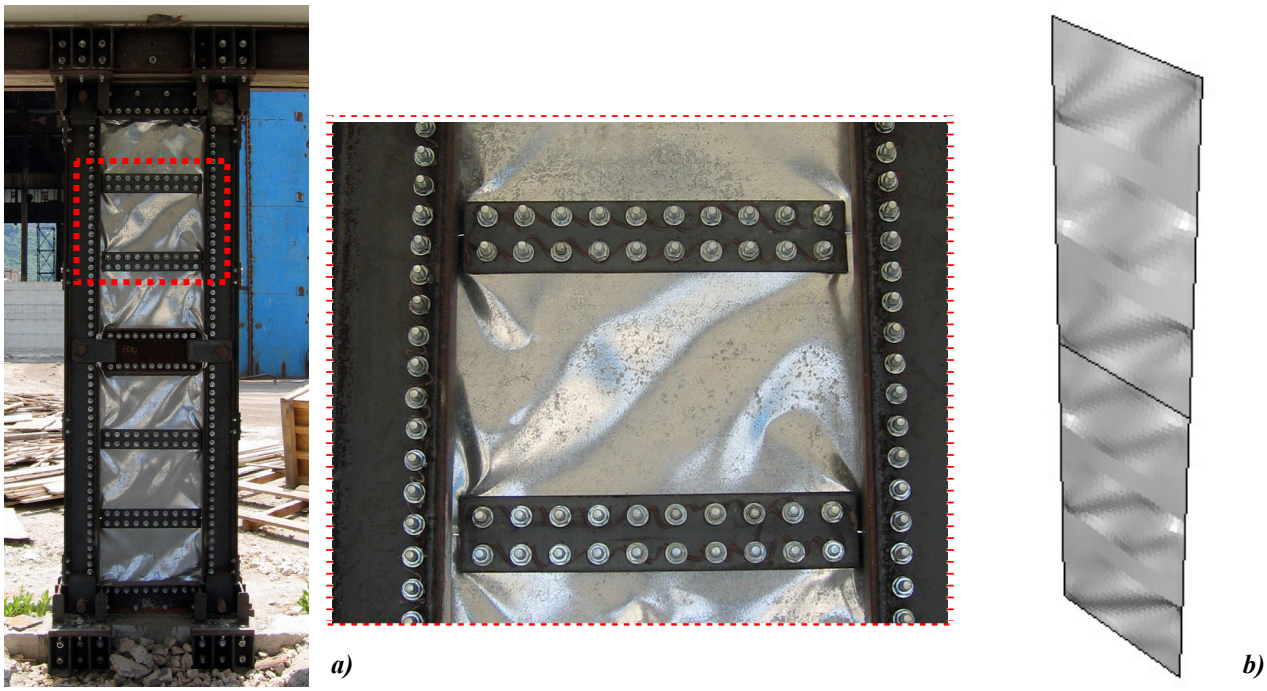

*a)* *b)*

Figure 33. Final Experimental (a) and Numerical (b) Deformed Shape of the Tested Shear Panel

## 6. CONCLUSIONS

In the current paper the use of slender steel panels as seismic retrofitting systems of existing RC structure has been analysed. The retrofitting design, developed on the basis of a preliminary evaluation of the load-carrying capacity of the bare structure, has been set-up according to the performance based design methodology, allowing the definition of the testing panel geometry. On the basis of the panel structural configuration obtained from the design phase, an experimental test has been carried out on the compound RC frame – steel panel structure, showing as the proposed retrofitting system is able to increase both the strength and the stiffness of the original building up to 10 and 2 times, respectively.

Based on such results the proposed system appears to be suitably used for the seismic upgrading of existing reinforced concrete frame characterised by significant structural deficiencies.

## ACKNOWLEDGEMENTS

This paper has been developed within both the European FP6 project “Earthquake Protection of Historical Buildings by Reversible Mixed Technologies” (PROHITECH) and the research theme n.5 “Development of innovative approaches for the design of steel and composite structures” of the Italian project RELUIS.

## REFERENCES


[1] Mazzolani, F.M., Dolce, M., Landolfo, R. and Nicoletti, M., "Seismic Upgrading of RC Buildings by Means of Innovative Techniques: The ILVA-IDEM Project", Proceedings of the 11th National Congress "L'ingegneria Sismica in Italia", Genoa, 2004, CD-ROM.

[2] De Matteis, G., Landolfo, R. and Mazzolani, F.M., "Seismic Response of MR Steel Frames with Low-yield Steel Shear Panels", Journal of Structural Engineering 2003, Vol. 25, pp. 155-168.

[3] De Matteis, G., Mazzolani, F.M. and Panico, S., "Steel Bracings and Shear Panels as Hysteretic Dissipative Systems for Passive Control of MR Steel Frame", Costruzioni Metalliche, 2003, Vol. 6, pp. 41-53.

[4] De Matteis, G., Formisano, A., Mazzolani, F.M. and Panico, S., "Experimental Tests and Numerical Simulation on Stiffened Pure Aluminium Shear Panels", Proceedings of the 10th International Conference on Civil, Structural and Environmental Engineering Computing, Rome, 2005, CD-ROM.

[5] Astaneh-Asl, A., "Seismic Behavior and Design of Steel Shear Walls", Steel TIPS Report, Structural Steel Educational Council, Moraga, CA, 2001.

[6] Mazzolani, F. M. (co-ordinator & editor), "Seismic upgrading of RC buildings by advanced techniques - The ILVA-IDEM Research Project", Polimetrica International Scientific Publisher, Monza, 2006, ISBN 88-7699-038-0.

[7] ATC-40, "Seismic Evaluation and Retrofit of Concrete Buildings", Applied Technology Council, Report n. SSC 96-01, 1996.

[8] De Matteis, G. and Mistakidis, E.S., "Seismic retrofitting of moment resisting frames using low yield steel panels as shear walls", Proceedings of the 4th International Conference STESSA 2003, "Behaviour of Steel Structures in Seismic Areas", Naples, 2003, pp. 677-682.

[9] Mistakidis, E.S., De Matteis, G., Formisano, A., "LYM Shear Panels as an Alternative for the Seismic Upgrading of Concrete Structures", Advances in Engineering Software, Elsevier, Noor, A.K., Adey, R.A. and Topping, B.H.V. editors, ISSN 0965-9978, N. 38, 2007, pp. 626-636.

[10] Hibbitt, Karlsson, Sorensen, Inc., ABAQUS/Standard, v. 6.4, Patwtucket, USA, 2004.

[11] Formisano, A., De Matteis, G., Panico, S., Calderoni, B. and Mazzolani, F.M., "Full-scale Test on Existing RC Frame Reinforced with Slender Shear Steel Plates", Proceedings of the 5th International Conference STESSA 2006 "Behaviour of Steel Structures in Seismic Areas", Yokohama, 2006, pp. 827-834.

[12] Sabouri-Ghomi, S., Ventura, C. and Kharrazi, M.H.K., "Shear Analysis and Design of Ductile Steel Plate Walls", Proceedings of the 4th International Conference STESSA 2003, "Behaviour of Steel Structures in Seismic Areas", Naples, 2003, pp. 189-195.

[13] Canadian Standards Association (CSA), "Limit States Design of Steel Structures", CAN/CSA S16-01, Canadian Standards Association, Willowdale, Ont., Canada, 2001.

[14] Formisano, A., De Matteis, G., Mazzolani, F.M. and Panico, S., "Seismic Retrofitting of an Existing RC Structure by Means of Steel Shear Panels: the Proposed Design Solution", Proceedings of the 20th C.T.A. National Congress, Ischia, 2005, pp. 475-482.

[15] Formisano, A., De Matteis, G., Panico, S and Mazzolani, F.M., "Metal Shear Panels as Innovative System for Seismic Upgrading of Existing RC Buildings: from Numerical Analyses to Full-scale Experimental Tests", Proceedings of the 15th International Conference on the Computational Mechanics in the UK (ACME 2007), Glasgow, 2-3 April 2007.

# BEHAVIOUR OF COLD-FORMED STEEL SINGLE AND COMPOUND PLAIN ANGLES IN COMPRESSION

S. Vishnuvardhan [1] and G. M. Samuel Knight [2,*]

[1] *Assistant Professor, Department of Civil Engineering, Tagore Engineering College, Vandalur, Chennai 600 048, India*
[2] *Professor, Department of Civil Engineering, Anna University, Chennai 600 025, India*
[*] *(Corresponding author: E-mail: gmsk@annauniv.edu)*

*Received: 28 November 2006; Revised: 4 May 2007; Accepted: 9 July 2007*

**ABSTRACT:** Compression tests were carried out on cold-formed steel single angles, double angles welded back-to-back and starred angles under three different end connections. Eight plain sections of different sizes of two different thicknesses of different strengths were tested as stub and as short columns. The effect of flat width to thickness ratio, the effect of size of the section, the effect of material yield strength and the effect of symmetricity of the cross-section on the load carrying capacity is studied. Load versus axial shortening behaviour, load versus lateral deflection behaviour and load versus strain behaviour is also studied. The initial stiffness and ductility co-efficient for different sections are computed and compared. The ultimate loads of double angles welded back-to-back and starred angles with ball end connection is found to be more than twice when compared to single angles irrespective of the slenderness ratio. It was found that initial stiffness of double angles welded back-to-back is 1.25 times more than that of single angles. There was reversal of strain from compression to tension for compound angles beyond 70% of ultimate load. The effect of symmetricity on the mode of buckling of the specimens under different slenderness ratios is also reported.

**Keywords:** Cold-formed; single angle; compound angle; double angle; starred angle; stub column; short column; buckling

## 1. INTRODUCTION

Cold-formed steel structural members can lead to more economic design than hot-rolled members as a result of their high strength to weight ratio, ease of fabrication and construction. These sections are essentially thin-walled members with moderate to very high flat width to thickness ratio of the web or flange plate components. These members can be produced in a wide variety of sectional profiles such as angles, channels, hat sections, zed sections and sigma sections. Angles are the most common structural shape found in almost any structure due to their simplicity and ease of fabrication and erection. Single angles are usually used as web members in steel joists and trusses, members of latticed transmission towers or communication structures and bracing members to provide lateral support to the main members. Compound angles either as double angles or as starred angles or as built up sections are frequently used as main members in trusses and in transmission line towers.

Murray and Sherief [1] reviewed the Simple Column Design Practice followed in Canada and United States and Load and Resistance Factor Design of AISC Design Practice for single angle compression members attached by one leg. The failure loads obtained in an experimental study were compared with the compressive resistances calculated in accordance with these design approaches. Finite element results were also compared with the experimental results. It was concluded that the AISC approach reflects the behaviour of single angles correctly.

Compression tests on pin-ended and fixed-ended cold-formed in-line galvanised angle sections over various slenderness ratios taking into account detailed measurements of material properties, residual stresses and geometrical imperfections was conducted by Popovic, Hancock and Rasmussen [2]. It was found that the capacities of stub column tests are 15 and 40% higher than those calculated according to Australian and American specifications for cold-formed and

hot-rolled steel structures. Popovic, Hancock and Rasmussen [3] conducted a series of compression tests on equal angles with slender cross-sections. The angles were tested between pinned ends and loaded axially with eccentric load, which caused bending parallel to the leg. The test data were compared with the design rules of the Australian and American specifications for cold-formed and hot-rolled steel structures, and as well as ASCE standards. The rules of the specifications for cold-formed steel structures are shown to be very conservative.

Young [4] conducted series of tests on cold-formed steel plain angle columns compressed between fixed ends. Tests were performed over a range of lengths such that column curves could be obtained. Geometric imperfections and material properties of the specimens were measured. The test strengths were compared with the design strengths calculated using the American specification and Australian/New Zealand standard for cold-formed steel structures. It was shown that the design strengths predicted by the specification and standard are generally very conservative. Modified design equations for cold-formed steel plain angle columns were proposed.

An efficient and accurate finite element model incorporating geometric imperfections and material non-linearities was developed by Ellobody and Young [5] to understand the behaviour of cold-formed steel plain angle columns. The finite element analysis was performed on plain angles compressed between fixed ends over different column lengths, and column curves were obtained. The column strengths predicted from the finite element model were compared with the design strengths calculated using the American specification and Australian/New Zealand standard for cold-formed steel structures. The results obtained from the finite element model were also compared with the design strengths obtained from the design rules proposed by other researchers.

## 2. EXPERIMENTAL INVESTIGATION

### 2.1 Test Specimens and End Connections

The specimens used in the present investigation were fabricated from different steel sheets of two different thicknesses 2.00 and 3.15 mm having different material properties. Tensile coupons were prepared and tested according to ASTM A 370 [6] to determine the yield stress, ultimate stress and percentage elongation. Table 1 presents the average material properties obtained from the tension tests.

Table 1. Tension Coupon Test Results

| Type of Steel | Thickness (mm) | Modulus of Elasticity, MPa | Yield Stress ($f_y$), MPa | Ultimate Stress ($f_u$), MPa | $f_u/f_y$ | % Elongation |
|---|---|---|---|---|---|---|
| 1 | 2.00 | 182000 | 345 | 440 | 1.28 | 16 |
| 2 | 2.00 | 211000 | 415 | 495 | 1.20 | 10 |
| 3 | 3.15 | 201000 | 250 | 350 | 1.40 | 11 |
| 4 | 2.00 | 179000 | 205 | 300 | 1.46 | 13 |
| 5 | 2.00 | 210000 | 310 | 410 | 1.32 | 10 |
| 6 | 3.15 | 208000 | 250 | 365 | 1.46 | 26 |

Figures 1 (a) to (c) show the different cross-section geometries tested. Single angles of required sizes were obtained directly by brake-pressing, whereas the double angles welded back-to-back and starred angles were prepared by suitably welding the two single angles of same size confirming to AISI Manual - 1996 [7].

(a) Single Angle (b) Double Angle (c) Starred Angle

Figure 1. Cross-section Geometries of Angle Tested

Fifty seven experiments were conducted on single angles, double angles welded back-to-back and starred angles with three different end connections. The specimens were tested either as stub columns or as short columns. Thirty six specimens were tested as stub columns of slenderness ratio 10, 15 and 20. Stub columns are specimens whose height is not less than three times the largest dimension of the section and not more than twenty times the least radius of gyration as prescribed in the IS : 801 - 1975 [8]. Twenty one tests were carried on short columns of slenderness ratio 25 and 30. Table 2 shows the flat width to thickness ratio of the sections, limiting flat width to thickness ratio as per IS : 801 - 1975, type of steel from which the section is obtained, slenderness ratios of the specimens tested and the type of end connection. The sections chosen were those which are listed in IS : 811 - 1987 [9].

Table 2. Details of Test Specimens

| Sl. No. | Section Size (mm) | (w/t) | $(w/t)_{lim}$ | Type of Steel | Slenderness Ratios | End Connection |
|---|---|---|---|---|---|---|
| 1 | 35 × 35 × 2.00 | 15.00 | 9.02 | 1 | 15, 20, 25 | Ball |
| 2 | 45 × 45 × 2.00 | 20.00 | 9.02 | 1 | 15, 20, 25 | Ball |
| 3 | 40 × 40 × 2.00 | 17.50 | 8.23 | 2 | 15, 30 | Ball |
| 4 | 40 × 40 × 3.15 | 10.20 | 10.60 | 3 | 15, 30 | Ball |
| 5 | 50 × 50 × 2.00 | 22.50 | 11.71 | 4 | 10, 15, 20 | Welded |
| 6 | 60 × 60 × 2.00 | 27.50 | 9.52 | 5 | 20, 30 | Bolted |
| 7 | 60 × 60 × 3.15 | 16.55 | 10.60 | 6 | 20, 30 | Bolted |
| 8 | 70 × 70 × 3.15 | 19.72 | 10.60 | 6 | 20, 30 | Bolted |

Three different end connections were used in the present investigation to study their effect on the load carrying capacity. Figures 2 to 4 show the details of three different end connections for single angles, angles welded back-to-back and starred angles.

### *2.1.1 Ball End Connection*

This end connection is fabricated by welding the sections to an end bearing plate of 6 mm thick and in turn connected to a pair of flat bearing plates of sizes varying from 60 × 60 mm to 120 × 120 mm. The assembly consisted of two end plates of 16 mm thick with a spherical groove in between to accommodate a ball of 40 mm diameter at both ends.

### *2.1.2 Welded End Connection*

This end connection is fabricated by welding the section to the end plate of size varying from 60 × 60 × 6 mm to 120 × 120 × 6 mm through a gusset plate in such a way that the centre of the plate coincided with the centroid of the specimen. Then the section is tested with the load line coinciding with the centroid of the end plates.

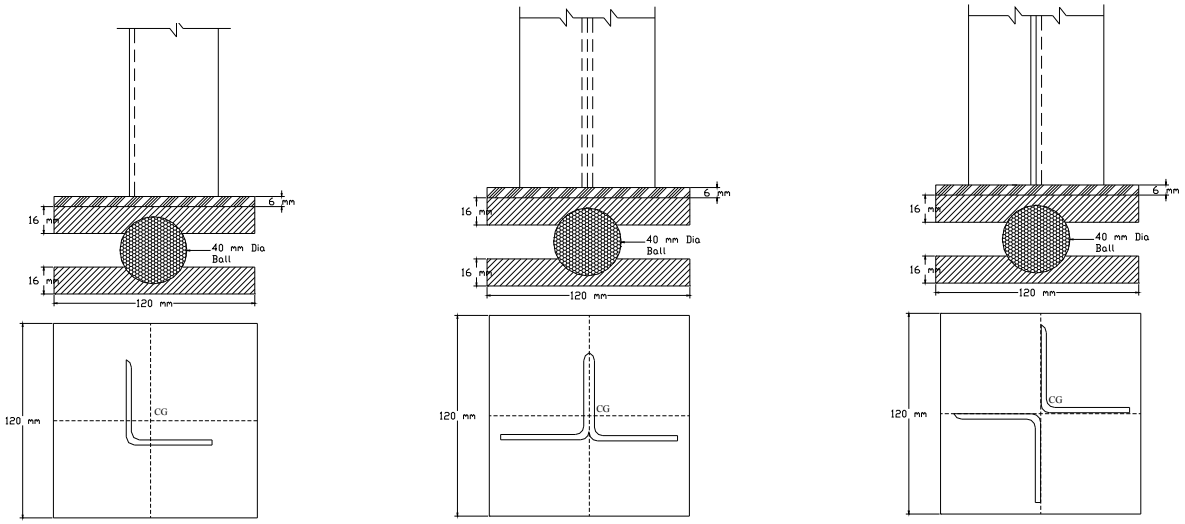


(a) Single Angles (b) Double Angles (c) Starred Angles

Figure 2. Details of Ball End Connection

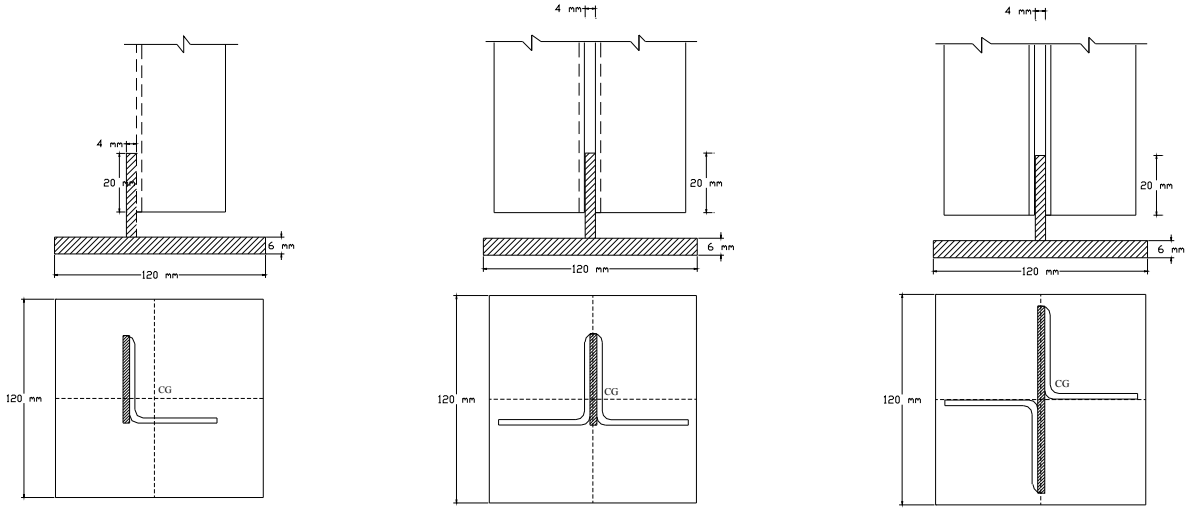


(a) Single Angles (b) Double Angles (c) Starred Angles

Figure 3. Details of Welded End Connection

### *2.1.3 Bolted End Connection*

The specimens were bolted to two hot-rolled ISAs of size varying from 50 × 50 × 6 mm and 75 × 75 × 6 mm connected to 20 mm thick base plate of size 200 × 200 mm. The angles which are welded to the base plates were provided with a slot arrangement to accommodate specimens of different sizes and maintains the centre of gravity of specimens in line with the base plate. Bolt holes of 12 mm nominal diameter were made in the specimens to connect to the gusset angles confirming to AISI Manual - 1996.

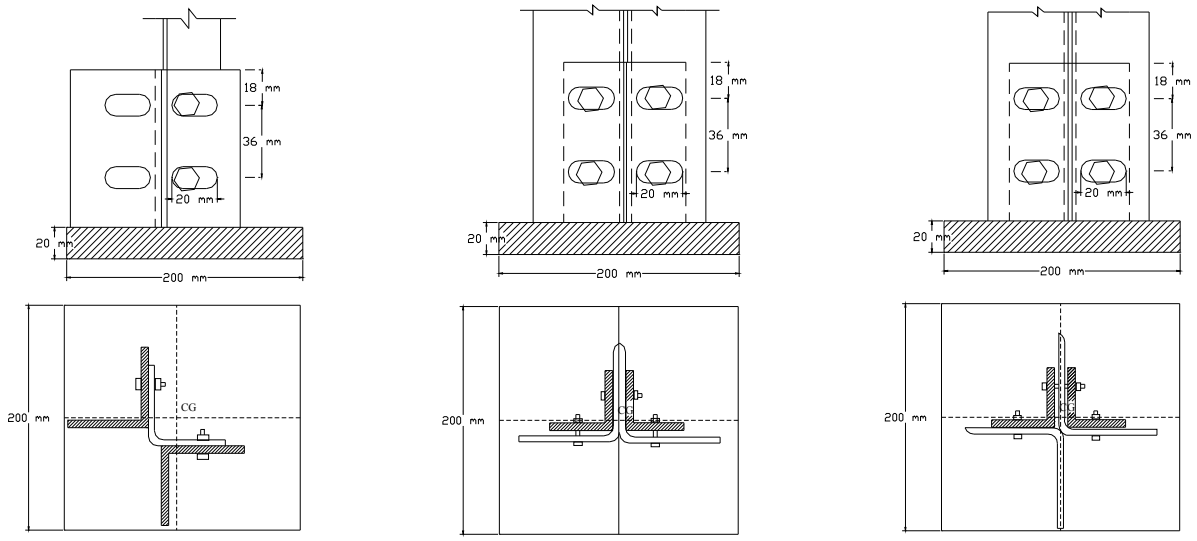


(a) Single Angles (b) Double Angles (c) Starred Angles

Figure 4. Details of Bolted End Connection

## 2.2 Compression Test Set Up

Compression tests were carried out on a column testing machine. The test specimens were connected to the end fixtures and were tested to failure. For each test the axial load was increased at a relatively faster rate in the elastic range and at a slower rate in the plastic range till the specimen collapsed. Mitutoyo and Batty dial gauges of least count 0.01 mm were used to measure the axial shortening and lateral deflections of the member. Dial gauges were placed at the mid height of the section and also at one fourth of the height of section with their tips touching the web and flange of the specimens to measure the lateral deflections. One dial gauge was placed with its tip touching the movable head of the column testing machine to measure the axial shortening of the test specimen. Electrical resistance strain gauges of type BKSA 20 with the gauge factor of 2.1 ± 0.6 were used to measure the strains at mid-height. Strain gauges were fixed on flanges at mid height of the specimen. Care was taken that these strain gauges were fixed farther away from the neutral axis and to check whether the cross-sections experience symmetric or unsymmetric buckling. Strain indicator with 10 channels was used to record the strain measurements. The strain gauge and dial gauge readings were taken at higher intervals in the elastic range and at closer intervals in the inelastic range until the specimen failed. Figure 5 shows the test set up for bolted end connection.

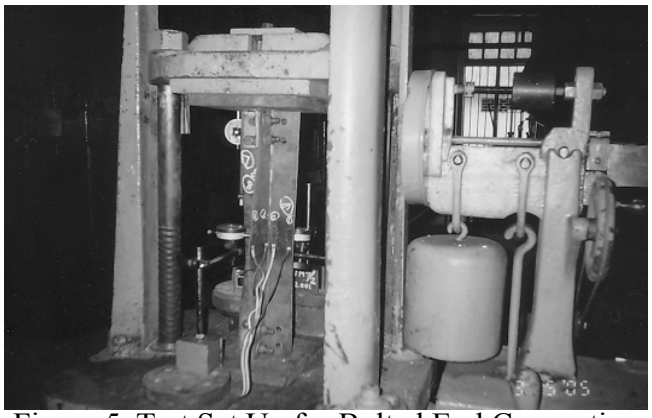

Figure 5. Test Set Up for Bolted End Connection

## 3. RESULTS AND DISCUSSION

The behaviour of cold-formed steel single angles, double angles welded back-to-back and starred angles under axial compression was studied. The load versus axial shortening behaviour, the load versus lateral deflection behaviour and the load versus strain behaviour under the elastic as well as in the plastic ranges of loading were studied. The effect of slenderness ratio, cross-section geometry of the angle, type of steel and the flat width to thickness ratio of the angle on the load carrying capacity were studied. The effect of symmetricity and the mode of buckling of the angles were also studied.

### 3.1 Load Carrying Capacity

The experimental ultimate loads obtained for single angles, double angles welded back-to-back and starred angles and also their ratios are presented in Table 3.

Table 3. Experimental Ultimate Loads of Single and Compound Angles and Their Ratios

| Section Size (mm) | $\lambda$ | Ultimate Load ($P_{ex}$), kN | | | $\frac{P_{double}}{P_{sin\,gle}}$ | $\frac{P_{starred}}{P_{sin\,gle}}$ |
|---|---|---|---|---|---|---|
| | | Single Angles | Angles welded back-to-back | Starred Angles | | |
| Ball End Connection | | | | | | |
| 35 × 35 × 2.00 | 15 | 32.03 | 76.09 | 76.32 | 2.3756 | 2.3828 |
| | 20 | 31.59 | 73.87 | 74.87 | 2.3384 | 2.3701 |
| | 25 | 29.37 | 69.42 | 72.09 | 2.3636 | 2.4545 |
| 45 × 45 × 2.00 | 15 | 40.05 | 80.28 | 83.39 | 2.0045 | 2.0821 |
| | 20 | 32.69 | 75.46 | 77.87 | 2.3084 | 2.3821 |
| | 25 | 27.02 | 70.49 | 54.05 | 2.6088 | 2.0004 |
| 40 × 40 × 2.00 | 15 | 48.47 | 69.14 | 66.74 | 1.4264 | 1.3769 |
| | 30 | 46.90 | 65.10 | 59.86 | 1.3881 | 1.2763 |
| 40 × 40 × 3.15 | 15 | 62.12 | 127.30 | 117.50 | 2.0493 | 1.8915 |
| | 30 | 59.20 | 123.50 | 115.30 | 2.0861 | 1.9476 |
| Welded End Connection | | | | | | |
| 50 × 50 × 2.00 | 10 | 26.00 | 58.50 | 57.91 | 2.2500 | 2.2273 |
| | 15 | 25.75 | 55.00 | 56.05 | 2.1359 | 2.1767 |
| | 20 | 24.50 | 49.20 | 55.50 | 2.0082 | 2.2653 |
| Bolted End Connection | | | | | | |
| 60 × 60 × 2.00 | 20 | 31.15 | 64.52 | 66.75 | 2.0713 | 2.1429 |
| | 30 | 28.49 | 59.30 | 61.65 | 2.0814 | 2.1639 |
| 60 × 60 × 3.15 | 20 | 68.97 | 127.71 | 123.70 | 1.8517 | 1.7935 |
| | 30 | 52.51 | 123.23 | 117.53 | 2.3468 | 2.2382 |
| 70 × 70 × 3.15 | 20 | 73.42 | 128.38 | 121.65 | 1.7486 | 1.6569 |
| | 30 | 58.29 | 101.65 | 117.72 | 1.7439 | 2.0196 |

It is observed that in the case of angles tested with ball end connection the increase in ultimate load of double and starred angles is twice when compared with single angles irrespective of the slenderness ratio. Similarly, the ultimate loads of double and starred angles are 1.90 times more as compared to single angles with bolted end connection of slenderness ratio less than 20. For short

columns the increase is found to be 2.05 and 2.15 for double and starred angles, respectively. It is observed that in the case of angles tested with ball end connection there is only a marginal decrease in ultimate loads due to increase in the slenderness ratio from 15 to 30, irrespective of the type of angle whether single or compound. Similarly for angles tested with welded end connection the increase in ultimate loads is insignificant due to increase in slenderness ratio from 10 to 20. In the case of angles tested with welded end connection the increase in slenderness ratio from 15 to 30 decreases the ultimate load carrying capacity by 15% in the case of single angles and 10% in the case of double and starred angles. For the angles with bolted end connection the decrease in ultimate load is 16% for single angles, 8% for double and starred angles when the slenderness ratio is increased from 20 to 30.

### 3.2 Load Versus Axial Shortening Behaviour

The load versus axial shortening behaviour is initially linear in most cases up to 50% of ultimate load irrespective of the cross-section of the specimens. Figures 6 and 7 show the typical load versus axial shortening behaviour of stub and short angles with ball end connection. It is observed that the behaviour is steeper for stub columns as compared to short columns. Similarly for angles with welded end connection there is a sudden drop in the load after the ultimate load and the non-linearity in the behaviour starts at 70% of ultimate load for all angles.

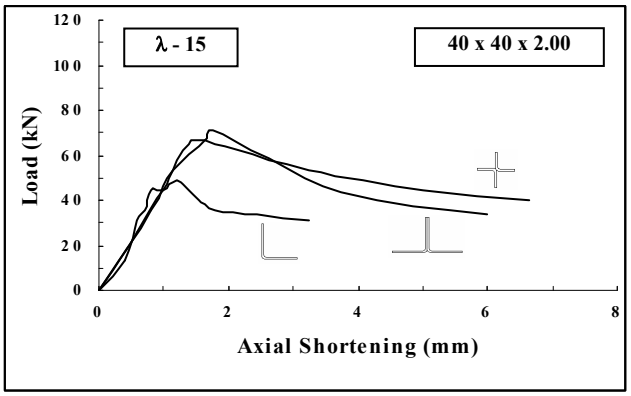


Figure 6. Axial Shortening Behaviour of StubAngles with Ball End Connection

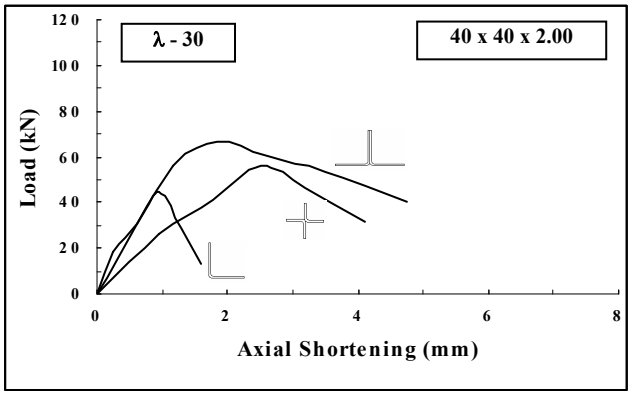


Figure 7. Axial Shortening Behaviour of Short Angles with Ball End Connection

Figures 8 and 9 show the typical load versus axial shortening behaviour of stub and short angles with bolted end connection. It is observed that the behaviour is similar irrespective of the cross-section and slenderness ratio. The long horizontal plateau after the ultimate load is noticed, indicates high degree of ductility. For specimens with higher flat width to thickness ratios the non-linearity starts at 40% of the ultimate load whereas for flat width to thickness ratio less than the limiting, the non-linearity starts at 50% of the ultimate load. Flat width to thickness ratio certainly plays a significant role in the load carrying capacity.

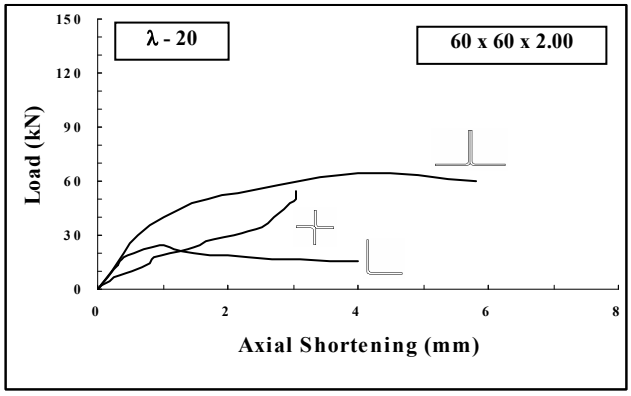


Figure 8. Axial Shortening Behaviour of Stub Angles with Bolted End Connection

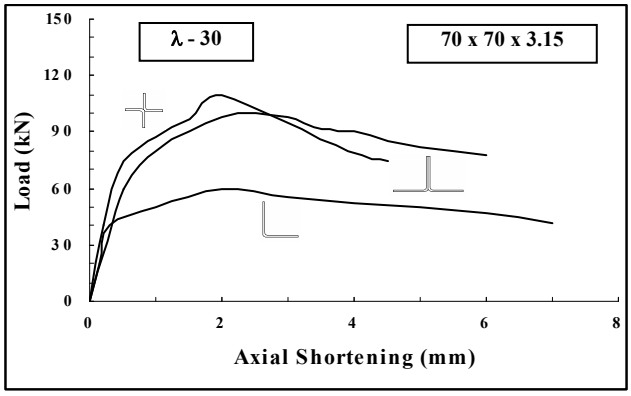


Figure 9. Axial Shortening Behaviour of Short Angles with Bolted End Connection

The initial stiffness is calculated for all the sections tested from the load versus axial shortening behaviour. In the case of angles tested with ball end connection it is observed that the initial stiffness of stub angles was always less than short angles by 25%, irrespective of the configuration of the section. The stiffness of single angles is higher compared to double and starred angles when tested as stub or as short columns. For angles tested with welded end connection, the stiffness of starred angles is over two times when compared to single angles and over 1.3 times as compared to double angles when tested as stub columns. Similarly, in the case of angles tested with bolted end connection, for single and starred angles the initial stiffness of stub columns is higher than that of short columns. For double angles the initial stiffness of short columns is higher than stub columns by 15%.

To quantify the ductility of stub and short columns under different end connections, ductility co-efficient $\mu$ as defined by Han, Zhao and Tao [10] is adopted. It is calculated as the ratio of the axial displacement ($\Delta_u$) corresponding to 85% of ultimate load in the post ultimate region to the axial displacement at yield load ($\Delta_y$). For angles tested with ball end connection, the co-efficient is more for starred angles as compared to single and double angles tested as stub columns by 15 and 45%, respectively. Similarly for angles tested as short column the ductility co-efficient is more for double angles as compared to single and starred angles by 20 and 45%, respectively. For angles with welded ends, the ductility co-efficient of double angles is more as compared to single and starred angles. It is observed that the ductility co-efficient of angles tested with bolted end connection was generally higher than that for angles tested with ball end as well as with welded end connection. The ductility co-efficient of short columns is more as compared to stub columns irrespective of the angle whether single, double or starred.

### 3.3 Load Versus Lateral Deflection Behaviour

The lateral deflections were observed to be meager up to 75% of ultimate load and beyond which the magnitude increases enormously indicating buckling of the flanges for specimens with ball ends. Whereas for angles tested with bolted ends the non-linearity in behaviour starts from the onset of loading. The lateral deflection of connected leg is higher than that of unconnected leg. In most of the cases the lateral deflection behaviour is found to be symmetrical with respect to both the legs indicating that the load transfer is through the axis of the angle. It is observed in general, that lateral deflection is predominant only after 60% of the ultimate load. There is a gradual increase in the elastic limit and at the attainment of the plastic stage there is a sharp increase in the lateral deflection. The load versus lateral deflection behaviour of double angles is distinctively different with those of single angles which have steep initial slope.

### 3.4 Load Versus Strain Behaviour

Figures 10 to 12 show the typical load versus strain behaviour of single angles, double angles welded back-to-back and starred angles with different end connections. In the case of single angles tested with welded ends, it is observed that the portion near the root of the unconnected leg buckled first, and remained compressive throughout. The toe end of the connected leg remained compressive in the initial stage and changed over to tension near the ultimate load, and remained tensile throughout, for all the slenderness ratios.

For double angles, at the toe end of the unconnected legs the compressive strains changed over to tensile strains at 75% of ultimate load. The toe end of the connected legs remained compressive till the failure of the specimen. In the case of starred angles almost the entire cross-section changed over to tension at 70% of ultimate load indicating a twist in the cross-section. The angle failed even before reaching the yield.

In the case of single angles tested with bolted ends, it is observed that the non-linearity in the strain behaviour started much earlier than yield strain. In single angles tested as stub column both compressive and tensile strains prevailed in the legs until failure. For single angles tested as short column, the strains measured at the corner of one of the legs remained tensile and in other locations remained compressive.

For double angles tested as stub column the strains in most of the locations remained within the yield strain irrespective of the configuration of the section. The non-linearity in the behaviour started at 75% of ultimate load. The strains increased more steeply with the increase in load in the case of double angles tested as short columns compared to stub columns. In starred angles when tested as stub column the strains were tensile in all the legs except in one leg, where tensile strain changed over to compressive at 40% of the ultimate load. Similarly in starred angles tested as short columns the strains were initially compressive and later changed over to tensile.

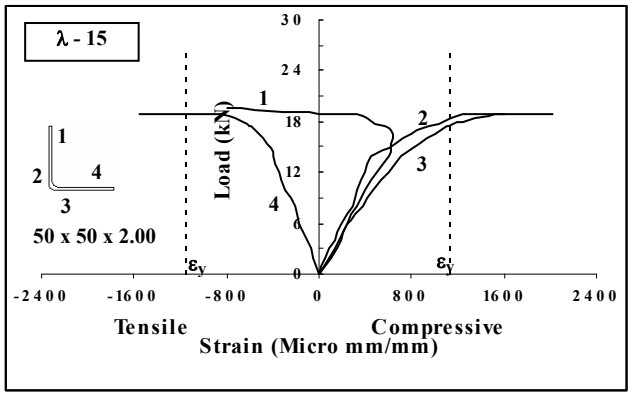


Figure 10. Load Versus Strain Behaviour of Single Stub Angles with Welded End Connection

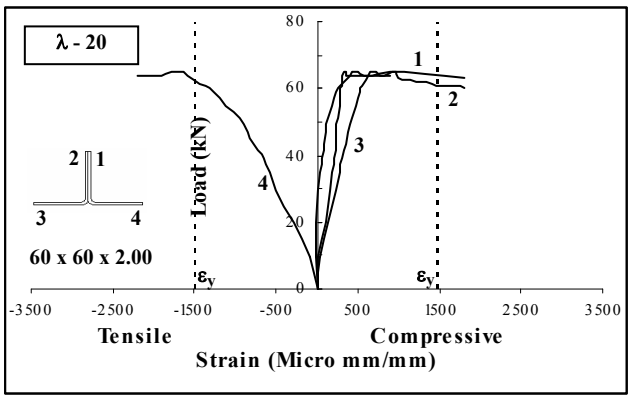


Figure 11. Load Versus Strain Behaviour of Double Stub Angles with Bolted End Connection

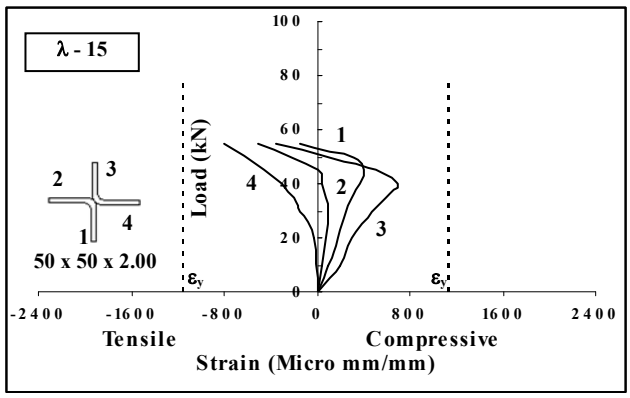


Figure 12. Load Versus Strain Behaviour of Starred Stub Angles with Welded End Connection

## 3.5 Failure Modes of Angles

The mode of failure of all the specimens tested with three different end connections were noticed during testing. The angles failed either by local plate buckling, flexural buckling about the weak axis, torsional-flexural buckling or torsional buckling. The failures were distinctly different for singly symmetric sections and doubly symmetric sections. The mode of failure and the location of failure depends on the slenderness ratio, cross-section and symmetricity of the section. The different failure modes of the angles tested under different end connections are discussed. Local plate buckling was observed in the case of single angles tested with ball end connection. The local buckling occurred at mid height of flange or between mid height and one third of flange of the angle irrespective of the section whether it is stub or short column. Local plate buckling was also noticed in the flanges of stub and short columns of single angles with welded end connection.

Figure 13 shows the failure of single angle by local buckling. In the case of starred angles, local plate buckling was noticed when tested as short columns at mid height of the section with welded end connection. Similarly stub columns tested as double angles welded back-to-back with bolted ends predominantly failed by local buckling caused either at the end of the section or at one-fourth height of the section. In the case of single angles tested as stub columns with bolted end connection, most of the sections failed by local plate buckling initiated either at the mid height or at one-fourth height or at the ends.

Figure 13. Failure of Single Angle by Local Plate Buckling under Bolted End Connection

Failure of double angles welded back-to-back with ball end was also failed by flexural buckling irrespective of the slenderness ratio of the section. The failure of these sections occurred always in the flanges of the sections either at mid height or at one-third height. Single angles tested as short column with bolted end connection failed by flexural buckling at one-fourth height of the section or by local plate buckling initiated at the end of the section. In the case of short columns of double angles and stub columns of starred angles the failure is by flexural buckling. Torsional-flexural buckling was noticed in most of the double angles. It is observed that failure is caused either by flexural or torsional buckling in the case of starred angles tested with ball end connection. The failure occurred between the mid and one-third height of the section in the flanges. Starred stub angles with welded ends failed by flexural buckling. In the case of starred angles tested as short columns with bolted end connection the failure is by torsional buckling. Figure 14 shows the torsional buckling failure of starred angle.

Figure 14. Torsional Buckling of Starred Angle with Bolted End Connection

## 4. CONCLUSIONS

Based on the experimental investigation carried out on the compression behaviour of single angles, double angles welded back-to-back and starred angles, the following conclusions are drawn.

- In the case of angles tested with welded end connection the increase in slenderness ratio from 15 to 30 decreases the ultimate load carrying capacity by 15% in the case of single angles and 10% in the case of double and starred angles.

- For angles with welded end connection the ultimate loads of double and starred angles are 2.10 and 2.20 times more than that of single angles when tested as stub columns.

- For specimens with higher flat width to thickness ratio non-linearity in axial shortening behaviour starts at 40% of the ultimate load whereas for smaller flat width to thickness ratio non-linearity starts at 50%. For stub columns the behaviour is steeper as compared to short columns.

- The initial stiffness of starred angles is twice as compared to single angles and one and a half times more as compared to double angles when tested as stub columns with welded end connection.

- The ductility co-efficient of angles with welded ends is 50% more as compared to angles with ball ends. Similarly the ductility co-efficient of angles with bolted ends is twice as compared to angles with ball ends.

- For double angles with welded ends the compressive strains at the toe end of the unconnected legs changed over to tensile strains at 75% of ultimate load.

- Double angles welded back-to-back with bolted ends failed by local buckling which occurred at the end of the section or at one-fourth the height and starred angles with welded ends also failed by local plate buckling at mid height of the section.

- Single angles tested as short column with bolted ends failed by flexural buckling at one-fourth the height of the section and starred angles tested as short column with bolted ends failed by torsional buckling.

## REFERENCES

[1] Murray, C. Temple and Sherief, S.S. Sakla, "Consideration for the Design of Single Angle Compression Members Attached by One Leg", Proceedings of Structural Stability and Design, Rotterdam, 1995, pp. 107-112.

[2] Popovic, D., Hancock, G.J. and Rasmussen, K.J.R., "Axial Compression Tests of Cold-formed Angles", Journal of Structural Engineering, ASCE, 1999, Vol. 125, No. 5, pp. 515-523.

[3] Popovic, D., Hancock, G.J. and Rasmussen, K.J.R. (2001), "Compression Tests of Cold-formed Angles Loaded Parallel with a Leg", Journal of Structural Engineering, ASCE, Vol. 127, No. 6, pp. 600-607.

[4] Young, B., "Tests and Design of Fixed-Ended Cold-Formed Steel Plain Angle Columns", Journal of Structural Engineering, ASCE, 2004, Vol. 130, No. 12, pp. 1931-1940.

[5] Ellobody, Ehab and Young, Ben, "Behaviour of Cold-formed Steel Plain Angle Columns", Journal of Structural Engineering, ASCE, 2005, Vol. 131, No. 3, pp. 457-466.

[6] ASTM : 370 - 92, "Standard Test Methods and Definitions for Mechanical Testing of Steel Products", 1996.

[7] AISI Manual, "Cold-formed Steel Design Manual", American Iron and Steel Institute, 1996.

[8] IS : 801, "Code of Practice for Use of Cold-formed Light Gauge Steel Structural Members in General Building Construction", Bureau of Indian Standards, 1975.

[9] IS : 811, "Specification for Cold-formed Light Gauge Structural Steel Sections", Bureau of Indian Standards, 1987.

[10] Han, L.H., Zhao, X.L. and Tao, Z., "Tests and Mechanics Model for Concrete-filled SHS Stub Columns, Columns and Beam-columns", Steel and Composite Structures, 2001, Vol. 1, No.1, pp. 51-74.

# THE BEHAVIOUR AND DESIGN OF LAP-JOINTS IN THIN-WALLED BAR CONSTRUCTIONS

W. Wuwer[1]

[1] *Associate Professor, D.Sc., PhD. Eng., Faculty of Civil Engineering, Department of Building Structures, Silesian University of Technology, Gliwice, Poland*
[*] *(Corresponding author: E-mail: Walter.Wuwer@polsl.pl)*

*Received: 12 March 2007; Revised: 2 May 2007; Accepted: 3 August 2007*

**ABSTRACT:** The paper presents the results of checking experimentally the way of calculating an m-bolt single-cut joint with blind-bolts, dealt with by Wuwer [1, 2]. The method of calculating any arbitrary lap-joint was checked there by testing symmetrical five-blind-bolt and eight-blind-bolt joints of cold-bent profiles, the walls of which were 5.0 mm thick, respectively: stretched eccentrically and alternately bent. The present report, however, deals with the results of investigations on test elements with asymmetrical four-blind-bolt joints of walls, 4.0 mm thick, which were simultaneously subjected to bending and shearing. In all the three kinds of joints single-cut blind bolts type BOM-Rl6-4 were used [3]. Loads increasing proportionally until the destruction of the joint, were reiterated cyclically on stabilized levels. The set of equations describing the static behaviour of a joint was solved numerically, and the results were compared with the results of experimental investigations. For the bolt subjected to the highest effort in the 4-blind-bolt joint boundary curves of the load-carrying capacity were plotted for three cases of boundary states I, II and III. Moreover, the boundary curve of the load-carrying capacity was determined for the boundary state I. Basing on the example of a frame with flexible joints attempts have been made as well to assess the influence of interactive connections between three rigidities in a lap-joint, combined with a rotation and two shifts (perpendicular to each other) between the joined walls of sheet-metal sections. Each of the three instantaneous rigidities has been expressed by the coefficient of rigidity reduction and the parameter of rigidity degradation, depending on the quantities acting in the joint of the loads $M$, $V$ and $H$.

**Keywords:** sheet-metal section; single-cut joint; instantaneous centre of rotation; rotational friction; boundary curve of the load-carrying capacity; instantaneous rigidity; coefficient of rigidity reduction; rigidity degradation

## 1. INTRODUCTION

The correctness of the method of calculating single-cut lap-joints of thin walls with blind bolts was checked experimentally on the example of three different single-cut lap-joints (Figure 1):
a) a symmetrical 5-blind-bolt joint of walls, 5.0 mm thick, presented by Wuwer [1],
b) a symmetrical 8-blind-bolt joint of walls, 5.0 mm thick, presented by Wuwer [2],
c) an asymmetrical 4-blind-bolt joint of walls, 4.0 mm thick, presented by Wuwer [4].

All the joints in the test elements consisted of five, eight and four blind bolts, type BOM R16, class 12.9, with a diameter of $d$ = 13.6 mm [3]. In the case of walls with a thickness of 5.0 mm the blind bolts were mounted in holes ∅14.0 mm in diameter, whereas in the case of walls with a thickness of 4.0 mm the diameter of the holes amounted to 14.3 mm. Steel profiles with walls 4.0 and 5.0 mm thick were made of the same kind of steel: St3SX (according to Polish standard), S235 JR (according to Eurocode 3). The technology of joining permitted, according to the recommendations of their producer, holes with diameters of 13.8÷14.8 mm. After the bolt had been inserted by means of a so-called embedder, it was quite tight (Figure 2). With the growing load, the bolts were gradually tilted, and they began to work in a complex state of stresses.

All the numerical calculations were carried out by Dr Ryszard Walentynski from the Chair of the Theory of Designing, Silesian University of Technology, by means of the programme Mathematics, among others in Reference [5]. These calculations consisted in the solution of a set of ($m$ + 3) equations, describing the static behaviour of a joint comprising three equations of equilibrium and $m$ physical equations, formulated by means of the geometrical connections in the joint, where $m$ –

number of the blind bolts in the joint. A physical (constitutive) equation was the anti-function versus the exponential dependence $S_1$-$\delta_{L+E}$, which connects the load $S_1$ of a single bolt with the mutual displacement $\delta_{L+E}$ of the stretched walls, 4.0 mm or 5.0 mm thick, in the single-cut lap-joint.

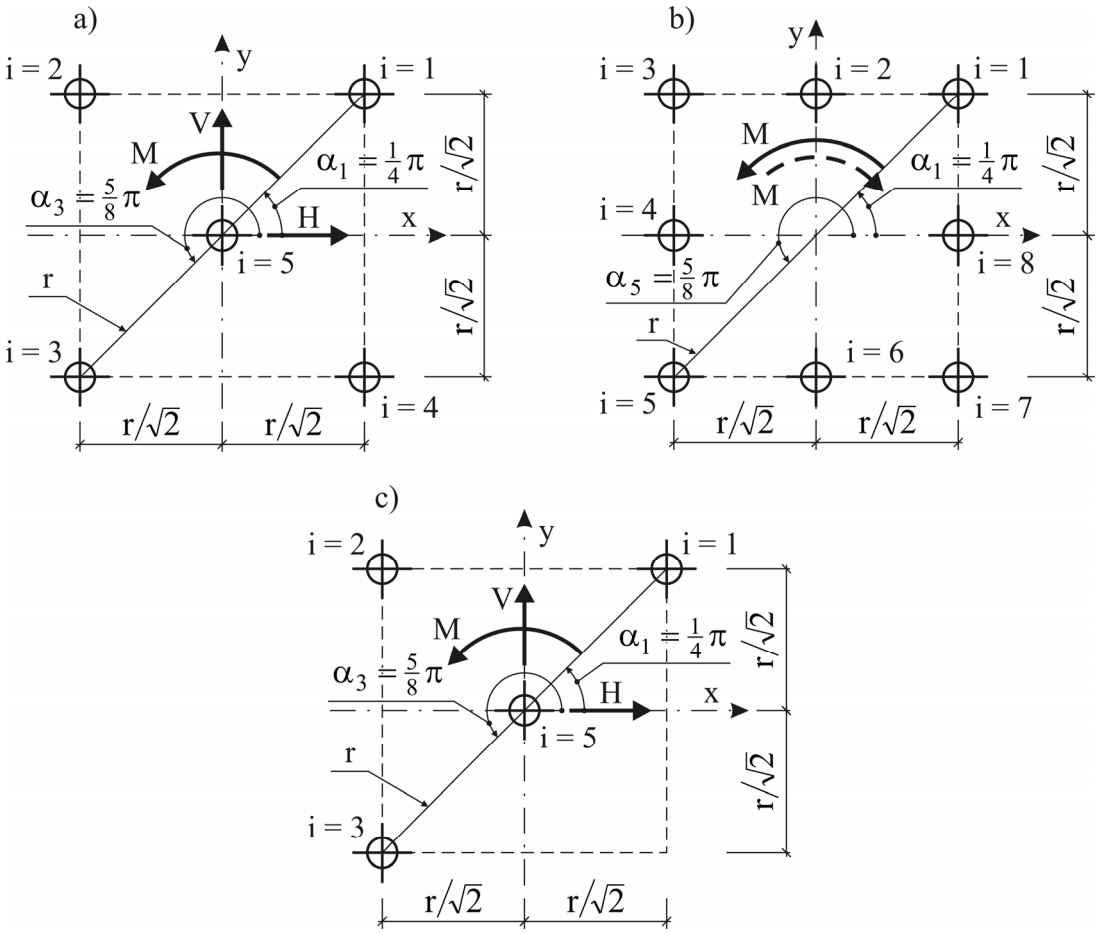


Figure 1. Numerically and Experimentally Tested Joints:
a) Symmetrical Five-blind-bolt Joint of Walls, 5.0 mm thick,
b) Symmetrical Eight-blind-bolt Joint of Walls, 5.0 mm Thick,
c) Asymmetrical Four-blind-bolt Joint of Walls, 4.0 mm Thick

Figure 2. State of the Filling of Holes in Sheet Iron by Bolts

## 2. RESULTS OF INVESTIGATIONS CONCERNING SYMMETRICAL JOINTS

In two identical experimental elements "V", denoted as V-200,5.1/5 and V-200,5.2/5, a lap joint with five bolts of the type BOM R16-6 (cf. Figure 1a) was cyclically loaded and relieved at various levels of loading $F$. To this joint were transmitted: the shearing force $V = F$ and the bending moment $M = F \cdot e = V \cdot e$ (Figure 3a). The displacements were measured by means of two pairs of dial indicators, mounted on the axes of two connected rods 200×60×5 (Figure 3b).

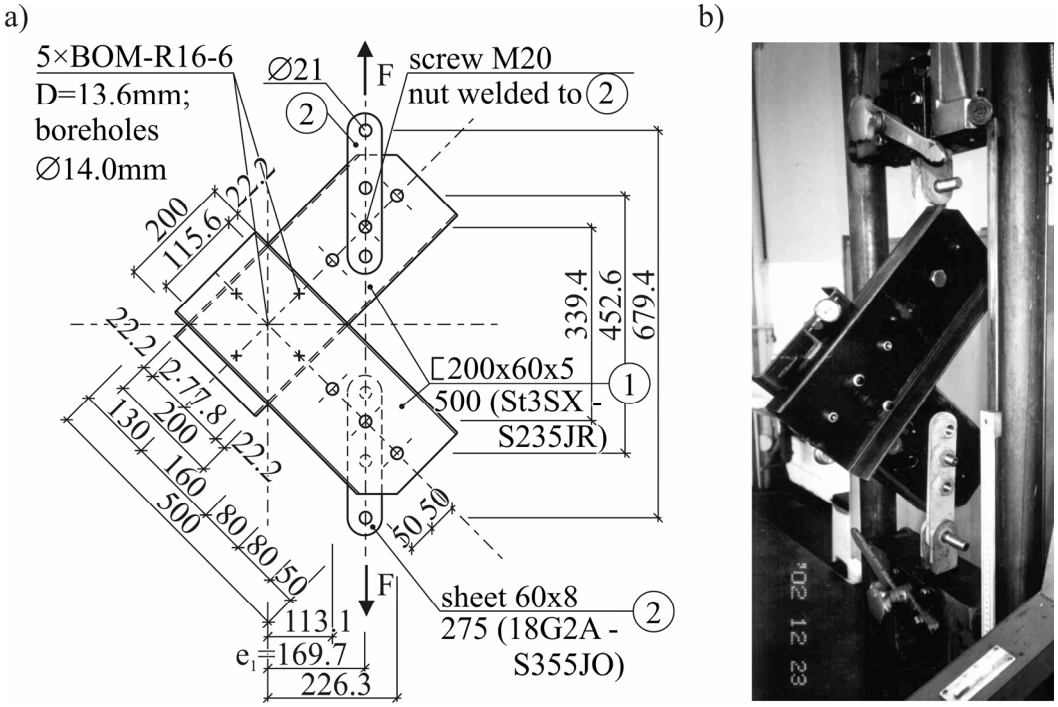


Figure 3. Test Element "V": a) Dimensions, b) View of the Investigated Element, [1]

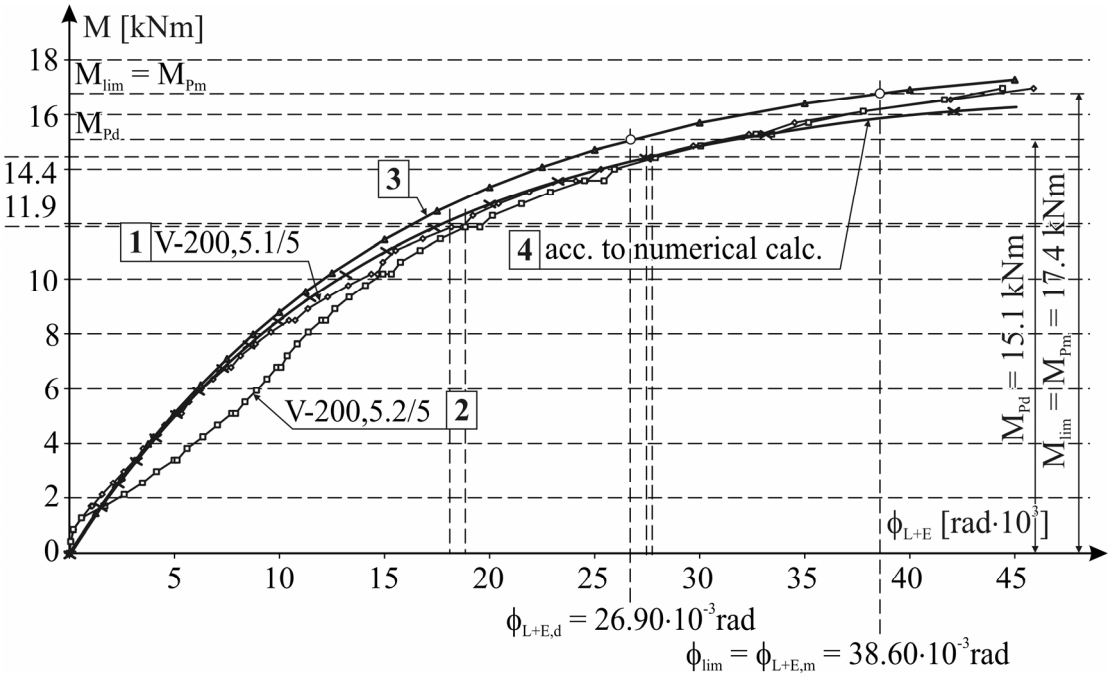


Figure 4. Relation $M$-$\phi$: Broken Lines 1 and 2 for Joints in the Test Elements "V", Curve 3 – for Joint Loaded Only by the Moment M, Curve 4 – acc. to Numerical Calc., [1]

The equations describing the behaviour of a five-blind-bolt joint in the test element "V" were solved numerically by means of the programme "Mathematica". The obtained results of calculations permitted to plot the curve 4 in the diagram $M$-$\phi$ (Figure 4). The broken lines 1 and 2 correspond to the envelope curves of static equilibrium, obtained in two experimental elements "V". Curve 3 illustrates the behaviour of a five-blind-bolt joint, analogical to the joint tested in the test element "V", but loaded only by the moment $M$.

In two identical test elements, denoted as X-200,5.1/8 and X-200,5.2/8, a eight-blind-bolt joint was tested, loading it cyclically with alternate bending moments $M = \pm\sqrt{2} \cdot b \cdot F$ (Figure 5).

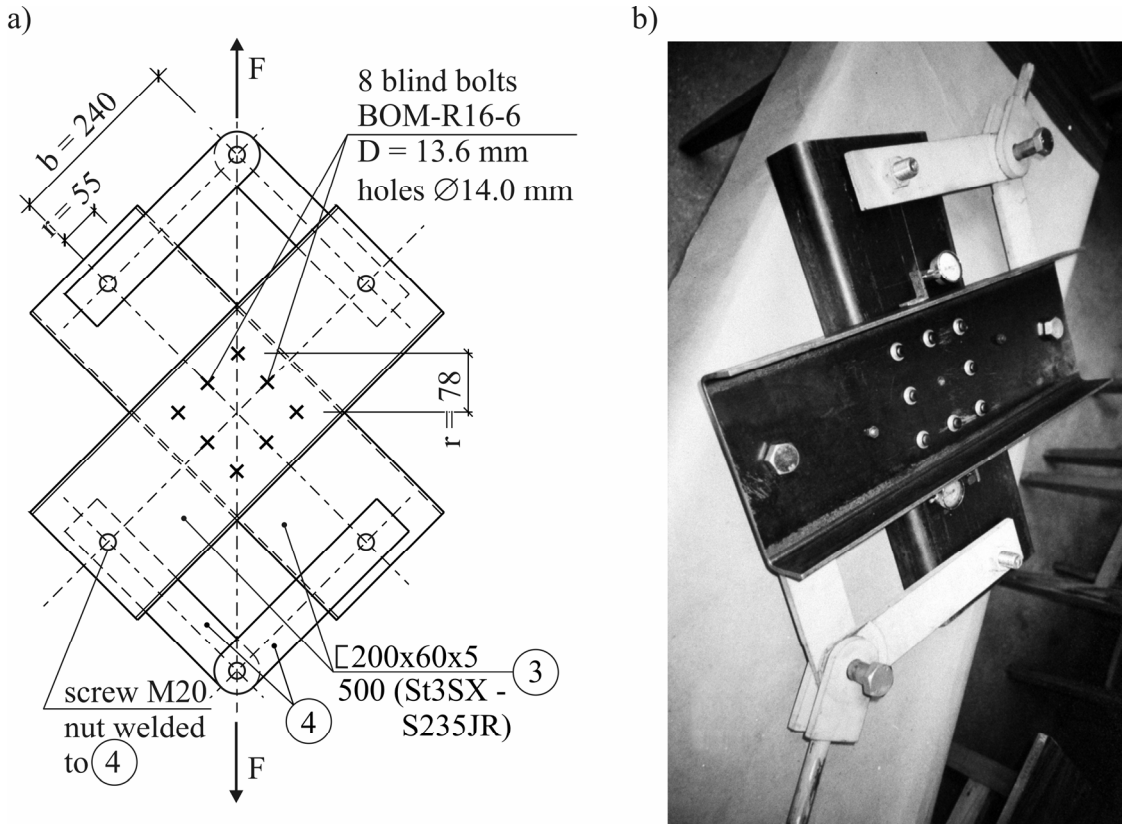


Figure 5. Experimental Element X-200,5.1/8:
a) Construction and Dimensions of the Element, b) Element Anchored in the Testing Machine

The behaviour of these joints is illustrated by two paths of static equilibrium (Figure 6). It is to be noted that in the case of more fasteners in the joint, the envelope curves of the paths of static equilibrium 1 and 2 are more or less similar coinciding better than in the case of 5-blind-bolt joints (cf. Figure 4). We may suppose that when there are more fasteners, the sensitivity to the accuracy of the drilling the holes in the joint is smaller, and so is the sensitivity to the sequence of mounting the blind bolts in the holes.

It is obvious that the investigated eight-blind-bolt are actually more rigid than might be assumed basing on numerical calculations, the results of which were used to plot the curve No. 3 in the diagram.

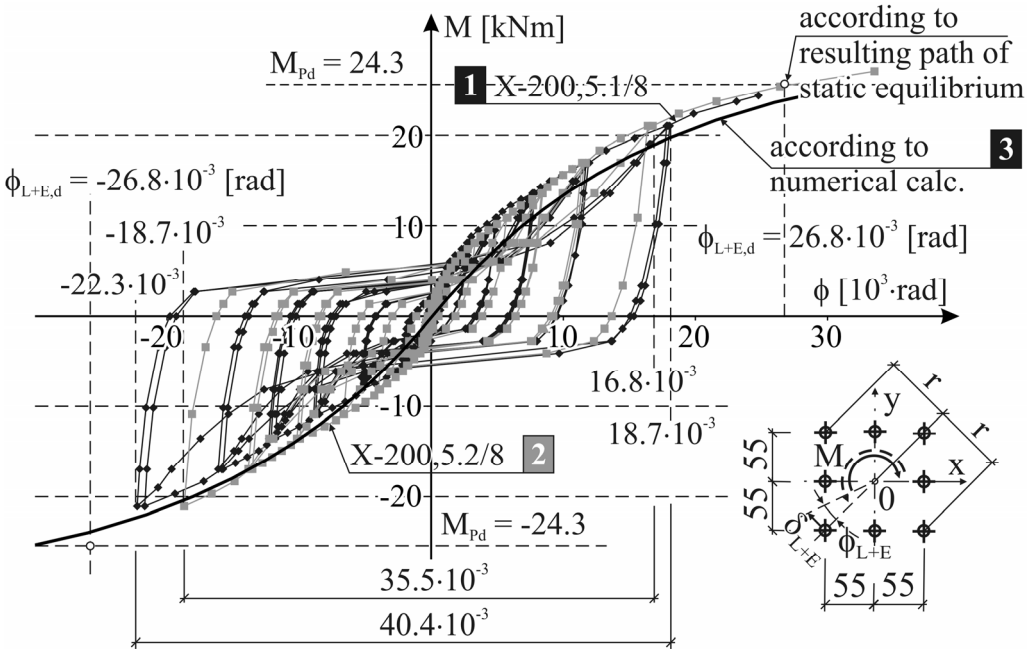


Figure 6. Relation $M$-$\phi$ of the Eight-blind-bolt Joints in Experimental Elements X-200,5.1/8 and X 200,5.2/8

## 3. THE EFFORT OF AN ASYMMETRIC JOINT WITH FOUR-BLIND-BOLTS OF SHEET-METAL

### 3.1. Experimental Investigations

In result of experimental investigations:
- the load-carrying capacity of a bolt in a single-cut joint of walls, 4.0 mm thick, was determined,
- the resulting path of static equilibrium, for the relation $S_1$-$\delta_{L+E}$, was determined,
- three analogical 4-blind-bolt joints were stretched.

In order to determine the calculated load-carrying capacity of a bolt five analogical test elements "I" with a 2-blind-bolt joint, subjected to monotonically increasing axial stretching by the force $F$, were tested. The behaviour of a joint, e.g. in the element I-100, 4.2/2, is demonstrated by the path of static equilibrium in Figure 7.

In compliance with the Recommendations [6] the force which destroys a single bolt in the joint, i.e. the value $S_1 = P_m$ should, be determined as a load which leads to the mutual displacement of the joined walls amounting to $\delta_{lim}$ = 3.0 mm. In the five tested 2-blind-bolt joints the values of the forces $P$ amounted to 40.84 kN, 40.26 kN, 42.12 kN, 40.75 kN and 37.61 kN. Basing on these values the mean boundary value $P_{m,med}$ = 40.315 kN was found, after which the value of the characteristic load $P_k$, was calculated, making use of the formula

$$P_k = P_{m,med} - c \cdot s\,, \tag{1}$$

where: $c$ – a coefficient depending on the number of investigated test elements; in the case of five elements it had been assumed to be $c$ = 2.13; $s$ – standard deflection, calculated in compliance with the guidelines, amounting to $s$ = 1.664 kN; thus, according to (1) $P_k$ = 40.313 – 2.13 · 1.654 = 36.77 kN. The calculated load-carrying capacity $P_d$, of the investigated joint was determined to be equal to $P_d = P_k / \gamma_m$; for the partial factor of safety $\gamma_m$ = 1.1 it amounted to $P_d$ = 36.77 / 1.1 = 33.43 kN.

The doubled values $P_d$ =33.43 kN and $P_{m,med}$ = 40.315 kN were plotted in the diagram $F$-$\delta_{L+E}$ (cf. Figure 7).

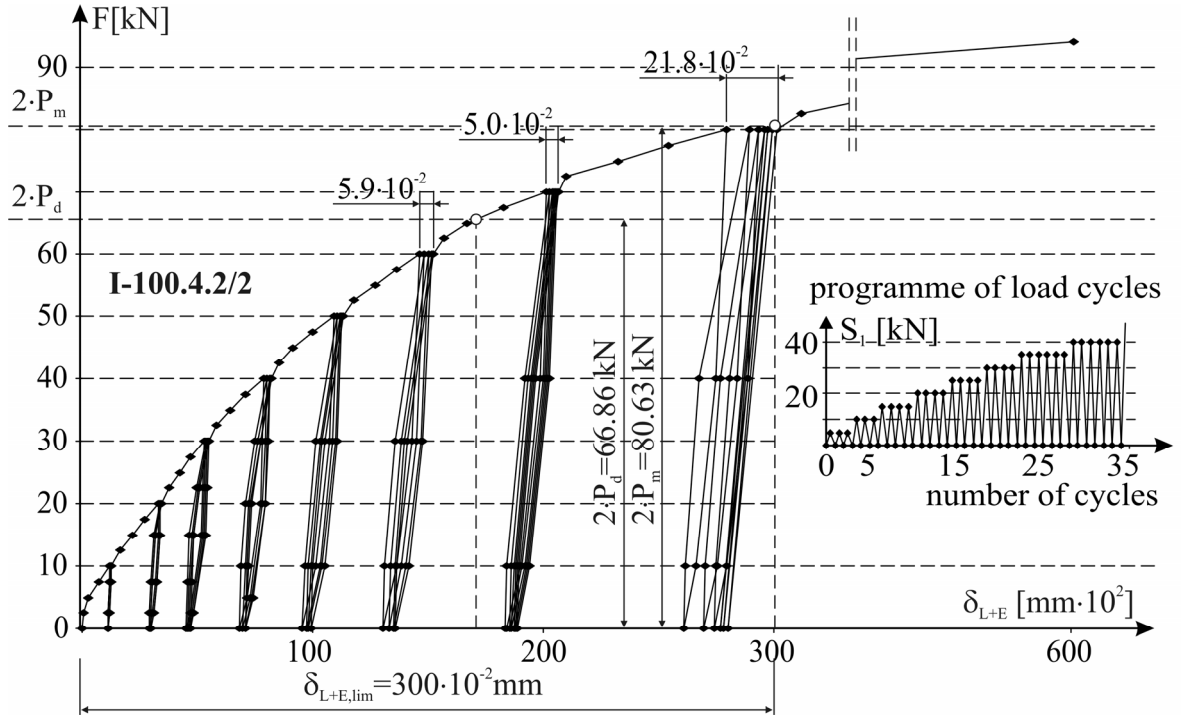


Figure 7. The Path of Static Equilibrium $F$-$\delta_{L+E}$ for a Joint in the Element I-100, 4.2/2 (36 cycles of loading), [4]

The envelope curves of the paths of static equilibrium, denoted by broken lines, obtained in five test elements "I", were compared in a common diagram of the relation $S_1$-$\delta_{L+E}$ (Figure 8). Making use of; the programme Curve Expert the following exponential function of the regression curve, describing the behaviour of a bolt in the joint, was determined statistically:

$$S_1 = a_s\left(1 - e^{-b_s \cdot \delta_{L+E}}\right). \tag{2}$$

In compliance with Eq. 2 the mutual displacement of the joined iron-sheets equal to $\delta_{L+E,d}$ = $205.7 \cdot 10^{-2}$ mm, corresponds to the calculated load-carrying capacity of the bolt $P_d$. The scattered results are characteristic, particularly the irregular ones in the range of displacements $\delta_{L+E} \leq \delta_{L+E,d}$, i.e. below the calculated load-carrying capacity $P_d$ = 33.43 kN.

Additionally, a diagram of the relation "load $S_1$ – increment of the displacement $\Delta\delta_{L+E}$" (Figure 9) was plotted, which also proves that the "breakdown" of the load-carrying capacity of the bolt really occurred in the loading range $S_1$ = (30 ÷ 40) kN, containing the load-carrying capacity $P_d$ = 33.43 kN. The values, of the increments of displacements $\Delta\delta_{L+E}$ exerted on each single joint, correspond in the diagram to the increase of the load $\Delta S_1$ equal to 5.0 kN.

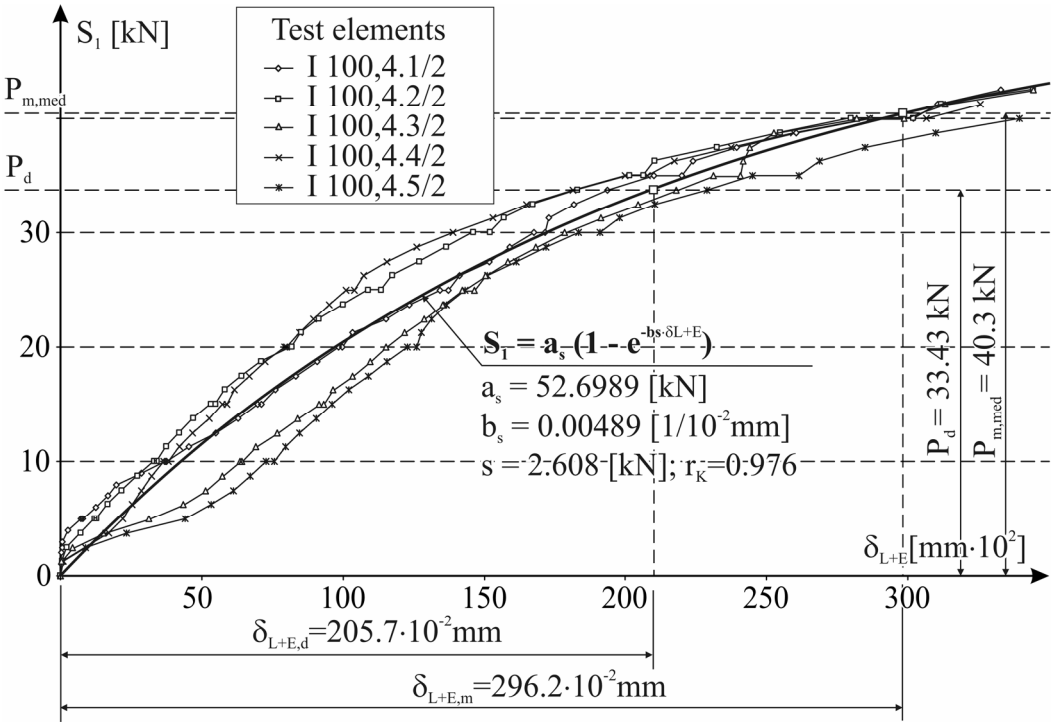


Figure 8. The Relation $S_1$-$\delta_{L+E}$ in the Case of Joining Walls, 4.0 mm Thick, in Five Elements of the Type "I", [1]

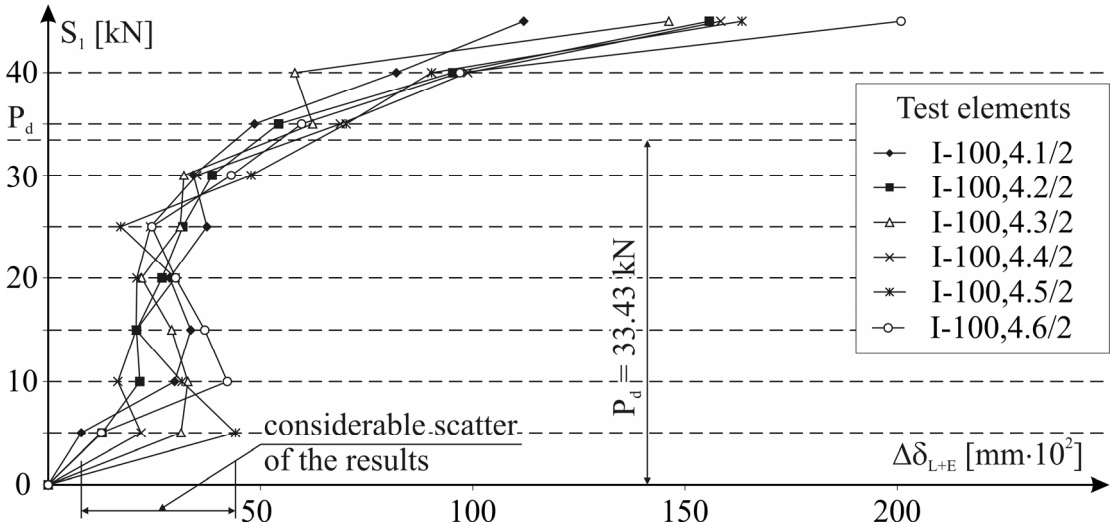


Figure 9. The Dependence $S_1$-$\Delta\delta_{L+E}$ of 2-blind-bolt Joints in Five Test Elements "I", [4]

Similarly, according to Recommendations [6] the calculated load-carrying capacity of the BOM R16-6, joining two walls, 5.0 mm thick, $P_d$ = 48.6 kN, as well as its corresponding value of the mutual displacement of the walls $\delta_{L+E,d} = 209.3 \cdot 10^{-2}$ mm, were determined first experimentally and then statically Wuwer [1]. The resulting paths of static equilibrium $S_1$-$\delta_{L+E}$ for two tested thickness 4.0 mm and 5.0 mm of the walls illustrates diagram on Figure 10.

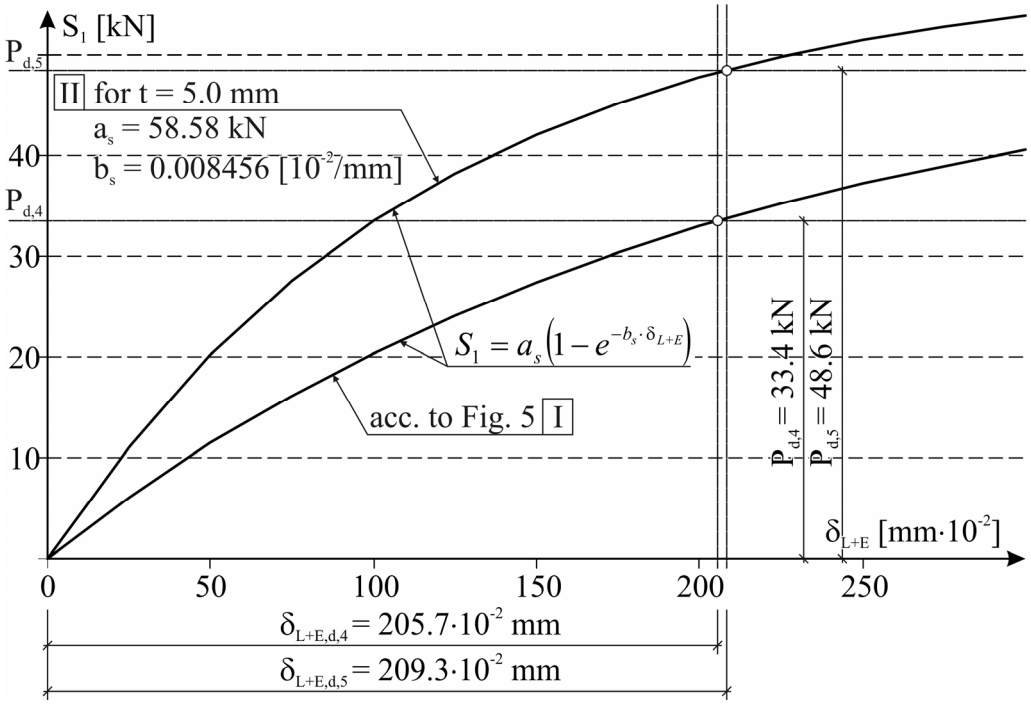


Figure 10. The Resulting Paths of Static Equilibrium $S_1$-$\delta_{L+E}$: I – for Thickness of the Wall $t$ = 4.0 mm, II – for Thickness of the Wall $t$ =5.0 mm

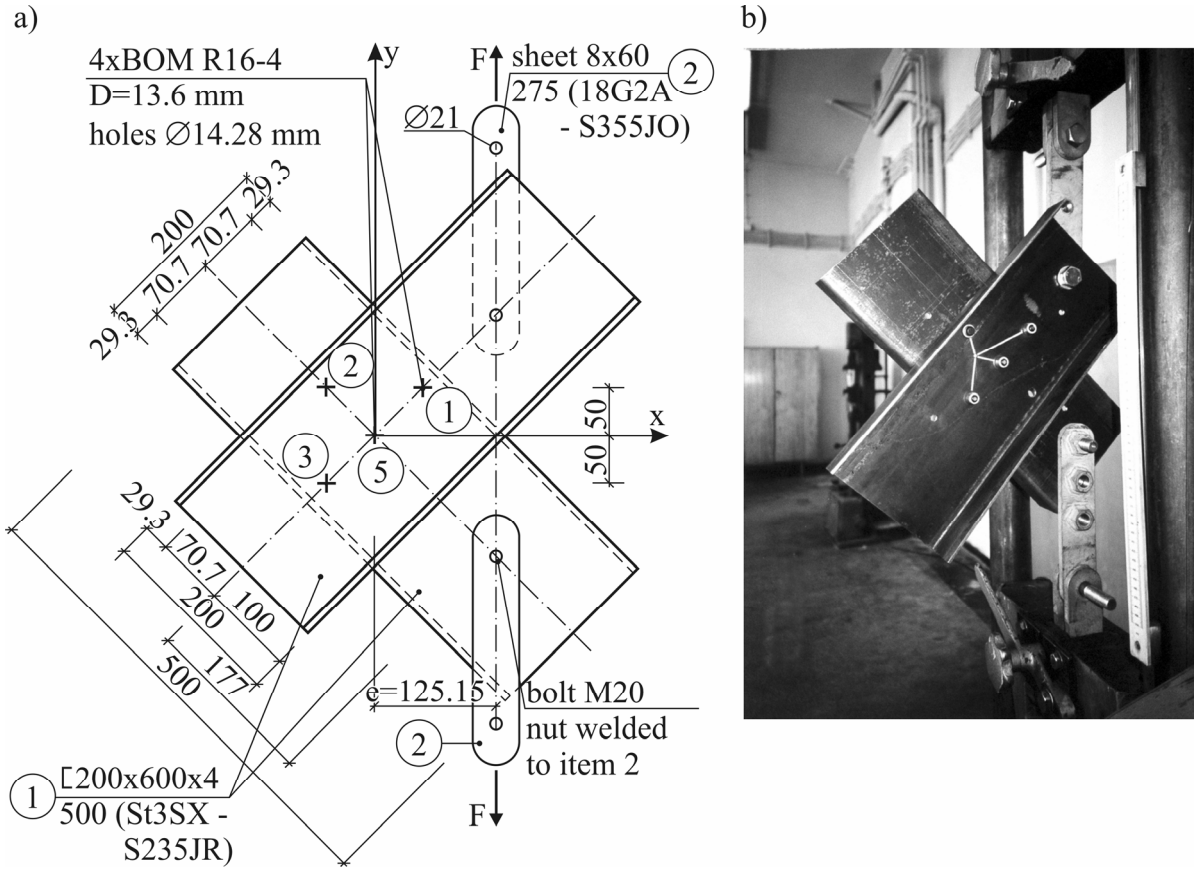


Figure 11. Test Element “V”: a) Construction and Dimensions, b) Element Anchored in the Press

Four-bolt joints were investigated in three identical test elements: V-200.4.1/4, V-200.4.2/4 and V-200.4.3/4 (Figure 11). Bolts of the type BOM R16-4 with diameters of 13.6 mm were placed in holes $d$ = 14.3 mm, drilled simultaneously in both walls, the channel bars being mutually immobilized. The joint was stretched eccentrically by the force $F$, pulsating and monotonically increasing to destruction.

The displacements were measured by means of two dial indicators, attached in the axes of the joined bent channel bars 200×60×4 to the shelves – parallelly to the axes of these sections (Figure 11b). In the plan of displacements occurring in the joint (Figure 12) the average displacements of the "upper" wall $\delta_{ig}$ (the web of the "upper" channel bar) were plotted, corresponding to the $i$-th bolt, denoted in the axis of the indicator, and the axis of the bolt $\delta_{ig,cz}$ (the displacement constituted a half of the entire value $\delta_{i,sw}$). The radii $r_{i,R}$ connecting the instantaneous centre of rotation $R$ with axes of four bolts were denoted subsequently as $r_{1,R}$, $r_{2,R}$, $r_{3,R}$ and $r_{5,R}$.

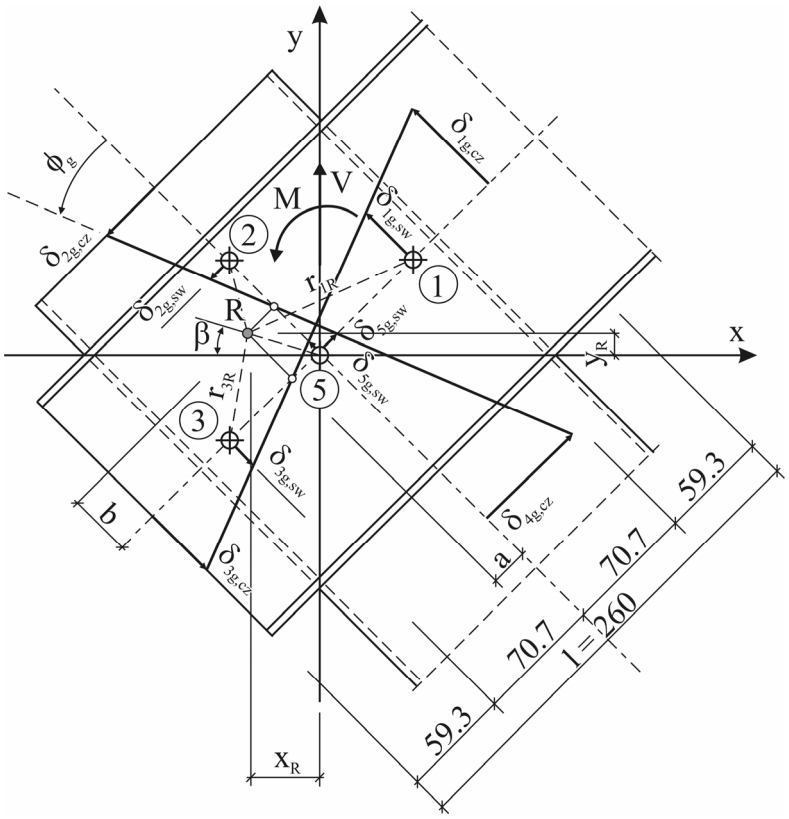


Figure 12. Plan of Displacements in the Axes of Dial Indicators and Blind Bolts in a Joint of the test element "V"

The geometrical relations in the destorted joint permitted to determine the values of the angles of rotation $\phi$ between the values of the coordinates $x_R$ and $y_R$ of the instantaneous "wandering" centre of rotation.

The behaviour of three joints is displayed by the paths of static equilibrium in the diagram $M$-$\phi$ (Figure 13). One of them proved to be stiffer than the other two.

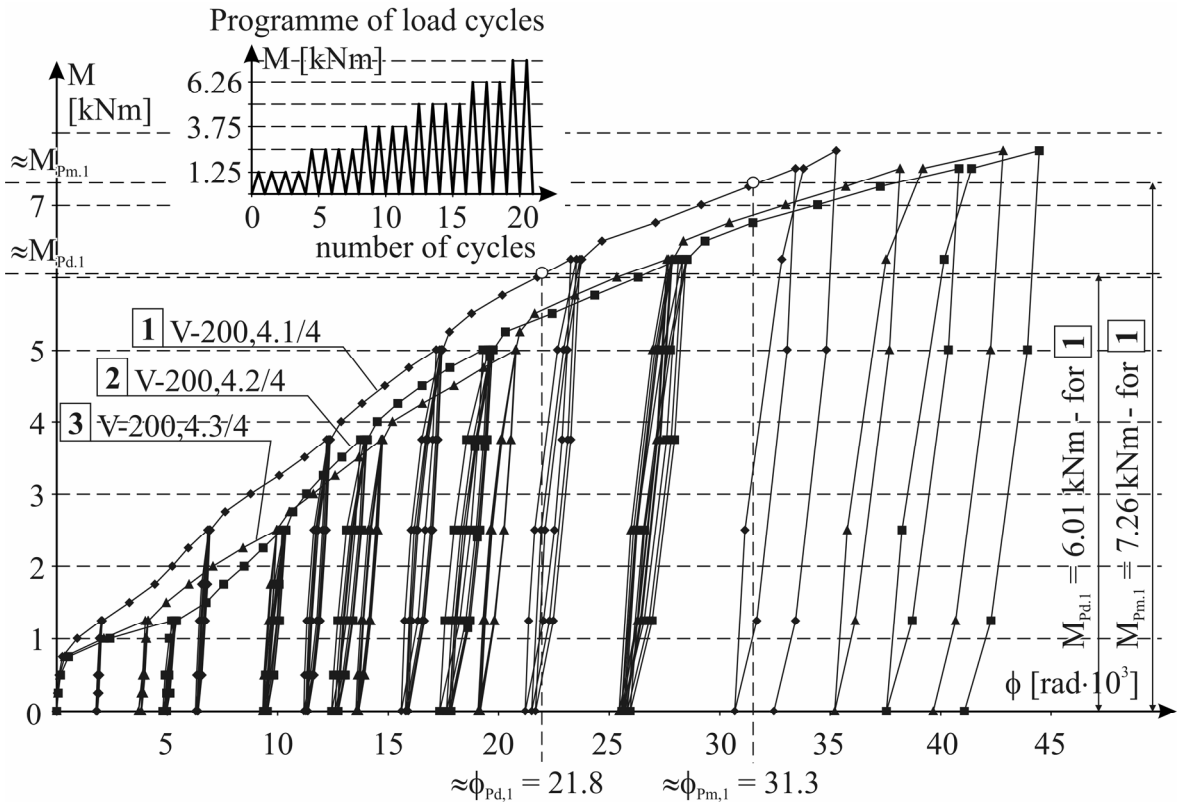


Figure 13. Paths of Static Equilibrium $M$-$\phi$ of a 4-bolt joint in the Test Elements: V-200,4.1/4, V-200,4.2/4 and V-200,4.3/4

### 3.2. The Set of Equations Describing the Behaviour of a 4-blind-bolt Joint

The set of seven equations formulated in compliance with the suggestion put forward by Wuwer [1] comprises:

- three equations of equilibrium:

$$H - u\left(\frac{S_1}{\delta_1} + \frac{S_2}{\delta_2} + \frac{S_3}{\delta_3} + \frac{S_5}{\delta_5}\right) + \frac{r\cdot\phi}{\sqrt{2}}\left(\frac{S_1}{\delta_1} + \frac{S_2}{\delta_2} - \frac{S_3}{\delta_3}\right) = 0\,, \tag{3}$$

$$V - v\left(\frac{S_1}{\delta_1} + \frac{S_2}{\delta_2} + \frac{S_3}{\delta_3} + \frac{S_5}{\delta_5}\right) - \frac{r\cdot\phi}{\sqrt{2}}\left(\frac{S_1}{\delta_1} - \frac{S_2}{\delta_2} - \frac{S_3}{\delta_3}\right) = 0\,, \tag{4}$$

$$\sqrt{2}\frac{M}{r} + u\left(\frac{S_1}{\delta_1} + \frac{S_2}{\delta_2} - \frac{S_3}{\delta_3}\right) - V\left(\frac{S_1}{\delta_1} - \frac{S_2}{\delta_2} - \frac{S_3}{\delta_3}\right) - \sqrt{2}\cdot r\cdot\phi\left(\frac{S_1}{\delta_1} + \frac{S_2}{\delta_2} + \frac{S_3}{\delta_3}\right) = 0\,, \tag{5}$$

- four constitutive (physical) equations, which after the introduction of the geometrical relations in the joint take the following form:

$$\delta_1 - \sqrt{\left[u - \frac{r\cdot\phi}{\sqrt{2}}\right]^2 + \left[v + \frac{r\cdot\phi}{\sqrt{2}}\right]^2} = 0\,, \tag{6}$$

$$\delta_2 - \sqrt{\left[u - \frac{r \cdot \phi}{\sqrt{2}}\right]^2 + \left[v - \frac{r \cdot \phi}{\sqrt{2}}\right]^2} = 0\,, \tag{7}$$

$$\delta_3 - \sqrt{\left[u + \frac{r \cdot \phi}{\sqrt{2}}\right]^2 + \left[v - \frac{r \cdot \phi}{\sqrt{2}}\right]^2} = 0\,, \tag{8}$$

$$\delta_5 - \sqrt{u^2 + v^2} = 0\,. \tag{9}$$

In the Eq. 6 ÷ Eq. 9 the initial constitutive equation had the form $\delta_i = f(S_i)$ and was an anti-function to the exponential function Eq. 3. The unknown values in the set of equations are the total displacements $u$, $v$ and $\phi$ occurring between the joined walls and the combined forces $S_i$, exerted on the four bolts in the joint, i.e. $S_1$, $S_2$, $S_3$ and $S_5$.

### 3.3. Comparison of Experimental and Numerical Results

The diagram $M$-$\phi$ (Figure 14) provides a comparison of the three broken lines 1, 2 and 3, corresponding to the envelope curves of the paths of equilibrium in three test elements "V", with the curve 4 obtained by numerical calculations. The curve 5 was obtained making use of the programme Robot Millennium v.15 [9], which did not take into account the interactive relations, occurring in the joint between the rigidity with respect to the direction of the shearing force $V = F$ and the rotational rigidity at the bending moment $M = V \cdot e$. The investigated joints were, therefore, actually stiffer (cf. the broken lines 1, 2, 3) than the results of the numerical analysis (curve 4) would indicate, and more flexible, when in the calculations the interaction between two rigidities (curve 5) is neglected.

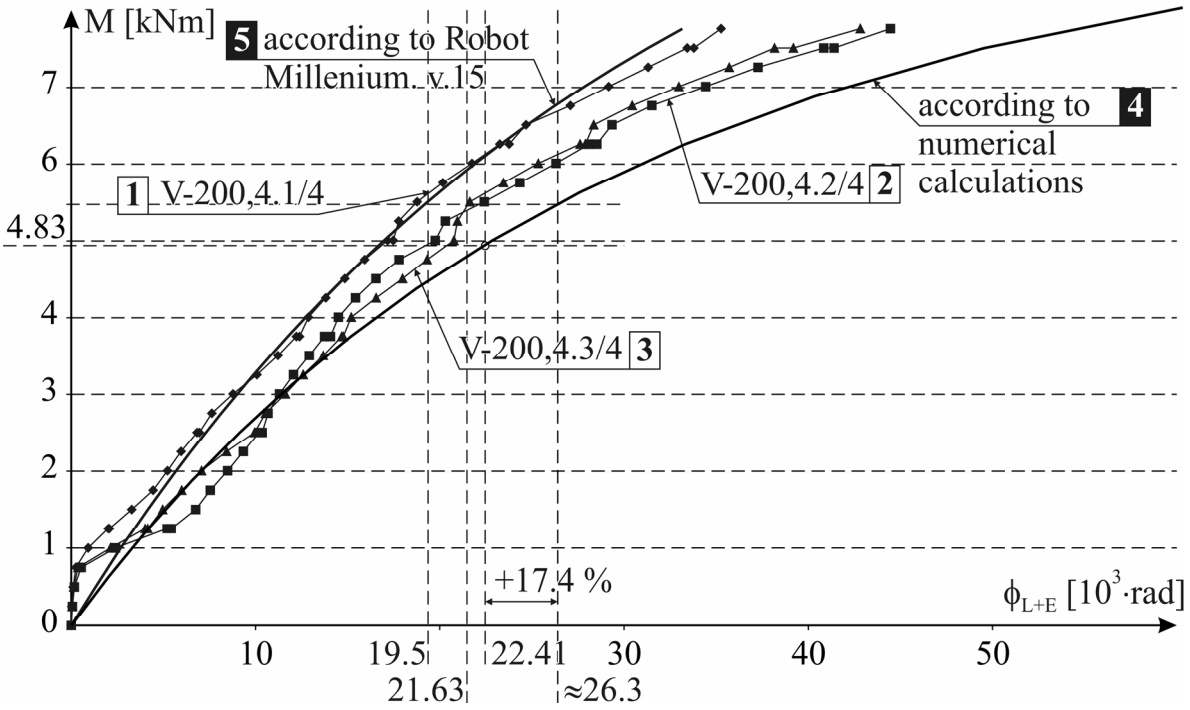


Figure 14. Relation $M$-$\phi$: Broken Lines 1, 2 and 3 – for 4-blind-bolt Joints in "V" Elements;
Curve 4 – According to Numerical Calculations;
Curve 5 – According to Robot Millennium v.15, [9]

The obtained results can also be assessed by comparing in Table 1 the values of the measured coordinates of the instantaneous centre of rotation $x_R$ and $y_R$, with the values obtained as the result of numerical analysis.

Table 1. Values of the Coordinates of the Instantaneous Centre of Rotation $x_R$, $y_R$ for the Joint as in Figure 12

| Loads of the joints | | V-200,4.1/4 | | V-200,4.2/4 | | V-200,4.3/4 | | mean values | | acc. to numerical calculations. | | Difference in % | |
|---|---|---|---|---|---|---|---|---|---|---|---|---|---|
| $V = F$ [kN] | $M = V \cdot e$ [kNm] | $x_R$ [mm] | $y_R$ [mm] | $x_R$ [mm] | $y_R$ [mm] | $x_R$ [mm] | $y_R$ [mm] | $x_R$ [mm] | $y_R$ [mm] | $x_R$ [mm] | $y_R$ [mm] | [(9)/(11) -1] ·100 | [(10)/(12) -1]·100 |
| *1* | *2* | *3* | *4* | *5* | *6* | *7* | *8* | *9* | *10* | *11* | *12* | *13* | *14* |
| 0.0 | 0.0 | 0.0 | 0.0 | 0.0 | 0.0 | 0.0 | 0.0 | 0.0 | 0.0 | 0.0 | 0.0 | 0.0 | 0.0 |
| 10.0 | 1.252 | -42.6 | 11.2 | -46.8 | 8.5 | -34.5 | 11.4 | -41.3 | 10.4 | -37.7 | 12.4 | 9.6 | -16.1 |
| 20.0 | 2.504 | -36.9 | 10.7 | -42.4 | 13.0 | -36.5 | 5.6 | -38.6 | 9.8 | -38.0 | 12.2 | 1.6 | -19.7 |
| 30.0 | 3.756 | -33.1 | 10.3 | -39.9 | 13.4 | -37.4 | 8.7 | -36.8 | 10.8 | -38.3 | 12.1 | -3.9 | -10.7 |
| 40.0 | 5.008 | -34.2 | 10.9 | -39.6 | 12.5 | -37.4 | 10.7 | -37.1 | 11.4 | -38.6 | 11.9 | -3.9 | -4.2 |
| 50.0 | 6.260 | -35.7 | 11.3 | -39.9 | 12.9 | -37.9 | 11.4 | -37.8 | 11.9 | -39.0 | 11.8 | -3.1 | 0.8 |
| 60.0 | 7.512 | -37.5 | 12.3 | -40.3 | 12.8 | -38.4 | 13.0 | -38.7 | 12.7 | -39.4 | 11.8 | -1.8 | 7.6 |
| 62.0 | 7.762 | -37,8 | 12,3 | -40.4 | 12.5 | -38.9 | 13.3 | -39.0 | 12.7 | -39.5 | 11.8 | -1.3 | 7.6 |

### 3.4. Reasons of the Differences between Experimental and Theoretical Results

The scatter of results in bent and sheared 4-blind-bolt joints, which neither in their character nor in their quantity deviate from those occurring in stretched 2-blind-bolt joints (cf. Figures. 8 and 13). The scatter of results may be due to:

a) the technique of embedding the bolts in the holes,
b) the accuracy of drilling in the joined walls,
c) the fatigue of the material of the wall in the borehole, caused by the low-cyclic loading exerted by the side surface of the bolt mandrel,
d) the forces of sliding friction in the stretched joint,
e) the forces of .journal friction in a simultaneously stretched and bent joint.

The reason for which the producer permits to embed bolts with a diameter of 13.6 mm in boreholes, the diameters of which are contained in the range of 13.3÷14.8 mm, may be accounted for by the differentiated flexibility of the joints, but – as has turned out – this is not the most important reason. The accuracy of drilling all the bore-holes separately in the individual walls of the elements "I" by hand may affect to some extent the filling of the holes with the material of the blind bolt sleeve, although not essentially, because in the case of "V" elements in which the holes were drilled and the bolts were embedded in immobilized sections the values were still scattered.

Presumably the fatigue of the material in the vicinity of the bolts may also have influenced the variety of results. The crystalline structure of steel in the pressed wall of the hole may have undergone changes caused by the reiterated cyclic loading with the forces $S_i$, the stresses in the wall considerably having exceeded the yield point. In the loaded wall may – according to Dietrich [7] – have started the development of the slipping line and cracking.

It is characteristic that displacements $\delta_{L+E}$ between the joined walls are not repeated in the case of stretched 2-blind-bolt joints in elements of type "I" during the initial phases of loading, when the first displacements are "released" (Figure 15). The mutual displacement of joined walls is connected with the mastering of some forces of sliding friction caused by rather small tensile forces in the mandrels of the bolts, remaining in them after having been embedded in the holes.

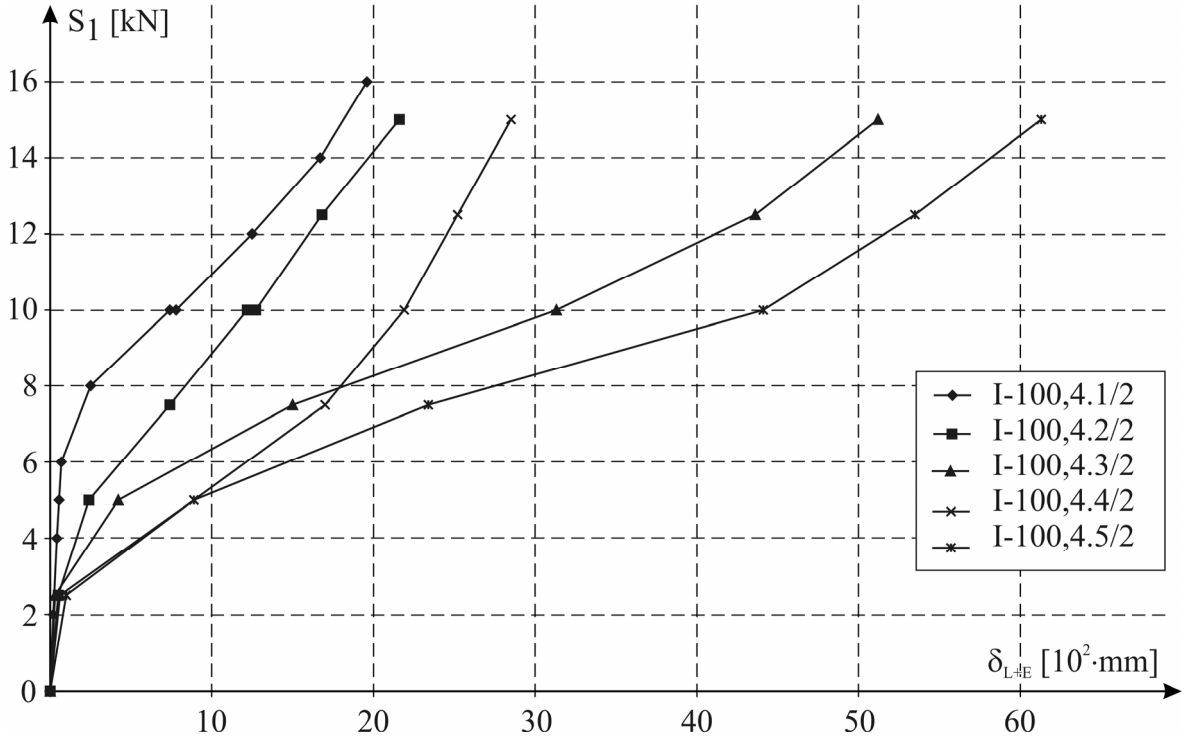


Figure 15. Displacements during the Initial Phases of the Torsion of 2-blind-bolt Joints in Five Test Elements "I"

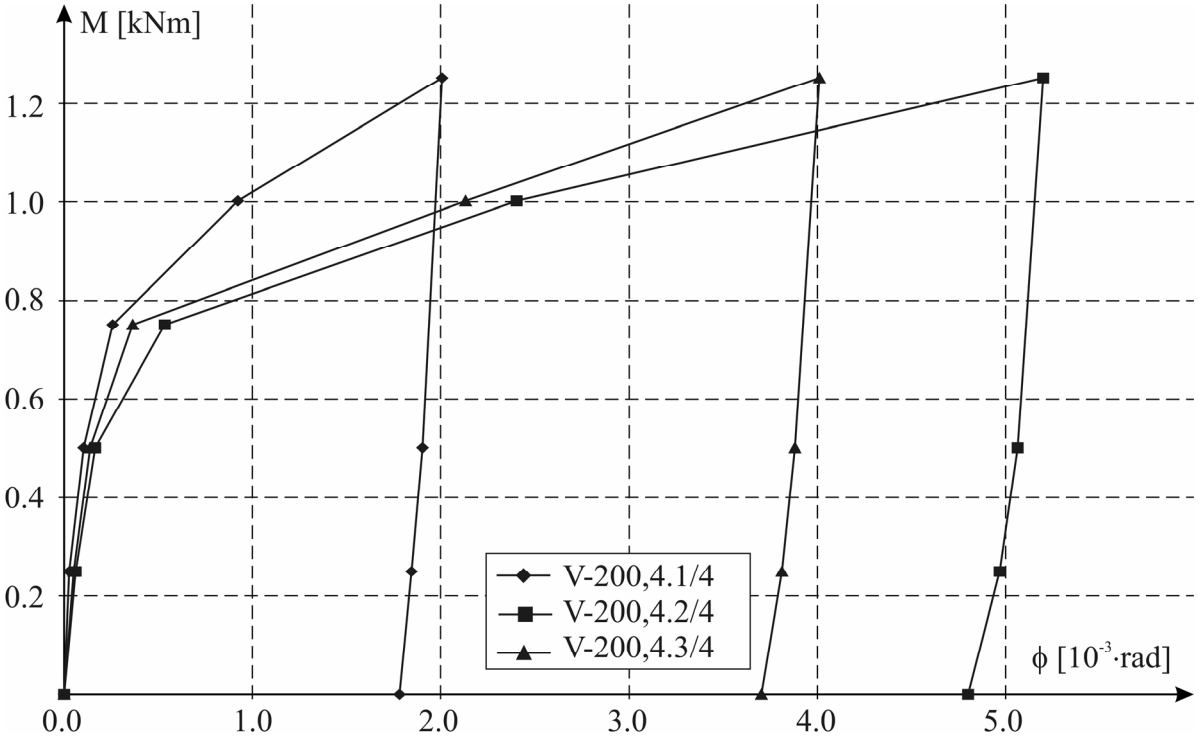


Figure 16. Relation $M$-$\phi$ in the Initial Increments of Load in "V"-type Joints

Similar differences have been observed in angular displacements occurring in simultaneously sheared and bent walls (Figure 16). The relaxation and creeping, as well as the degradation of rigidity in the case of greater loads, were doubtlessly indications of a local fatigue of the material; durable displacements, which in the case of $S_i > P_d$, increased successively and did not stabilize after several iterations, as has been the case earlier, may also serve as a prove of this phenomenon.

A certain role may also be played by the forces of sliding and journal friction. The former ones have been taken into account in the set of Eq. 3 ÷ Eq. 9, the latter, however, have been neglected. In a joint transferring the loads $M$, $H$ and $V$, in the axis of the $i$-th blind bolt a torque moment $M_{i,\phi}$, occurs counteracting the mutual torque of the joined walls by the angle $\phi$ (Figure 17). In a joint with m links the mutual torque of the walls by the angle $\phi = \phi_g + \phi_d$ (cf. Figure 12) is counteracted by the sum of torque moments $\sum M_{i,\phi}$, which may cause a certain reduction of angular displacement $\phi$.

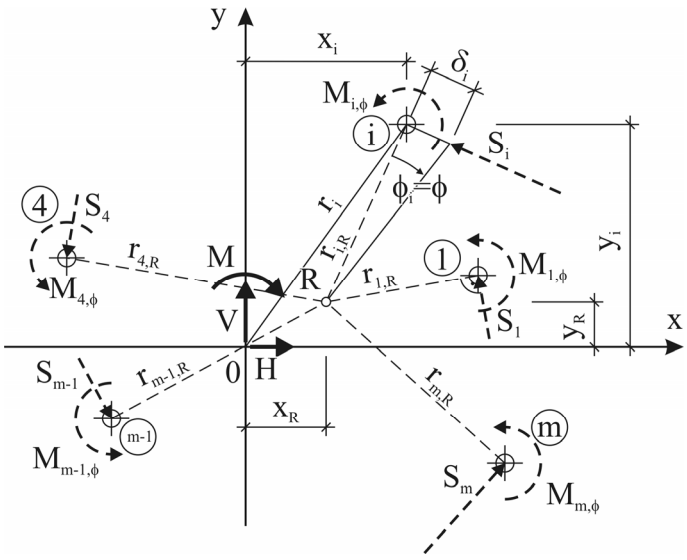


Figure 17. Diagram of the Interactions $S_i$ of the "Bottom" Disk with Torque Moments $M_{i,\phi}$ during the Transfer of the Loads $H$, $V$ and $M$ from the "Upper" Disk

The value of the $i$-th torque moment $M_{i,\phi}$, depending on the load $S_i$, shearing the bolt "i", consists of journal friction forces existing between (Figure 18):

- the blind bolt heads and the external surfaces of the joined walls,
- the cylindrical side surface of the blind bolt and the wall in the hole,
- the adjacent internal surfaces of the joined walls, brought about by the tilt of the blind bolt inside the hole.

The increasing forces $S_i$ accompanied by a simultaneous tilting of the bolts in the holes may have caused an increase of rigidity of the 4-blind-bolt joint.

### 3.5. Boundary Curves of a 4-Blind-bolt Joint

In the investigated joints three variants of boundary states were tested in a dimensionless set of rectangular coordinates $M/M_{\lim}^{III}$ and $V/V_{\lim}^{III}$. Variant I concerns the situation when at least one link in the joint is loaded with a force equal to the calculated load-carrying capacity $P_d$, the variant II – when the mutual linear displacement of the joined walls attains at the point with the most intensive effort the boundary the value $\delta_{lim}$ = 3.0 mm, and variant III corresponds to the theoretical boundary state of destruction of the joint, when the loads of all joints attain boundary values.

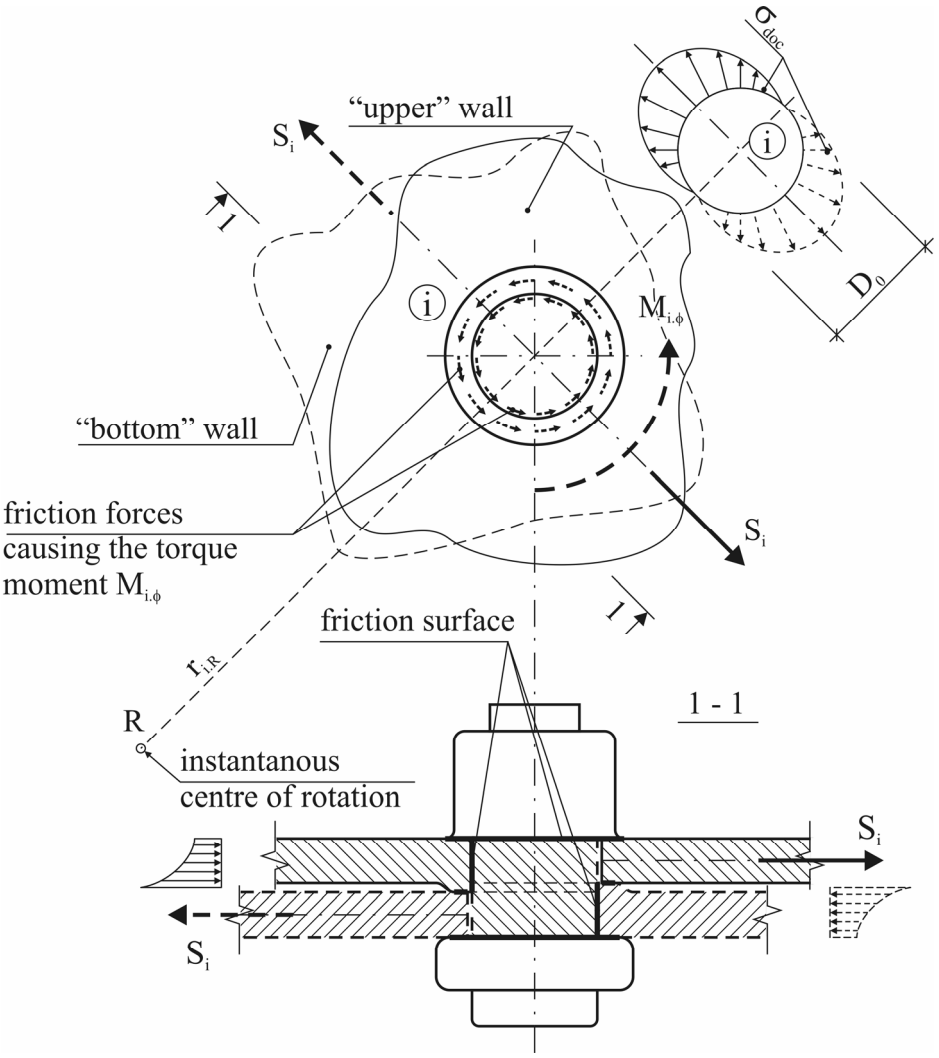


Figure 18. Friction Forces in the Axis of the Bolt "i" in a Lap Joint Loaded with the Bending Moment *M* and Shearing Forces *H* and *V*

The set of Eq. 3 ÷ Eq. 9 ought to satisfy the following conditions concerning the joint "i" with the most intensive effort:

- in the case of boundary state I – with respect to the calculated load-carrying capacity of the joint

$$S_{i,\max} \le S_{\lim}^{\mathrm{I}} = P_d , \tag{10}$$

- in the case of boundary state II - with respect to boundary displacements of the joined walls

$$\delta_{i,\max} = f\left(S_i\right) \le \delta_{\lim} = 3.0\ \mathrm{mm} , \tag{11}$$

when $S_{i,\max} \le S_{\lim}^{\mathrm{II}} = P_{m,med}$,

- in the case of boundary state III - with respect to the theoretical destruction of the joint

$$S_{i,\max} \le S_{\lim}^{\mathrm{III}} = P_{destr} . \tag{12}$$

Basing on results obtained in some other tested joints, also internally statically indeterminable, it was acknowledged that the compatibility of experimental and numerical results is satisfying and the model of calculations is correct. The quoted set of equations could, therefore, be used to plot boundary curves separately for each of the four joints in the system of dimensionless rectangular coordinates $M/M_{\text{lim}}^{III}$ and $V/V_{\text{lim}}^{III}$ ($H = 0$).

In numerical calculations the load $V$ was exerted on the joint at the eccentricities $e$, both the positive and the negative one (cf. Figure 11a). The diagram in Figure 19, for instance, illustrates the areas, enclosed by the boundary curves I, II and III, respectively, for the boundary loads $S_{1,\text{lim}}^{I}$, $S_{1,\text{lim}}^{II}$ and $S_{1,\text{lim}}^{III}$, i.e. for the bolt No. 1 (cf. Figure 1c).

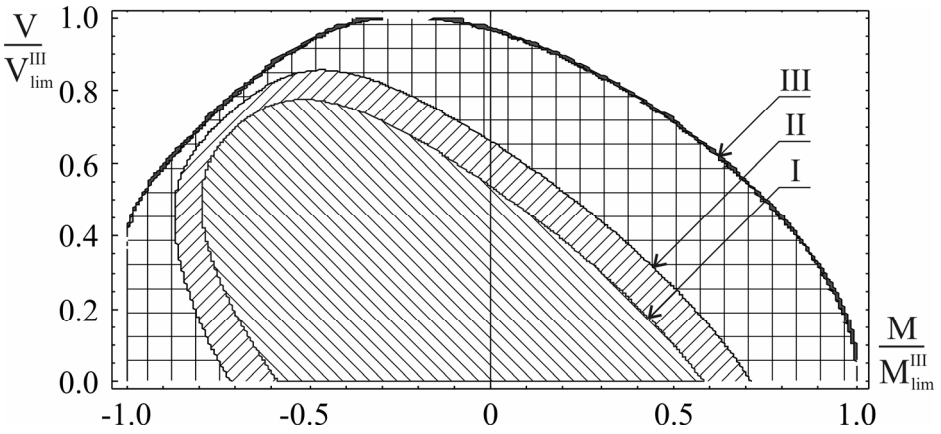


Figure 19. Areas Enclosed by Three Boundary Curves I, II and III of the Force Si for the Bolt No. 1 in the Joint, as in Figure 1c, [4]

The boundary curves for the four bolts in the joint, corresponding to the boundary state I, ware plotted in a common diagram (Figure 20). The surface enclosed by the boundary curves $S_1$ and $S_2$, below their point of intersection at the height of the abscissa $V/V_{\text{lim}}^{III}$ = 1.0, determines the area corresponding to the calculated load-carrying capacity of the joint.

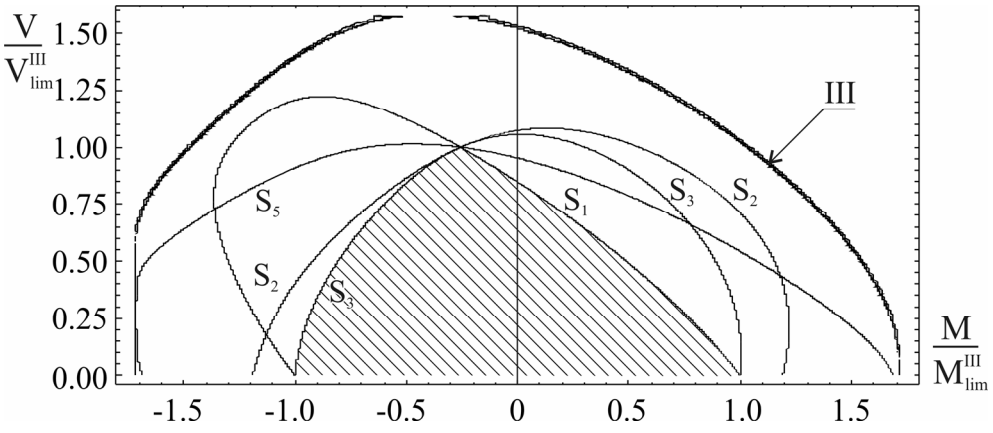


Figure 20. Boundary Curves of the Forces $S_1$, $S_2$, $S_3$ and $S_5$ of the Case of the Boundary State I, Respectively for the Bolts No. 1, 2, 3 and 5 in the Joint Presented in Figure 1c, and the Boundary Curve III (Boundary of the Mathematical Model), [4]

## 4. DESIGN OF A FRAME WITH FLEXIBLE NODES

### 4.1. Assumptions and Fundamentals of Calculation

Basing on the example of a frame designed by Wuwer and Kowolik [8] of sheet-metal sections with closed and open cross-sections and eccentrically joined bars in the nodes, the effect of the instantaneous rigidity of the joints on the static behaviour of the frame was assessed (Figure 21). The walls of sections 5.0 mm thick (of steel S235 JR) were joined in the nodes by blind bolts of the type BOM R16-6, class 12.9. The values of single-cut 5-blind-bolt joints change non-linearly due to the ovalization of the holes (approved by the standard [10]), affecting a plastic failure of the walls in the holes, propagating with the increase of the axial forces $V$, the transverse forces $H$ and the bending moment $M$. The way of calculating a multi-blind-bolt lap-joint was presented by Wuwer [1, 2].

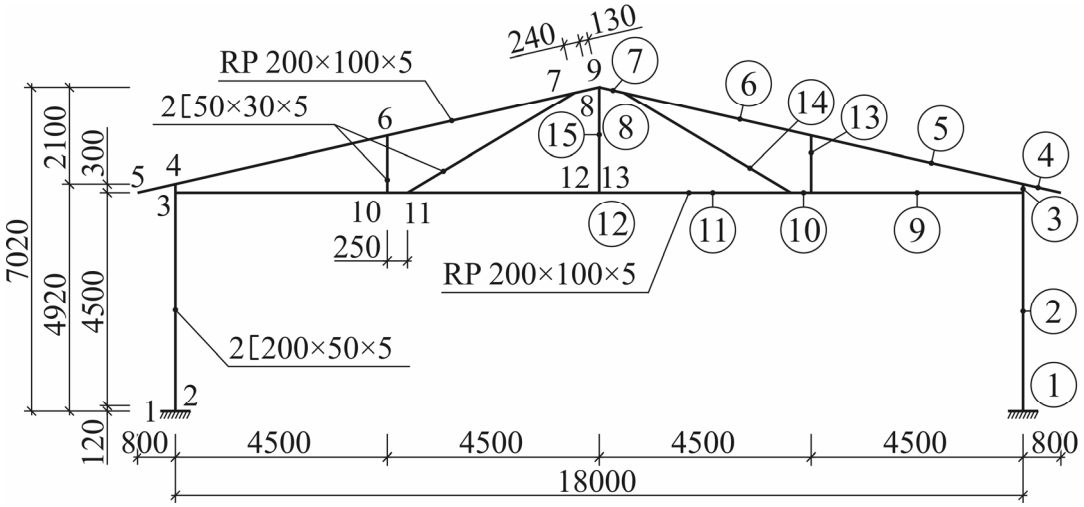


Figure 21. Diagram of a Frame with the Cross-sections of the Bars and the Numeration of the Bars and Nodes

Up to now the authors of the paper Wuwer and Kowolik [11] have carried out static calculations of a lattice frame with a span of 20.0 m and nodes constructed using the same joints, introducing values of the secant rigidity and strain rigidity, instead of the an instantaneous rigidity. The influence of interactive dependences occurring in the nodes of the frame between the values of the three rigidities which go together with the loads $V$, $H$ and $M$, respectively, was there neglected. This influence was taken into account in calculations concerning the frame presented in Figure 21, applying formulae quoted by Wuwer [2], describing the nonlinearly changing values of the rigidity of the joints by means of three reductive coefficient of rigidities; the coefficient $\upsilon_M$ reduced the value of the rotating rigidity combined with the bending moment $M$ in result of the simultaneous shearing of the joints by the two other forces $V$ and $H$; whereas the reductive coefficients $\upsilon_V$ and $\upsilon_H$ reduce the rigidity in the direction of the forces $V$ or $H$, respectively, due to the jointly acting forces $M$ and $H$ or $M$ and $V$. The values of the reductive coefficients were taken from contour lines constructed by solving a set of eight equations describing the static behaviour of a 5-blind-bolt joint, Wuwer [2]. The developed contour lines of three coefficients of the reductive rigidity were presented by Wuwer and Walentynski [5]. The contour lines were plotted on diagrams of dimensionless rectangular co-ordinates $M/M_{\lim}$ and $W/W_{\lim}$, concerning cases in which the directions of inclination of the resultant force $W$, the components of which are the forces $H$ and $V$, change every 15°. In each node of the frame presented in Figure 1 single-cut joints were assumed, either as 5-blind-bolt joints or single-blind-bolt joints. Calculations concerning this frame were carried out by applying the programme Robot Millennium v.15 [9], making use of the option of nonlinear releases of the bars.

## 4.2. Load-carrying Capacity of a 5-Blind-bolt Joint

Single-cut lap-joints of the upper and the bottom flange (RP 200×100×5) in the nodes 8 and 12, i.e. in the vicinity of the roof ridge joints, connecting the columns (2[200×50×5) subsequently with the anchoring elements at the bottom and the bottom and upper flanges (cf. Figure 21), were constructed by means of 10 bolts, 5 in each joint connecting two adjacent walls of the sections (Figure 22).

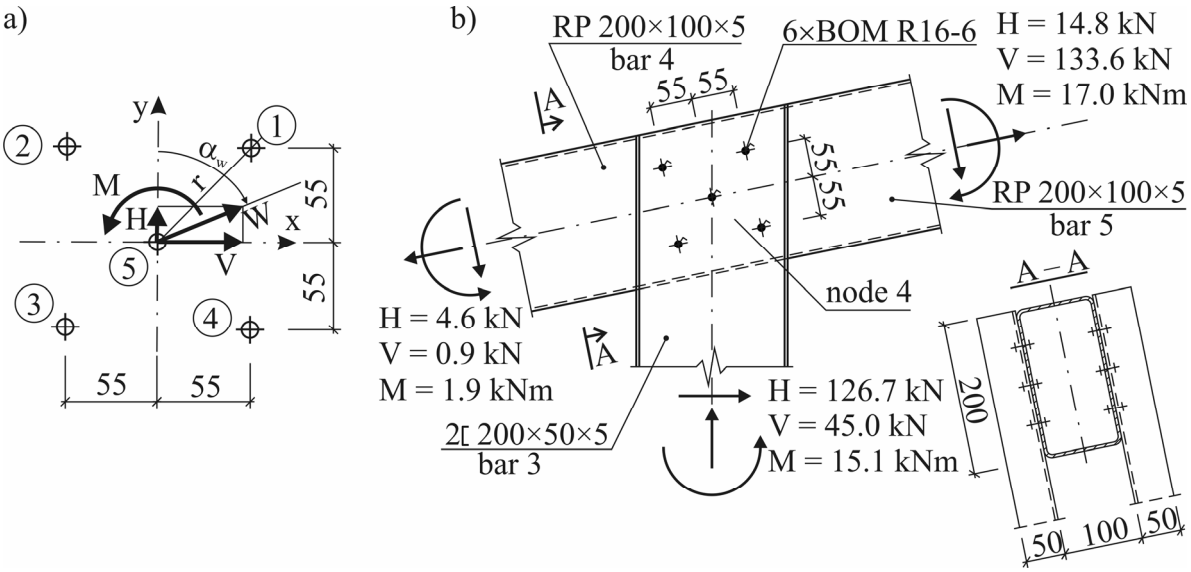


Figure 22. Assumptions for Calculations: a) Draft of a 5-Blind-bolt Joint bent by the Momentum M and Sheared by the Force W inclined Versus the Axis y at the Angle $\alpha_W$, b) Construction of the Quoin of the Frame in the Node 4 and the Loads $M$, $H$ and $V$ of the Bars, According to the Final Results of Calculations (cf. Column 5 in Table 2)

The number of bolts assumed in the calculations was not rational, because in some joints the load-carrying capacity was not taken into account. In the dimensioning of the joints already existing diagrams of the boundary curves were used, as well as the contour lines of the reduction coefficients, developed so far only for a 5-blind-bolt joint (cf. Figure 22a). Double-branch bars 13 and 14 (2[50×30×5) were joined with the flanges in an articulated way, i.e. by two joints in each node 6, 10, 7 and 11.

Calculations concerning a 5-blind-bolt joint were carried out by solving a set of equations, consisting of three equations and geometrical relations and a constitutive equation, providing five equations, Wuwer [1]. The constitutive equation had the form of a function reciprocal to the relation $S_1$-$\delta_{L+E}$, connecting the load $S_1$ of a single bolt with the mutual displacement $\delta_{L+E}$ of the joined walls, in compliance with the relation (2) (cf. Figure 10, curve II).

The numerical solution of this set of equations provided results expressed by the values of the forces $S_i$ exerted on the individual joints and of the displacements $\delta_i$ between the joined walls of the sections, where "i" denotes the subsequent joints numbered 1÷5 (cf. Figure 22a) in the considered joint.

The values of the forces $S_i$ and the displacements $\delta_i$ were compared on contour lines with the boundary values, Wuwer and Walentynski [5]. As examples of the behaviour of the bolts 1 and 2 (cf. Figure 22a) may serve the contours of the forces $S_1$ and $S_2$ (Figure 23) and the corresponding contours of displacements $\delta_1$ and $\delta_2$ (Figure 24). The contours corresponding to the calculated load-carrying capacity $S_1 = S_2 = P_d = 48.6$ kN (in the case of the boundary state I) and the boundary

load-carrying capacity $S_1 = S_2 = P_m = 55.85$ kN, as well as the contours corresponding to the displacements $\delta_{L+E,d} = 209.3 \cdot 10^{-2}$ mm and $\delta_{lim} = 3.0$ mm (the case of the boundary state II) have been singled out in the diagrams.

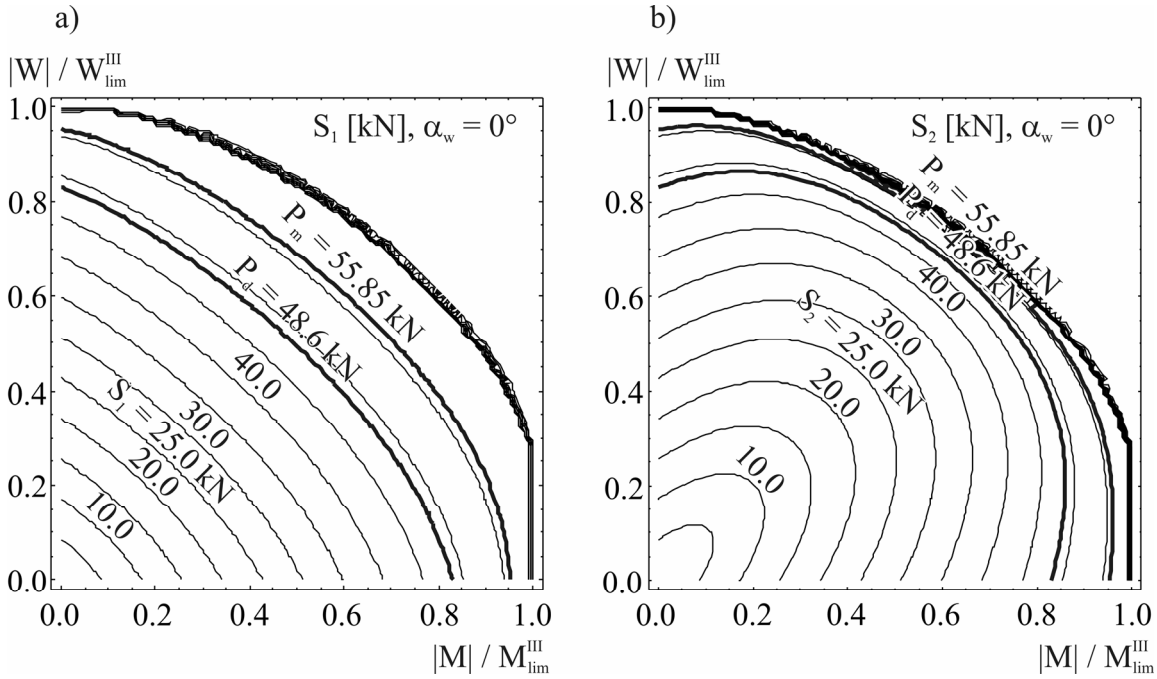


Figure 23. Contour Lines of the Forces $S_1$ and $S_2$ Exerted in a 5-Blind-bolt Joint on a) the Bolt No.1, b) Bold No.2, Respectively, [5]

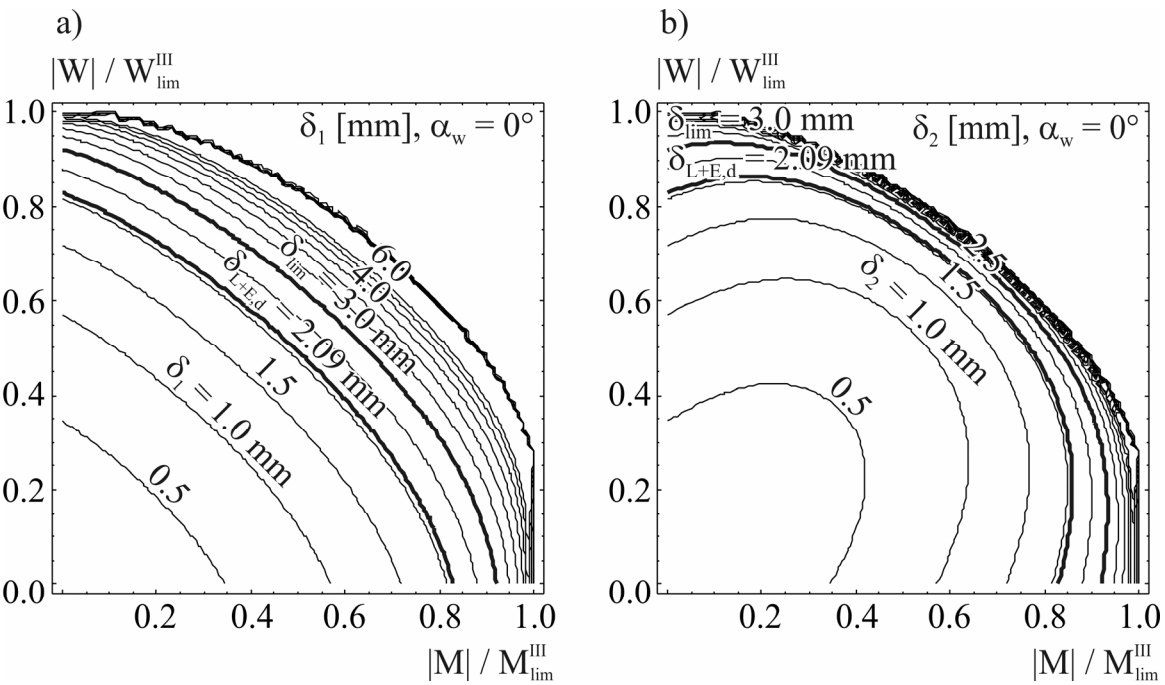


Figure 24. Contour Lines of the Displacements $\delta_1$ and $\delta_2$ Occurring Between the Joined Walls in a 5 Blind-bolt Joint in the Case of a) Bolt No. 2, b) Bolt No. 2, [5]

Concerning the behaviour of joints three cases of the boundary states were considered in the dimensionless rectangular coordinate system $M/M^{III}_{\text{lim}}$ and $W/W^{III}_{\text{lim}}$. The first case concerns the situation when at least one link in the joint is loaded with a force equal to its calculated load-carrying capacity $P_d$, and the second case the situation when the mutual linear displacement of

the joined walls achieves in the place of the: highest effort the boundary value $\delta_{lim}$ = 3.0 mm. The third case corresponds to the theoretical boundary state of destruction of the joint, i.e. when the loads on all the joints reach boundary values. The shapes of all the three boundary curves change with the angle of inclination of the resultant force $W$ in the joint, as is to be seen in Figure 25, corresponding to the case when $\alpha_W = 0$ or $\pi/2$ and $\alpha_W = \pi/4$.

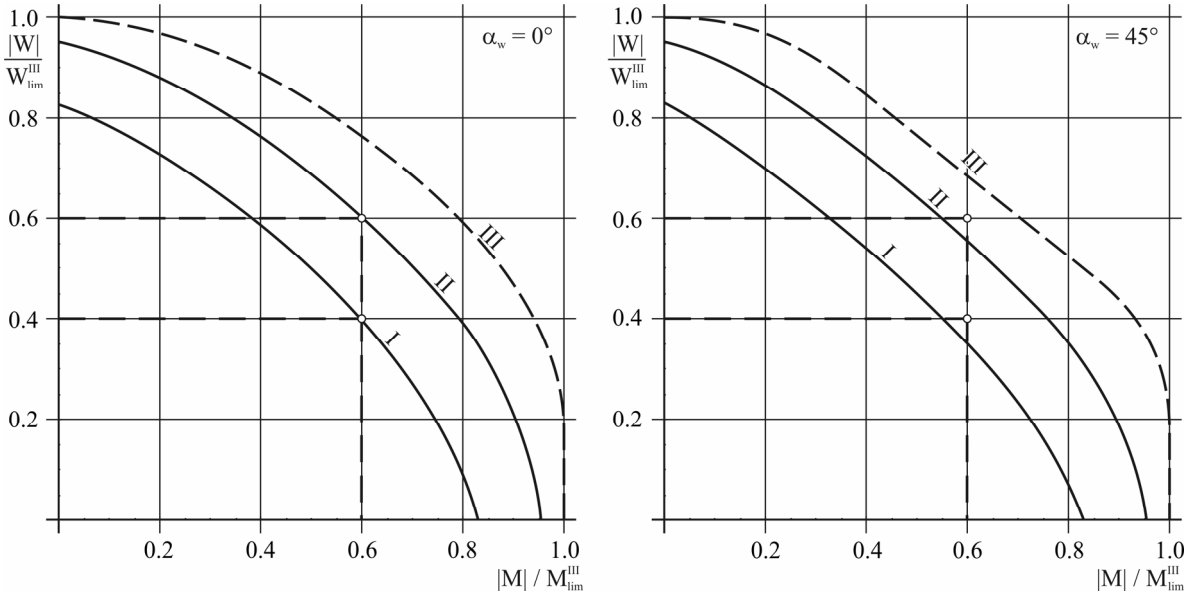


Figure 25. Boundary Curves of the Load-carrying Capacities I, II and III of a 5-Blind-bolt joint Loaded with the Forces $M$ and $W$ Concerning Two Different Loads:
a) When $\alpha_W = 0$ or $\pi/2$, b) When $\alpha_W = \pi/4$, [5]

The diagrams plotted basing on the results of numerical analyses indicated, for instance, that in the case of the load $M$ and $W$, when $W/W_{\lim}^{III}$ = 0.4 and $M/M_{\lim}^{III}$ = 0.6, the condition of the calculated load carrying capacity of a 5-blind-bolt joint is maintained at $\alpha_W = 0$ or $\pi/2$, but at the same values of the load $M$ and $W$ it is exceeded already when $W/W_{\lim}^{III} = M/M_{\lim}^{III} = 0.6$. Boundary curves I considerably felicitated the checking of the calculated load carrying capacity of the joints in the nodes numbered 2, 3, 4, 8 and 12.

### 4.3. Rigidity of a 5-Blind-bolt Joint

The rigidity of joints was calculated basing on the Eq. 2, which permits to express the rigidity of a single bolt in the joint by the equation Wuwer [1]:

$$K_{rt}^{S} = \frac{dS_1}{d\delta} = a_S \cdot b_S \cdot e^{-b_s \cdot \delta_{L+E}}, \tag{13}$$

but the values of three instantaneous rigidities associated with the forces $V$, $H$, $M$ are calculated by means of the formulae:

$$K_{rt}^{V} = m \cdot K_{ri}^{S} \cdot (1 - \omega_V) \cdot \upsilon_V, \tag{14}$$

$$K_{rt}^{H} = m \cdot K_{ri}^{S} \cdot (1 - \omega_H) \cdot \upsilon_H, \tag{15}$$

$$K_{rt}^{M} = (m-1) \cdot r^2 \cdot K_{ri}^{S} \cdot (1 - \omega_M) \cdot \upsilon_M. \tag{16}$$

As there are two 5-blind-bolt joints in the nodes 2, 3, 4, 8 and 12, the values of rigidity calculated according to Eq. 13, Eq. 14 and Eq. 15 were taken in the calculations as twice as high. In order to simplify the calculations it has been assumed that in each joint the load consists of the bending moment $M$ and only one shearing force $W$, which always equals the larger force of the two component loads $V$ and $H$, i.e. which is parallel either to the axis $y$ or $x$ of the coordinate system; thus, for $\alpha_W = 0$ or $\alpha_W = \pi/2$, respectively (cf. Figure 22b).

The reduction coefficients $\upsilon_M$ and $\upsilon_W$, were taken from the contour lines plotted in the diagrams as a system of non-dimensional quantities $W/W_{\text{lim}}^{III}$ and $M/M_{\text{lim}}^{III}$. Figure 26 presents the contours of the coefficients $\upsilon_M^{III}$ and $\upsilon_W^{III}$ plotted in a common diagram versus the third boundary state with the boundary values of the load amounting to $W_{\text{lim}}^{III} = 5 \cdot S_{\text{lim}}^{III} =$ $5 \cdot 58.58$ kN = 292.9 kN and $M_{\text{lim}}^{III} = 4 \cdot r \cdot S_{\text{lim}}^{III} = 4 \cdot 0.055 \cdot 2 \cdot 58{,}58 = 18.2$ kNm (cf. Figure 10, $S_{\text{lim}}^{III} = a_S$ – for curve II). Thus, for example, for the values $W/W_{\text{lim}}^{III} = 0.275$ and $M/M_{\text{lim}}^{III} = 0.325$, the diagram in Figure 26 quotes, interpolating linearly, the values of both reduction coefficients, namely $\upsilon_W^{III} = 0.81$ and $\upsilon_M^{III} = 0.89$.

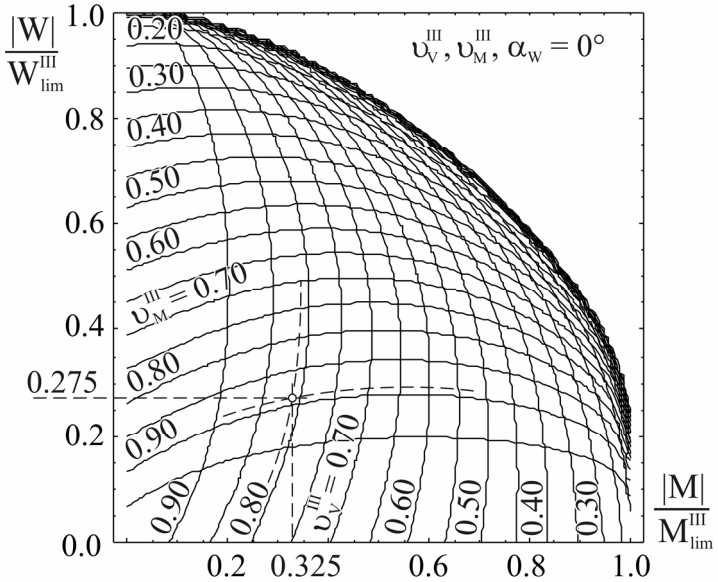


Figure 26. Contour Lines of the Reduction Coefficients of the Rigidities $\upsilon_M^{III}$ and $\upsilon_W^{III}$ in a 5-Blind-bolt Joint, [5]

## 4.4. Analysis of the Results of Calculations

In the static calculations of the frame several variants of combined loads were taken into account; considering the load-carrying capacity of the bars and nodes, of much importance proved to be the variant I (dead load of the frame, covering, walls, installations, snow in zone II, temperature), variant 2 (constant loads, wind in zone II) and variant 3 (variant I plus wind). Table 2 provides a comparison of selected results of static calculations for a frame with rigid, flexible and articulated nodes, loaded according; to variant 1. The values of the forces $M$, $H$ and $V$ in the bars are quoted for two kinds of flexible joints: in column 4 the rotational rigidity and two rigidities corresponding to the mutual displacement of the joined walls in the direction of the loads $V$ and $H$ have been introduced, disregarding the reduction coefficients of rigidity; in column 5 the rigidities were calculated applying the formulae Eq. 14 ÷ Eq. 16, i.e. taking into account the values of the reduction coefficients $\upsilon_W$ and $\upsilon_M$, quoted in Table 3 (numbers above 100 correspond to the

symmetrical nodes of the frame). The values of the reduction coefficients and are contained within the range $0.79 \leq \upsilon_W \leq 1.0$ and $0.89 \leq \upsilon_M \leq 1.0$.

Table 2. Results of Statistical Calculations Concerning a Frame with Rigid, Flexible and Articulated Nodes

| No. of the bar/ node | Forces $H$,$V$ [kN] moment $M$ [kNm] | Values $M$, $H$, $V$ in the bars of a frame with nodes | | | |
|---|---|---|---|---|---|
| | | rigid | flexible | | articulated |
| | | | no reduction of rigidity | reduced rigidity | |
| *1* | *2* | *3* | *4* | *5* | *6* |
| 2/2 | M | -2.1 | -2.7 | -3.0 | 0 |
| 2/3 | M | 3.2 | 9.6 | 9.9 | 45.10 |
| | H | 56.7 | 56.7 | 56.7 | 56.67 |
| | V | 1.4 | 2.9 | 3.0 | 10.23 |
| 3/3 | M | 17.6 | 22.7 | 22.9 | 45.10 |
| | H | 50.2 | 50.0 | 50.0 | 50.34 |
| | V | -123.8 | -126.9 | -126.7 | -148.87 |
| 3/4 | M | -19.6 | -15.4 | -15.1 | 0 |
| | H | 49.7 | 49.5 | 50.0 | 49.84 |
| | V | -123.8 | -126.9 | -126.7 | -148.87 |
| 5/4 | M | -21.5 | -17.3 | -17.0 | -1.88 |
| | H | 130.8 | 133.8 | 133.6 | 155.25 |
| | V | 15.7 | 14.9 | 14.8 | 10.15 |
| 9/3 | M | -14.4 | -13.1 | -13.0 | 0 |
| | H | -125.2 | -129.8 | -129.7 | -159.09 |
| | V | 5.7 | 5.9 | 6.0 | 5.61 |

Table 3. Values of the Reduction Coefficients of the Rigidities $\upsilon_W$ and $\upsilon_M$

| No. of the nodes | variant I | | variant II | |
|---|---|---|---|---|
| | $\upsilon_M$ | $\upsilon_W$ | $\upsilon_M$ | $\upsilon_W$ |
| 2<br>102 | 0.950 | 0.990 | 1.000<br>0.970 | 0.880<br>0.970 |
| 3<br>103 | 0.920 | 0.830 | 0.950<br>0.955 | 0.920<br>0.835 |
| 4<br>104 | 0.920 | 0.790 | 0.950<br>0.955 | 0.890<br>0.805 |
| 8<br>108 | 0.930 | 0.935 | 0.950<br>0.950 | 0.950<br>0.960 |
| 12<br>112 | 0.890 | 1.000 | 0.910<br>0.910 | 1.000<br>1.000 |

In the case of the frame bars the conditions of the load-carrying capacity have been checked, which have been satisfied as follows (cf. Figure 21): in the bottom section (bar 2) and upper section (bar 3) of the pillar $0.932 < 1.0$ and $0.862 < 1.0$, respectively, and in the flanges of the upper spandrel beam (bar 5) and the bottom flange (bar 9) $0.790 < 1.0$ and $0.580 < 1.0$, respectively. Table 4 presents the values of maximum vertical and horizontal displacements of the spandrel beam on the level of the quoins, which do not exceed the boundary values.

Table 4. Values of Vertical and Horizontal Displacements in the Spandrel Beam at the Quoins of a Frame with Rigid, Flexible and Articulated Nodes

| No. of the nodes | Displace-ments | Displacements in a frame with nodes [mm] | | | | Boundary displace-ments [mm] |
|---|---|---|---|---|---|---|
| | | rigid | flexible | | articulated | |
| | | | no reduction of rigidity | reduced rigidity | | |
| 9 | vertical | 13.5 | 20.5 | 21.6 | 39.3 | 72.0 |
| 3 | horizontal | 6.1 | 13.5 | 13.7 | 544.4 | 32.0 |

Figure 27 presents a comparison of the percentage changes of the values of bending moments concerning the cases quoted in columns 3 and 5 in Table 2. The differences are considerable and in the average they are as large as some score of percent. Thus, for instance, in the span of bar 6 (cf. Figure 21) the values of the moments are in a frame with flexible nodes larger by 39% in relation to a frame with rigid nodes.

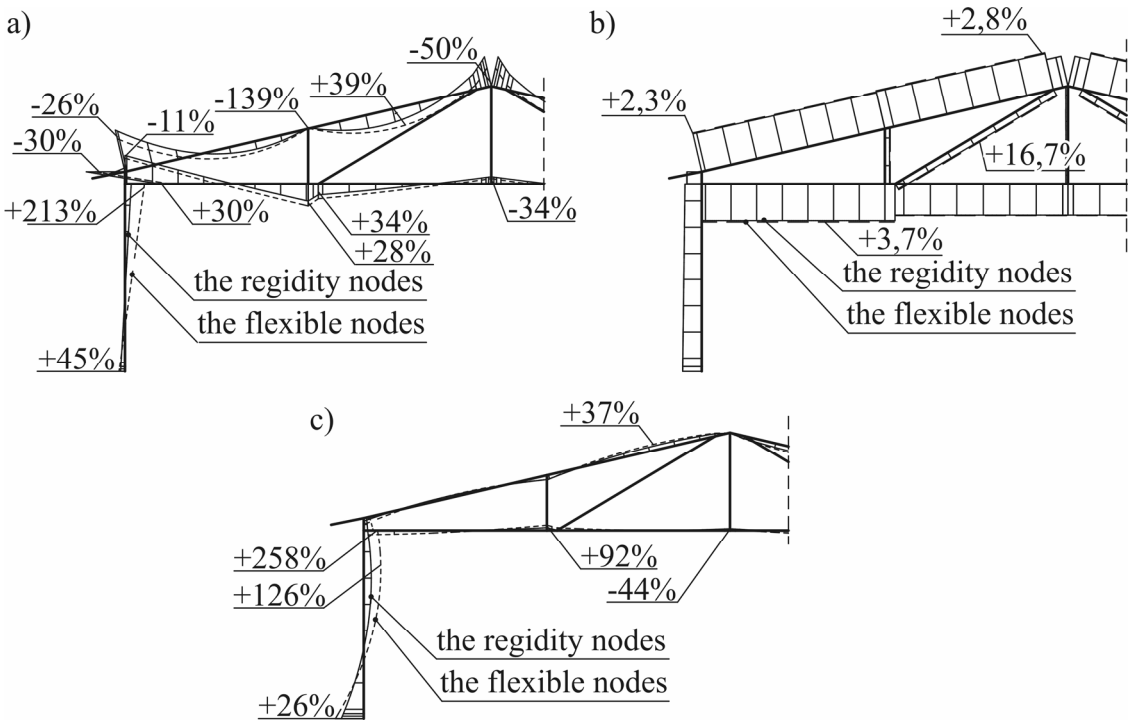


Figure 27. Diagrams of the Forces in the Bars of the Frame: a) Bending Moments in Variant 1 of Loads, b) Axial Forces in Variant 1 of Loads, c) Bending Moments in Variant 2 of Loads

## 5. CONCLUSIONS

The results of single-cut joints with bolts, investigated by the author, including alternately loaded joints, are characterized by considerable scatters within the frame of identical cases of constructions. These scatters cannot be eliminated – as has been found – by a better accuracy in the construction of the joints, although their rigidity can be improved by embedding the bolts in holes with smaller diameters, within the range recommended by the producers of the joints.

Keeping all this in mind, the suggested way of calculating the joints may be considered to be accurate enough. If the relation between the load $S_i$, the value of the torque moment $M_{i\phi}$ and the angular disp1aceraent $\phi$, were known, which might be achieved only experimentally, it would become possible to modify the set of equations and to solve it once again, assessing – basing on the example of a four-blind-bolt joint or eight-blind-bolt joint – how much the friction forces can improve the compatibility of experimental and numerical results.

Referring to the results obtained in calculations of a frame with flexible nodes it has been found that the differences between the values of the bending moments, occurring in the bars of the frame connected with each other rigidly or flexibly, are considerable.

The rather small effect of the reduction coefficients $\upsilon_M$ and $\upsilon_W$ on the values of internal forces in the bars of the frame result from redimensioning of the 5-blind-bolt joints in the nodes 2, 8 arid 12, which had too large reserves. The interaction of three rigidities would mean a greater share in the static work of the frame, if the joints in these nodes were designed with a respectively reduced number of links, as the values of the coefficients $\upsilon_M$ and $\upsilon_W$ in Table 2 suggest; in some nodes the values of the rigidity of the joints are reduced by 11% at bending and 21% due to the effect of the longitudinal force.

Contour lines of the reduction coefficients ought to be determined for several typical joints, e.g. 2-, 3- and 4-blind-bolt joints. Only then will it be possible to design the considered construction of the frame with an adequately chosen smaller number of links in the respective joints.

The important problem of alternate loads of the knuckle joints has not been taken into account in the calculations of the frame. Only one load cycle has been taken into account, resulting from the impact of the wind. Obviously, the changing the direction of the construction results in a change of the values and directions of the bending moments $M$ and shearing forces $W$ in the joints, particularly in the quoins of the considered frame.

The joints taking alternately over the exerted forces $\pm M$ and $\pm W$ behave depending on the course of the functions which describe the hysteresis loops, connected with changes of the rigidity of the joints.

In order to find out the shapes of the hysteresis curves, alternately loaded joints were investigated, including those stretched axially and bent (cf. Figure 8).

It has also been noticed that when the direction of the wind changes, the joints in the quoins may instantaneously attain a zero rigidity.

The problem concerning the effect of alternate loads on the behaviour of the considered joints requires a new analytical approach and also a new computer programme, which would permit to analysis properly the statics and strength of the construction. In the presented calculations of the frame the applied Robot Millennium, v.15 programme [9] did not facilitate such an analysis.
The feasibility of applying FEM for the purpose of testing the given joints cannot be excluded; in such a case the results of the numerical analysis may be compared with the results obtained by means of the analytical method suggested in the present paper.

It should be noticed that modelling any bent and sheared multi-blind-bolt joint in compliance with FEM may prove to be rather troublesome. A complete model permitting to obtain comparable results ought to be a spatial model. For the sake of simplification, e.g. a two-stage procedure should be applied: first the whole joint should be modelled applying elements of a lower order, i.e. "flat elements" (2D), and then "lump element" (3D) should be introduced into the analysis in the form of the separate surrounding for each single bolt, taking into account the respective boundary conditions. Of much importance would also be, among others, such effects as contact problems, the incomplete isotropy of the material that is to be joined, the fissures resulting from constant deformations as well as sliding and journal frictions occurring in the loaded joints.

Keeping all this in mind we may assume that a numerical analysis carried out by means of FEM would then involve the necessity of formulating untypical elements.

The problems of the effect of alternate loads on the behaviour of bar structures with single-cut joints and the elaboration of an FEM method for numerical investigations of such joints are topics which the author of the present report intends to deal with in the nearest future.

## REFERENCES

[1] Wuwer, W., "Investigations and Calculation of Lap Joints with Special Blind Bolts", Polish Academy of Sciences, Archives of Civil Engineering, Volume LI, Issue 2. Warszawa, 2005, pp. 253÷280.

[2] Wuwer, W., "Flexible Joints with Blind Bolts in Thin-walled Bar Constructions", Zeszyty Naukowe Politechniki Śląskiej Nr 1710 (z. 105), (Scientific Fascicles of the Silesian University of Technology). Gliwice, Poland, 2006.

[3] Technical Certificate of the Institute of Civil Engineering No. AT-15-3487/99, Bolts produced by Huck, 1999.

[4] Wuwer, W, The Effort of An Asymmetric Joint with Blind-bolts of Sheet-metal Sections. Proceedings of XITH International Conference on Metal Structures "Progress in Steel, Composite and Aluminium Structures", (ICMS-2006). Rzeszow, Poland, 2006, pp. 190÷191.

[5] Wuwer, W., Walentynski, R., "Interaction Relations in the Model of the Lap Joints of Thin-walled Structure under Complex Load State", Proceedings of International Colloquium of IASS Polish Chapter: Lightweight Structures in Civil Engineering, Warszawa, Poland, 2005, pp. 239÷246.

[6] Recommendations for Steel Construction, ECCS-TC7, The Design and Testing of Connections in Steel Sheeting and Sections. Constrado, No. 21, 1990.

[7] Dietrich, M., "Introduction to the Stochastic Theory of Machines", PWN (National Scientific Editors), Warszawa, Poland, 1972.

[8] Wuwer, W., Kowolik, B., "The Rigidity of Flexible Lap-joints Subjected to Complex Loads", Proceedings of XITH International Conference on Metal Structures, "Progress in Steel, Composite and Aluminium Structures", (ICMS-2006), Rzeszów, Poland, 2006, pp. 192÷193.

[9] User manual, Robot Millennium, v.15, 2002.

[10] PN-B-03207, Steel Structures, Constructions of Section and Cold-formed Sheet-metal. Design and realization (Polish standard).

[11] Wuwer, W., Kowolik, B., "Frames of Thin-walled Sections with Flexible Nodes" (in Polish), Proceedings of 7th Symposium of the Cycle: New Achievements in Science and Technology in Civil Engineering. Rzeszów, Poland, 2005, pp. 355÷366.